NOTE TO USERS

Page(s) not included in the original manuscript and are unavailable from the author or university. The manuscript was scanned as received.

36,70,90

This reproduction is the best copy available.

Université de Sherbrooke

Damage induced in DNA and RNA components by low energy heavy ions, electrons and photons

By

Sarvnaz Sarabipour

Department of Nuclear Medicine and Radiobiology
Faculty of Medicine, University of Sherbrooke
Sherbrooke, Québec, Canada, J1H 5N4

Mémoire présenté à la Faculté de Médecine et Science de la Santé
En vue de l'obtention du grade de
Maitrise èn Sciences (M.Sc.) en Radiobiologie

June 2008

Jury

Directeur de Mémoire: Professor Michael.A.Huels, Université de Sherbrooke

Examinateur : Professor Richard.J.Wagner, Université de Sherbrooke

Examinateur: Professor Klaus Klarskov, Université de Sherbrooke

Your file Votre référence
ISBN: 978-0-494-49582-7
Our file Notre référence
ISBN: 978-0-494-49582-7

"What I have to do will want true colours..."
Shakespeare,Hamlet iii,4

TABEL OF CONTENTS

List of Figures

List of Abbreviations and Symbols

IRL	Ion Reaction Laboratory
UHV	Ultra High Vacuum
SR	Synchrotron Radiation
VUV	Vacuum Ultraviolet
RBE	Relative Biological Effectiveness
SSB	Single Strand Break
DSB	Double Strand Break
XPS	X-ray Photoemission Spectroscopy
NEXAFS	Near Edge X-ray Absorption Fine Spectroscopy
R	D-Ribose
dR	2-deoxy-D-Ribose
Ade	Adenine
Gua	Guanine
Cyt	Cytosine
Ura	Uracil
Thy	Thymine
dThd	Thymidine
BrdUrd	5-Bromouracil

Abstract

Hyperthermal heavy ion damage to DNA components

Ion beams have recently emerged as a promising radiotherapy technique for treatment of large, solid, deep seated tumours. As the primary beam of heavy particles traverses through the cell, secondary charged and neutral species are generated. In particular secondary ions with energies up to 100 eV are produced in large numbers along the ionization track. Ionization and fragmentation of DNA components is a key step in radiobiological damage to the cell.

An ultrahigh vacuum (UHV) ion beam system has been used to study the ionization and fragmentation pathways of DNA bases by ion irradiation in the condensed phase and electron impact in the gas phase. The apparatus consists of a low energy ion source, beam line, biomolecular film preparation system and a reaction chamber with high-resolution mass spectrometer to monitor desorbing ion yields Solid condensed films of DNA bases were prepared *in vacuo* by sample evaporation from an oven and were subsequently irradiated with (1-100 eV) Ar^+ ions. Upon bombardment, desorbing positive and negative fragments were collected using a Quadrupole Mass Spectrometer (QMS).

Ionization and fragmentation of Adenine (A), Guanine (G), Cytosine (C) and 5-aminouracil bases has been observed by low energy (10-100 eV) Ar^+ ions in the condensed phase and 70 eV electrons in the gas phase. These observations demonstrate fragmentation mechanisms involve site specific concerted dissociation reactions,

deamination of Ade, Gua, Cyt in the condensed phase and the gas phase as well as amination of Adenine in the condensed phase. Of significant features of the mass spectra of all four bases are the production of NH_4^+ (18 amu) and CH_3^+ (15 amu) fragments with high intensities relative to the most intense peak in each spectrum ($HCNH^+$, 28 amu). Utilizing isotopically labelled Ade, Gua and Cyt common purine and pyrimidine bond cleavage pathways and fragment origin sites were identified. Experiments performed with 5-aminouracil confirmed the demination hypothesis of A, G and C bases by low energy Ar^+ ion impact in the condensed phase as well as the low energy electron impact in the gas phase.

These results demonstrate induction of effective damage to the DNA by low energy heavy ions. Various physical and chemical mechanisms may involve initiation of this damage by fragmentation and ionization of DNA bases. In the gas phase, intra-molecular proton/hydrogen transfer may aide formation of NH_4^+, CH_3^+ and other intense fragments from within the base molecule. In the condensed phase however, adjacent base molecules may share a proton between two electron lone pairs. Ion desorption spectra of films of nucleobases suggest that intra/inter-molecular hydrogen transfer/proton tunnelling processes, tautomeric equilibrium and geometric characteristics of the nucleobases molecular structure and base stacking phenomena between nucleobases on different film layers may be responsible for emergence of masses 15 and 18 amu in the mass spectrum of all these bases.

Deamination of DNA base pairs occurs naturally in the cell a very low rate of 100-500 events per cell per day. Moreover enzymatic deamination has been observed in the genome of mammalian cells by enzymatic DNA deamination pathways. Chemical

deamination processes may take place in the single strands of DNA, transforming Cytosine into Uracil, which upon replication implies a change of G into A in the opposite strand (and similar for deamination of A and G).The change induced can result in Transition mutation (also induced by amination of DNA bases). These results show that a process of physically induced deamination of DNA is mediated by hyperthermal heavy ion impact.

Key words: heavy ion, low energy, deamination, proton tunnelling, condensed phase.

Résumé

Impact des ions de faible énergie sur les composants de l'ADN

L'émergence récente de la hadronthérapie (thérapie avec des particules lourdes) constitue à l'heure actuelle une technique de radiothérapie prometteuse pour le traitement de tumeurs solides ancrées en profondeur. L'émission d'un rayonnement primaire composé de particules lourdes traversant les cellules a pour conséquence la génération d'espèces secondaires neutres et chargées. En particulier, la production importante d'ions secondaires d'énergie entre 10 à 300 eV, sur le trajet du faisceau ionisant, engendre l'ionisation et la fragmentation des constituants de la molécule d'ADN, processus-clé des dommages radiobiologiques au niveau moléculaire et finalement cellulaire.

L'utilisation d'un système générateur de faisceaux d'ions sous ultravide a permis l'étude des mécanismes d'ionisation et de fragmentation des bases de l'ADN par irradiation ionique en phase condensée et par impact électronique en phase gazeuse. L'appareillage est constitué d'une source d'ions de faible énergie, d'un système de focalisation, d'une chambre de préparation des films moléculaire et d'une chambre de réactions couplée à un spectromètre de masse de haute résolution, permettant le monitoring des rendements des produits de l'irradiation générés. La condensation des bases de l'ADN en forme de films a été préparée in vacuo par évaporation d'un four, ce film étant ensuite irradié aux ions argon Ar^+ possédant une énergie entre 1 et 100 eV. Sous l'effet du bombardement, les fragments positifs et négatifs désorbés ont été collectés par un spectromètre de masse quadrupole.

L'ionisation et la fragmentation des bases adénine (A), guanine (G), cytosine (C) et 5-aminouracile (5-NH_2-uracile) ont été étudiées par observation de l'émission des ions positifs et négatifs pendant l'irradiation avec Ar^+ de faible énergie (10 à 100eV) dans la phase condensée et d'électrons (70 eV) dans la phase gazeuse. Ces observations impliquent des mécanismes de fragmentation engendrés par des réactions de dissociation concertée telles que la désamination des bases A, G et C tant dans la phase condensée que dans la phase gazeuse, ainsi que l'amination de l'adénine dans la phase condensée. Les caractéristiques significatives relevées dans les spectres de masses des quatre bases sont la production d'ions NH_4^+ (18 amu) et CH_3^+ (15 amu) pour la cytosine et le 5-aminouracile, avec des intensités relatives élevées, par comparaison avec le pic le plus haut de chaque spectre ($HCNH^+$, 28 amu). L'utilisation d'isotopes marqués d'A, G et C a révélé les mécanismes initiateurs de clivage des liaisons chimiques, communs à toutes les bases puriques et pyrimidiques constituant l'ADN. Des expériences conduites avec du 5-aminouracile ont confirmé l'hypothèse de désamination des bases A, G et C, par l'impact des ions Ar^+ de faible énergie dans la phase condensée et d'électrons dans la phase gazeuse.

Ces résultats démontrent clairement les lésions causées par les ions lourds de faible énergie sur notre matériel génétique. Divers mécanismes physiques et chimiques seraient impliqués dans l'initiation de ces dommages, par fragmentation et ionisation des bases de l'ADN. Dans la phase gazeuse, le transfert intramoléculaire de protons pourrait contribuer à la formation d'ions ammoniums quaternaires (NH_4^+), de radicaux méthyles (CH_3^+) et d'autres fragments, à partir de la même molécule. Dans la phase condensée, les bases adjacentes pourraient partager un proton H^+ entre deux paires d'électrons. Le spectre de désorption/ionisation obtenu à partir des biofilms suggère le transfert d'énergie intra et

inter-moléculaire durant le processus de fragmentation de l'ADN, alors que l'équilibre tautomérique et les caractéristiques géométriques des nucléobases, c'est à dire leur structure moléculaire et leur géométrie dans les films, contribuent à la génération d'ions NH_4^+ et CH_3^+.

La désamination des paires de bases d'ADN survient spontanément dans la cellule avec une fréquence très faible de 200 événements par cellule et par jour. De plus, dans le génome des cellules mammaliennes, le processus de désamination est contrôlé par des enzymes appartenant à la famille des désaminases. Ce processus biochimique transforme la cytosine en uracile et provoque par conséquent le changement d'une guanine en adénine sur le brin d'ADN opposé, lors de la réplication (cette conséquence est retrouvée pour l'adénine et la guanine). À l'inverse, l'amination des bases engendre le même type de mutations ponctuelles. Nos résultats montrent pour la première fois que le phénomène de désamination de l'ADN est engendré par l'impact hyperthermique d'ions lourds.

Chapter 1. Introduction

1.1 Radiobiology

The understanding of life on a molecular level and the processes underlying its evolution presents a challenging problem in physical, chemical and biological sciences. Consequently, investigations leading to the in-depth comprehension of the fundamental aspects concerning the building blocks of life (e.g. DNA and RNA structures) and their complexities, such as dynamics and reactivity on an atomic level, and their inter- and intra-molecular properties are of immense importance in life sciences research. When ionizing radiation interacts with the cell, ionization and fragmentation of the vital constituents of the cell occurs during discrete steps of energy loss. Most significantly damage induced in DNA holds the key to the radiobiological damage in the cell. The direct biological damage induced by the passage of ionizing radiation through matter is strongly dependent on the energy density of deposition events and on the excited and ionized species. Interactions where radicals (e.g. water radiolysis products such as $^{\cdot}OH$, $H^{\cdot}$, and e_{aq}^{-}) and secondary particles chemically attack DNA are categorised as indirect radiobiological damage. Ions are of primary significance in this context both as high energy primary ions, i.e. low energy track-end primary ions, and low energy secondary ions which can also interact with DNA components in the cell.

1.2 Some Applications of Radiobiology

Numerous fundamental applications have stemmed from radiation biology in a wide range of field of biological sciences and medicine.

1.3 Heavy Ion Therapy

One of the most widespread applications of ions in medicine is the concept of hadron therapy, which is radiation therapy using fast ion beams. Most remarkable advantages of this type of therapy compared to conventional radiation therapy techniques, such as photon therapy, is the better control of the beam during therapy, improved dose conformation to the tumour cells, and better sparing of the healthy tissue surrounding the target. The C^{6+} ion radiotherapy for instance, has been recognized as an effective treatment for skull based chordomas (Schulz-Ertner *et al*, 2007) and prostate cancer (Nikoghosyan *et al,* 2004). As charged particles traverse the tissue, they slow down, loosing energy as they interact with atomic electrons in the medium. These atomic interactions reduce the energy of the particles which results in increased energy loss, reaching a maximum at the end of the ion range (Bragg peak, Figure 1). As the ions slow down, the ionization sharply amplifies. This amplification is approximately eight times for the lower energy particles and yet more than three times for the high energy (Stelzer, 1998). The ratio of Bragg peak dose versus dose in the entrance region is larger for heavy ions than for protons. Since ions have larger mass, angular and energy straggling is negligible compared to protons. As a result, heavy ions provide highly improved dose conformation compared to protons and photon radiation therapy as well as improve the

tissue sparing around the tumour. Thus using proton and heavy ion therapy, better outcomes can be achieved for solid, deep seated tumours without increasing the risk of side effects. Light ions such as lithium (^{7}Li) or beryllium (^{9}Be) have been introduced recently as an even better treatment option since they induce less conclusive biological effects to normal tissue (Brahme, 2004). Helium ions are very similar to protons in terms of their biological effectiveness, however carbon (^{12}C) or argon (^{40}Ar) ions exhibit an enhanced relative biological effectiveness * (RBE) in the Bragg peak as compared to the entrance region, where a decrease in RBE is observed due to fragmentation. Nuclear fragmentation processes result in fragment tail observed in the dept dose distribution that extends beyond the Bragg peak (Figure 1).

* Relative Biological Effectiveness (RBE) is defined as the ratio of absorbed dose of a reference beam of photons to the absorbed dose of any other particle (most significantly high LET radiation) to produce the same biological effect (ICRU 1979).RBE is calculated using the following equation:

$$RBE = D_X / D_T$$

Where D_X is the dose of a standard low linear energy transfer (LET) X-ray beam and D_T is the dose of the test radiation type required to induce the same biological level of effect (IAEA 2008).

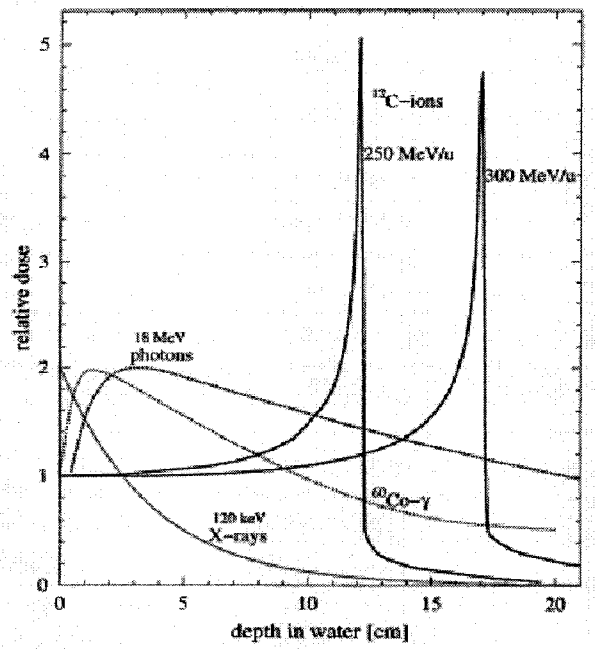

Figure 1. The Bragg curve: Dose distribution comparison: photon and heavy ions (Kraft, 2002).

It is generally believed that the essential difference between high Linear Energy Transfer (LET) and low LET radiations is the local density of the ionization events along the ionization track of the primary particle. However studies with high energy ions have demonstrated that abundant singly and multiply charged secondary cations with energies ranging from few tens of eV up to few hundreds of eV are produced upon high energy, heavy primary projectile impact on biomolecules such as thymine and uracil (Schlathölter *et al,* 2004). Besides the important effect of cell killing, there are other radiobiological effects which make heavier ions superior for therapy purposes. For instance, for low LET radiation, cell survival heavily relies on the oxygen content of the cell which is due to production of oxygen radicals in the cell upon irradiation. Consequently, solid tumours with hypoxic areas therefore exhibit strong resistance low LET radiation. On the contrary,

for high LET radiation, presence of oxygen in the cells has a minor role hence these particles are particularly efficient in treatment of radio-resistant tumours.

Heavy ion therapy centers have increased in number worldwide today. Heavy ions demonstrated distinctive advantages compared to types of other ionizing radiations in radiation therapy, most remarkably, the energy deposition of heavy ions increases with the penetration depth and peaks just before they stop (Bragg peak). Moreover heavy ion beams exhibit a much smaller lateral scattering and their range can be adjusted by tuning the beam energy (Kraft *et al*, 1999; Kraft 2002). The tail of dose behind Bragg peak is induced by lighter fragments, which have a longer range compared to the primary particles.

It is an accepted fact that DNA in the cell is the main target for ionizing radiation damage to the cell (McMilan *et al*, 1997) specifically for highly charged energetic (HZE) particles such as heavy ions which produce high density ionization track. Based on Watson and Crick's classic proposal for the structure of DNA, deoxyribonucleic acid, consists of two polynucleotide strands, running in opposite directions and coiled around each other in a double helix (Watson and Crick, 1953). There are four different heterocyclic bases in deoxyribonucleotides. Two are substituted purines (adenine and guanine) and two are substituted pyrimidines cytosine and thymine. Adenine, guanine and cytosine also occur in RNA, but thymine is replaced in RNA by a different pyrimidine base called uracil. Figure 2 illustrates the molecular structure DNA nucleobases adenine, guanine, cytosine RNA base uracil and modified base 5-aminouracil where an amino group is attached to C5 position of uracil molecule. The asterisks in this figure shows the atomic sites which are ^{13}C and ^{15}N isotope labelled.

The most lethal damages induced on DNA of the cell is due to a combination of direct and indirect effects and may be classified as Single Strand Break (SSB) and Double Strand Break (DSB) and clustered lesions. Radiolysis of the water molecules surrounding the DNA molecule in the cell accounts for the majority of damage induced by the indirect effects. The free radicals induced as a result of water radiolysis damage the DNA nucleobases and sugars by producing SSBs and loss of nucleobases as well as modified DNA bases.

DSBs are induced by direct and indirect effects of ionization of the cellular DNA and are fewer in numbers in comparison to SSBs. Nonetheless, despite their lower frequency, clustered DSBs are believed to be the primary responsible element in cellular death (Elkind, 1985).

In living cells, SSBs have a higher probability of being repaired compared to DSBs. If accompanied in large numbers and close vicinity on the strand, multiple ionization events are even more difficult to repair for the cell (Sutherland *et al*, 2000; Ward, 1981, 1988, 1994). Several studies on plasmid DNA have demonstrated induction of SSBs and DSBs by keV Ar^+ and C^+ ions (Lacombe *et al*, 2004; Hunniford *et al*, 2007). Moreover previous investigations at our laboratory have demonstrated that even low energy (1-100 eV) heavy Ar^+ ions are capable of producing SSB and DSB in plasmid DNA samples irradiated in vacuo (Sellami *et al,* 2007). The number and 3D distribution of DSBs induced by a given dose are important quantities which are to be studied in order to understand the mechanism of mutations, cellular repair and programmed cell death (apoptosis).

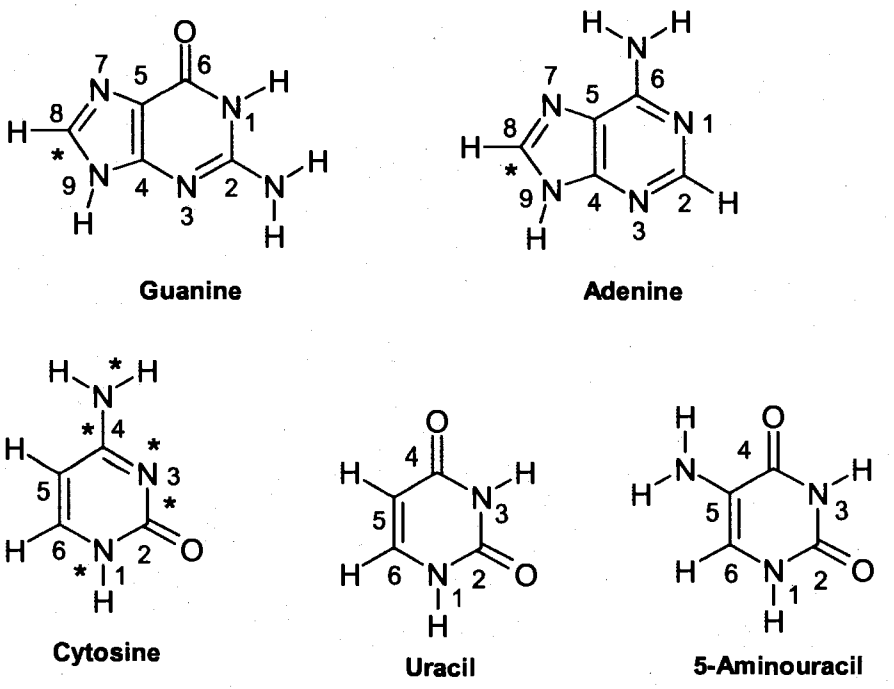

Figure 2. The Molecular Structure of Adenine ($C_5N_5H_5$), Guanine ($C_5N_5OH_4$), Cytosine ($C_4N_3OH_5$), Uracil ($C_4N_2O_2H_4$) and 5-Aminouracil ($C_4N_3O_2H_5$), the asterisk shows the atomic sites which were ^{13}C and ^{15}N isotope labeled. .

1.4 Environmental Background & Space Radiation

Radiation is found in natural environments. In space environments, alpha particles, hadrons and other types of heavy particles are of potential hazard to human space missions (Townsend *et al,* 1994; Cucinotta *et al,* 1994). Health effects induced by space radiation are of growing concern due to rapid advancement of space stations and Mars mission program which require longer astronaut exposure to space particles. The main contributing factors to the dose received during a space flight outside the Earth's geomagnetic field's protection stems from galactic cosmic rays (GCR) and solar particle

events (SPE) which both create the most significant hazard to space crew in interplanetary orbits. Protons contribute to approximately 87% of the galactic cosmic ray (Shapiro *et al*, 1983) and provide the largest role in the dose equivalent generated by the high flux of high energy (up to several GeV/amu), charged space particles encountered during the severe solar flares.

Health risks from radiation exposure may arise as acute effects and long term effects. Short term effects range from damage to the central nervous system or even death. Long term risks include and increase in probability of developing cancer. Biological experiments performed by NASA have demonstrated that the damage induced in the central nervous system (CNS) which is unique to high energy heavy ions encountered in the space is similar to that associated with aging. And this type of radiation is more effective in inducing damage which may ultimately lead to mutations and cancer in the tissue than the conventional gamma ray or x-ray commonly encountered on Earth. Inhaled radon and its decay products emit energetic alpha particles (He^{2+}) which pose significant damage potential to lung tissue (Burkart *et al*, 1997, Yamada, 2003).

At low doses (and low LET) which biological systems receive as background radiation on daily bases, cells can repair the damage rapidly. However at high doses (or high LET), cells may not be able to repair the extended, multiple damaged sites induced and they may change permanently or proceed to cell death.

1.5 Astrochemistry

Cosmic rays are composed of a spectrum of highly ionizing particles. The ionic part of cosmic ray mainly consists of α–particles and protons, a few percent is nuclei with Z< 10, and a few heavier nuclei (Figure 3) (Shapiro, 1983). The most common evidence of energetic ion impact on surfaces is indirect, from spectroscopic analysis of reflected stellar light that sometimes reveals the presence of molecules synthesized by radiation and from the observations of atmospheres of non-thermal origin around Europa and Ganymede (two satellites of Jupiter), Saturn's rings, the Moon and Mercury. Such atmospheres can be explained to result from sputtering by either magnetospheric ions or the solar wind (Sigmund, 2006). There have been connections identified with ion impact and life in response to the question that ion radiation was needed for primordial life, most remarkably the possibility of first organic complex molecules being synthesized by ion impact on icy surfaces or dust and grains in interstellar space or on comets or planetary icy surfaces.

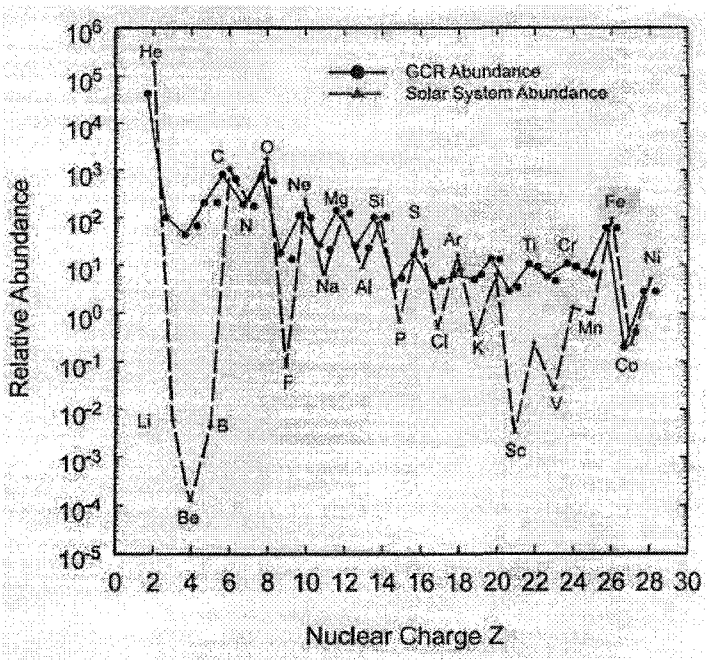

Figure 3. Relative abundances of elements from He to Ni in the Galactic Cosmic Ray (Shapiro, 1983).

1.6 Physical and Chemical mechanisms of radiation induced DNA damage

1.7 Interactions with high energy primary ions

When heavy charged particles traverse through matter, they experience various interactions with the target. At very high energies (e.g. 100 MeV and greater) electronic stopping phenomenon dominates, however at medium-high projectile energies nuclear stopping processes begin to play an important role in projectile energy loss and may lead to nuclear reactions and fragmentations. At low energies (low keV), binary collisions result in nuclear stopping via atomic scattering, displacements, recoil collisions, and

dissociations upon impact. One characteristic of highly charged, ions is the high potential (internal) energy they possess, which is the sum of their ionization potentials. Such energy is generated during ion production and remains available when these ions come in contact with neutral matter. For instance, Ar^{10+} carries a total potential of ~ 10 keV (Morgenstern *et al*, 2000). Multiply charged ions (MCI) can cause severe biological damage both as primary and secondary particles. An example of MCIs as primary quanta of radiation are α–emitters included in the human body as inhaled radon and its decay products which emit alpha particles of several MeV into the lung tissue and produce lethal damage.

Collisions of high energy ions with biomolecules fall in a regime where projectile ion velocity and typical velocities of the molecular valence electrons are roughly the same order of magnitude hence electron transfer processes lay a significant role in such collisions. Concurrently a keV ion pass through a molecule is subject to both electronic stopping and nuclear stopping. Nuclear stopping portrays the loss of projectile energy as a result of energy transfer to recoiling atoms in elastic collisions. Electronic stopping involves the electronic contributions to the slowing down of the projectile ions, e.g. electronic excitation. The interaction of different mechanisms turns into a very complex reaction dynamics for the ion-molecule interactions. In particular studies with DNA building blocks have demonstrated that DNA sugar is more sensitive to ion impact than nucleobases (Deng *et al*, 2005; Alvarado *et al*, 2006). It was also observed that at this energy range the dissociation dynamics are strongly dependent on the projectile ion's electronic structure and velocity as well as the properties of the target biomolecule. One of the most prominent effects which occur during the impact of highly charged, high

energy primary heavy ions by the strong field of these particles is Coulomb explosion. This phenomenon has been observed in uracil and thymine nucleobases by the strong field of 0.5 MeV $^{129}Xe^{25+}$ ion and results in the formation of singly and multiply charged, high kinetic energy atomic fragment ions (Schlathölter *et al*, 2004).

1.8 Interactions with low energy secondary ions

Multiply charged low energy secondary ions can be formed by various mechanisms, including Auger de-excitation after core ionization by primary particle impact. In most cases the energies of these secondary particles does not exceed a few tens of eV (Schlathölter *et al*, 2006). For fragmentation and production of cation fragments in films, the incident ion ionizes and excites a target molecule via charge transfer exchange, and further breaks the excited molecules via momentum transfer to the molecules. The former process provides the required kinetic energy for the ionic fragments to overcome an induced polarization potential and desorb from the surface. The low energy secondary ions are capable of scattering over very short ranges and hence inducing highly clustered damage in the films.

Previous studies have demonstrated severe damage induced by low energy ions on DNA and RNA components by fragmentation and ionization in the gas phase and condensed phase experiments. For instance, 10-100 eV Ar^+ ions irradiation of thymine, thymidine, and 2-deoxy-D-ribose have shown extensive damage beyond single ionization and bond cleavage (Deng *et al*, 2005). Moreover the impact of lighter atomic and diatomic ions such as N^+ and N_2^+ has shown to produce abundant negative and positive

and negative ions upon fragmentations of biomolecules such as dR, R, T and dT in the condensed phase (Deng *et al*, 2006). Studies on the RNA and DNA backbones, R and dR respectively, have demonstrated that these two molecules undergo severe decomposition upon low energy (1-100 eV) Ar^+ ion impact at kinetic energies as low as 15 eV (Bald *et al*, 2006). These results also suggest that DNA/RNA sugar moieties are vulnerable on carbon sites in particular C5 position in both molecules which link the nucleobases to phosphate groups to form DNA/RNA strand. Furthermore irradiation of (1-100 μg range) films of DNA by (100 eV) Ar^+ ions, in other words interaction of these ions with plasmid DNA, induces single and double strand breaks as well as nucleoside fragmentation involving N1-C1 glycosidic bond (Sellami *et al*, 2007). Energetic ions penetrate a solid and create secondary particles (e.g. ions and neutrals) on or below the film surface via electronic excitation and/or momentum transfer processes (Akbulut *et al*, 1997).

1.9 Interactions with low energy secondary electrons

Non-thermal secondary electrons with low kinetic energies (<100 eV) are among copious species created along the ionization track of high energy primary beam of ionizing radiation (e.g. hadron beams, x-rays, gamma rays). It has been demonstrated that such low energy electrons are capable of inducing severe DNA lesions such as SSB and DSB at energies as low as 15 eV through formations of molecular resonances involving DNA subunits (base, sugar, etc.)(Huels *et al*, 2003; Boudaïffa *et al*, 2000). At higher energies, e.g. 70 eV, used in our experiments here, electron impact results in dissociation

of the DNA strand inducing more complex strand break clusters i.e. multiple double strand breaks (MDSBs) in the DNA molecule (Huels *et al*, 2003).

1.10 Interactions with Ultraviolet photons and soft X-rays

I. Synchrotron radiation

When an electron travels at a relativistic speed along a curved path, it generates electromagnetic radiation. This light is known as synchrotron radiation (SR). The SR can have a continuous wavelength spectrum ranging from infrared to hard x-rays and is naturally emitted in a narrow cone. Moreover, SR exhibits well-defined polarization properties and is very bright. This characteristic of the beam offers high brilliance (intensity, brightness) in the vacuum ultraviolet (VUV) and x-ray regions which can not be achieved with other types of radiation sources. Furthermore SR is emitted in short pulses, having controllable time structure, and is generated in an UHV environment. SR can be used to induce excitation of specific core energy levels in specific atoms in a molecule, which often results in site-specific fragmentation. Core or site-specific fragmentation is of considerable importance in understanding localization phenomena in chemical reactions, and is also useful for synthesizing materials through selective bond dissociation. Hence monochromatized synchrotron radiation could be potentially used as an optical knife in this type of synthesis where selective bond dissociation around an atomic site is required.

In order to produce SR for research a special type of accelerator and a storage ring are utilized. In storage rings, the electrons (sometimes positrons) travel in a closed loop for hours, emitting synchrotron radiation whenever their paths are bent. To obtain SR, devices such as bending magnets, undulators and wigglers (arrays of magnets) may be inserted in the different sections of the storage ring in order to produce SR of higher intensity and variable polarization properties.

Numerous experiments have shown that unlike clinical hard X-rays or γ–rays, soft X-rays have a RBE similar to low energy electrons and some heavy particles, and hence are capable of inducing direct severe biological lesions resulting in mutations and apoptosis (cell death)(Hill, 2004; Resat *et al*, 2004; Brenner *et al* 1999). It is now well accepted experimentally and theoretically that the RBE of photons increases with decreasing photon energy (ICRU 1986; Brenner and Amols, 1989). The phenomena occurs since as the energy of photons decreases, the energy of the secondary electrons emitted as a result of photon interactions decreases, corresponding to an increase in the LET or stopping power of the secondary electrons. Low energy X-rays have been demonstrated to have an increased RBE in various biological systems (Virsik *et al*, 1977; Sasaki *et al*, 1989; Zeitz *et al*, 1977). Ultrasoft X-rays (X-rays with energies ranging from a few hundred eV up to a few thousand of eV) are lower in energy than the conventional X-rays and hence have a significantly higher RBE (Resat *et al*, 2004). This enhanced property of soft X-rays is in part due to the ability of these particles to induce core specific ionizations in DNA and RNA, which leads to resonant and non-resonant Auger cascades and violent fragmentation of these molecules (e.g. by Coulomb explosion) and hence resulting in more unrepaired damage in the cell. High energy primary heavy ions

induce a convolution of effects upon entrance to the biological medium, some of which are similar to soft X-rays (e.g. Coulomb explosions induced by core specific excitation/ionization of the atoms in the target biomolecule).

For primary high energy ions, in the Bragg-Peak region (As illustrated in Figure 1) the ions are slowed down to MeV, keV energies and below. As the energy of the particles decreases along the ionization track, the LET of the ions significantly increases. The density of the ionization events is very high at this region along the particle's track, the deposited dose is maximum and the RBE value peaks at the Bragg Peak region (Kraft *et al*, 1999).

In the present study we have investigated the physical and chemical mechanism underlying the damage induced in DNA and RNA bases by low energy heavy ions. We have utilized beams of 1-100 eV Ar^+ and Xe^+ ions to study the fragmentation and bond cleavage pathways induced in condensed films of DNA bases adenine, guanine, cytosine and modified RNA bases 5-aminouracil. Different types of ions during irradiation of biological media by electron, ions, X-rays or γ–rays appear to be different in charge state and chemical reactivity, and possess different potential and kinetic energies. As in the present experiments, secondary ions and the fragments induced by these species are capable of scattering over a short distance of a few nm in the biological medium; due to the fact that the DNA double strand in the cell is ~ 2 nm wide, secondary ions with energies like the ones used here may induce complex clustered damage in cellular DNA.

Furthermore the present work includes results of low energy electron impact experiments performed in the gas phase. These experiments have been performed to obtain cracking patterns of the same nucleobases investigated in the condensed phase to

compare the electron induced damage pathways with ion induced damage in these nucleobases. Low energy electrons interact with the target molecules differently, compared to low energy ions. At low energies heavy ions induce fragmentation due to binary collisions with individual molecules, or with individual atoms in the molecules, while here low energy electrons (70 eV) mainly interact with the valences electron in the molecules, leading to ionization and fragmentation. However, Ar^+ and Xe^+ ions along with kinetic scattering effects, will also damage the molecules due to their potential energy (PE), i.e. charge transfer from the molecule to the primary ion. Therefore, in ion impact there exists a combination of effects induced by mass, charge and energy of the projectile inducing biological damage.

Hence the motivation for a subsequent series of synchrotron photon experiments presented in this thesis, was to isolate the individual effect of ionization (i.e. electron removal) from the convolution of the above effects induced upon low energy heavy ion irradiation of biomolecules. Synchrotron photons carry no charge and possess virtually zero mass, hence making specific excitation and ionization of various electrons in the biomolecules, most significantly core and valence electrons feasible. Experiments were performed with soft X-rays to look at the degradation (damage) induced in films of DNA bases (Adenine) in the condensed phase. Also in cells, soft X-rays have a RBE close to that of low energy ions, hence a second motivation of these SR experiments is to study core excitation/ionization of specific atoms in biomolecular films that result in their severe degradation.

Finally experiments were performed with VUV synchrotron photons on DNA/RNA sugars in the gas phase, to investigate fragmentation of these molecules at different

photon energies, in particular threshold energies. This study focused on valence ionization of the electrons in D-Ribose and 2-deoxy-D-Ribose molecules to answer the questions on the dissociation of genetic sugars by mere removal of an electron.

Chapter 2. Experimental Apparatus

I. Condense Phase Experiments

Since biology takes place in a condensed medium, condensed phase experiments using biomolecules have been an active research area in many laboratories around the world. In ion impact experiments in the condensed phase, adjacent molecules play an undeniable role in the fate of different fragmentation pathways. In the condensed phase measurements, an incoming heavy ion can elastically scatter (no reactions occur if it recoils), extracts an electron and neutralizes. Subsequently ionization occurs following a binary collision between the projectile atom and the biomolecule. Singly charged hyperthermal ions used under conditions of our experiments cause fragmentation in the biomolecules via valence (positive) ionization, much like positive ionization induced by low energy ($E < 100$ eV) electrons or VUV photons.

II. Gas Phase Experiments

One motivation to study individual biomolecules in the gas phase, under defined conditions is the need to distinguish between intrinsic and externally imposed properties of these molecules. In particular, the differences measured between gas and condensed phase behaviour may assist identifying the environmental influence on the building blocks of life. Chemical and physico-chemical properties of bases can best be investigated by comparing the results of different experiments. Such properties include ionization energies, electron affinities, proton affinities, electronic structure.

2.1 Ion Beam Experiment

Our condensed phase experiments are carried out with the ion beam system at the Ion Reaction Laboratory in Sherbrooke, Canada (Figure 4). The apparatus is developed in-house, and is discussed in detail elsewhere (M.Imhoff, Ph.D. Thesis 2005, Université de Sherbrooke; Deng *et al* 2005; Deng *et al* 2006; Imhoff *et al*; 2008 in preparation; Bald *et al* 2006; Imhoff *et al* 2005), it consists of a low energy ion source, delivering a mass and energy selected ion beam in the 1-500 eV energy range into a UHV (10^{-9} Torr) reaction chamber for biomolecular film irradiation. The ions are extracted from the source chamber, accelerated and focused by lens system and guided into a 90° magnetic mass analyzer. The mass and energy selected ion beam is then refocused and directed by a second set of lenses to the surface of the target. The ion beam energy is measured by determining the electrical potential difference between the source and the target, and ranges between 1-500 eV at a current of 20-200 nA, depending on the type of ion formed. Preceding each experiment, the beam current is optimized using a Faraday cup.

To produce biomolecular films, an oven is located ~1 cm form the Pt substrate during the evaporation period, allowing the evaporating molecules to condense uniformly on the substrate.

The quadrupole mass spectrometer (QMS) is used to measure desorbing positive and negative ionic fragments with *in vacuo* energies between 0-5 eV during primary ion impact. The QMS is installed perpendicular to the axis of the ion beam and monitors the induced ionic fragments at an angle of 30° with respect to the target surface normal. The mass spectrometer is utilized in two different modes: using the ion count mode, the

incident ion energy is kept at a fixed value while the yield of the ionic fragments is monitored as a function of their mass. On the other hand appearance energy threshold of specific ionic fragments is determined as their intensity is monitored as a function of the incident projectile energy.

Films of DNA purine bases Adenine and Guanine, DNA Pyrimidine base Cytosine and modified RNA bases 5-aminouracil were prepared by evaporation of samples from an oven *in vacuo*. The 5-aminouracil film thickness (800 ng.cm^{-2}) and the Adenine, Guanine, Cytosine film thickness (200 ng. cm^{-2}) were determined by knowing the evaporation and condensation rates using the Quartz Crystal Microbalance (QCMB) earlier in the experiments. The use of thick films in these experiments guarantees that and ion-molecule interaction occurs between the incident ion and the intact nucleobase molecules. The sample evaporation temperatures were kept carefully at ~150-180 °C for all four molecules investigated, well below the decomposition temperature of Adenine, Guanine, Cytosine and 5-aminouracil (>300 °C).

To investigate the mechanisms and energies of ion fragmentation reactions, methods such as isotopic labelling and ionization and appearance energy measurements are used. The purpose of isotope labelling experiments is to locate the center of each reaction as well as the atoms involved in that reaction. In our experiments 2,4-^{13}C and 1,3,5-^{15}N Cytosine, 8-^{13}C Adenine, and 8-^{13}C Guanine molecules were used for the chemical identification of fragmentation pattern of Cytosine, Adenine and Guanine during both ion irradiation in the condensed phase, and electron impact in the gas phase. Comprehensive details of the experimental methods for each experiment can be found in the papers presented in Chapter III of the present thesis.

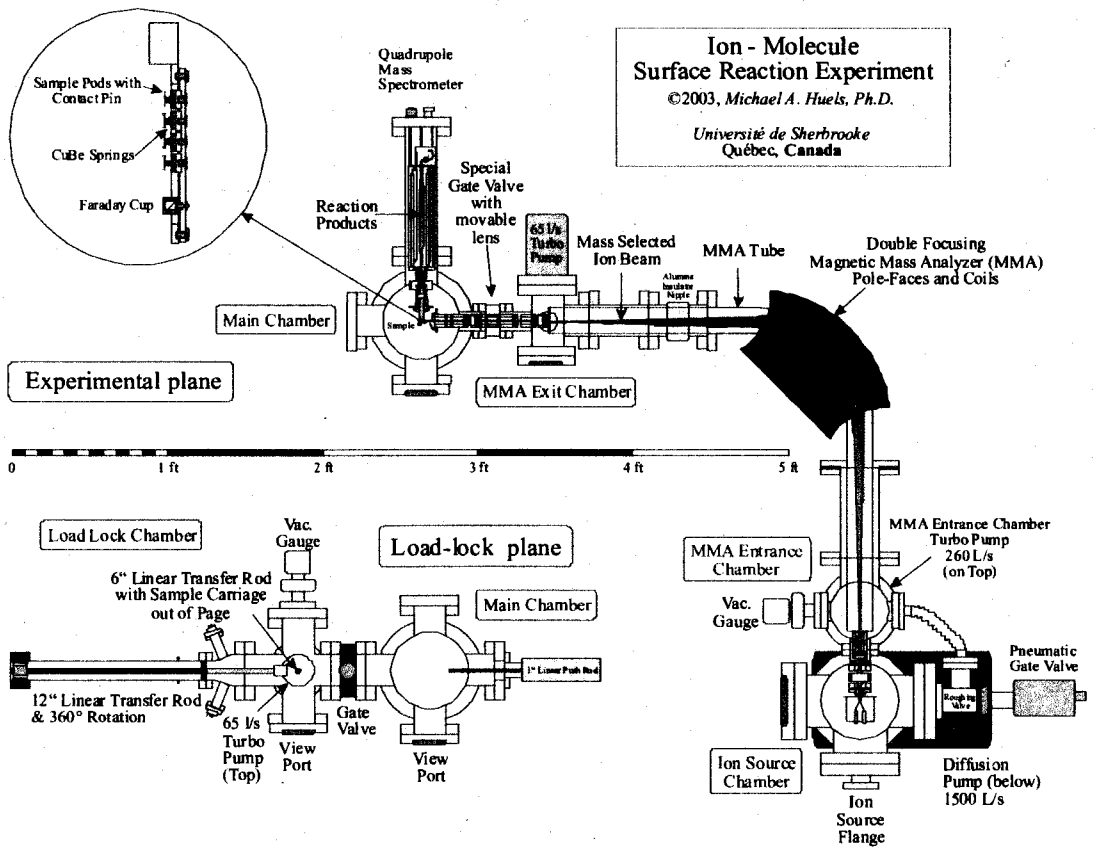

Figure 4. Schematic of the Ion Beam System at the Ion Reaction Laboratory, Sherbrooke, Canada (Imhoff *et al*, 2008).

I. Electron impact experiments in the gas phase

The gas phase experiments are a powerful tool to look at the cracking pattern of biomolecules. In electron impact experiments in the gas phase, the interaction of an electron with the electrons in the molecule is investigated. This interaction may result in the dissociative ionization of the molecule.

The electron impact set up consists of a co-axial, low profile ionizer installed between the quadrupole mass filter and the entrance ion optics of the QMS. The QMS is then used in the residual gas analyzer (RGA) mode in order to ionize and fragment neutral gas phase molecules. The results of electron impact measurements in the gas phase presented here are all taken in this mode with the electron impact energy set at 70 eV. A relatively large amount each base molecule (~ 800-1000 $ng.cm^{-2}$) is deposited on the Pt substrate and is subsequently placed in front of the QMS entrance. Afterwards, the base molecules are gently evaporated from the substrate into the QMS, by heating the substrate to 200-250 °C and subjected to electron impact in the QMS ionizer. A background spectrum of the gas present in the reaction chamber (at 10^{-9} Torr background pressure), is taken immediately prior to the sample evaporation and is subtracted from the nucleobase electron impact mass spectra presented here.

2.2 Synchrotron Experiments

Max II is a third generation light source with 1.5 GeV electron beam located in Max-Lab, Lund, Sweden. Third generation storage rings generally are specialized either in hard x-rays or soft-x-rays (sometimes called ultrasoft X-rays) of 50-1500 energy range. Max II utilizes additional superconducting wigglers in the storage ring, extending the spectral coverage to higher photon energies without sacrificing the performance at lower photon energies.

Max-I utilizes 1.5 GeV electron energy to generate low energy vacuum ultraviolet (VUV) photons of 5-30 eV energies. Use of synchrotron radiation is particularly important for the gas phase experiments where the sample densities are particularly low. Ion mass spectroscopy was used together with synchrotron radiation to study the dissociation channels of biologically relevant molecules during valence ionization. Thresholds for various molecular fragments were measured with SR and the fragment identification was performed using isotope labelled compounds with carbon atoms at different sites replace with ^{13}C, and hydrogen atom being replaced by deuterium.

2.3 Valence and inner shell ionizations/Excitations

I. Excitation

Ultrasoft x-rays ($E_{photon} < 1500$ eV) are used to excite electrons from the core orbitals of specific atoms (e.g. N, C, O) in particular molecules. The impact of a photon with energies just below the ionization edge energy (e.g. 285 eV for C(1s) K-Shell edge) induces excitation in the core electron of the specific atom in the molecule. As a result of the excitation, Auger decay of an electron or electron capture followed by fluorescent photon emission can occurs leading to ionization and dissociation of molecules. Valence excitations may lead to autoionization/dissociation (where the states subsequently decay to positive fragments) and neutral dissociation.

II. Ionization

Arriving at the edge energy of an electronic core shell (e.g. K-Shell or L-Shell), the incoming photon can directly ionize the core electron, i.e. eject a photoelectron to infinity (photoelectric effect). The binding energy ($E_{binding}$) of the emitted photoelectron is calculated using the Ernest Rutherford equation (1914):

$$E_{binding} = E_{photon} - E_{kinetic} - \Phi$$

Where E kinetic is the kinetic energy of the emitted photoelectron and Φ represents the work function of the detector. At low photon energies the photoelectric effect (PE) leads to (dissociative) ionization of molecular valence shells which also allows us to measure the lowest ionization threshold.

2.4 Techniques used

NEXAFS. (Near Edge X-ray Absorption Fine Structure) is an electron spectroscopy technique which provides information on the specific nature of the chemical bonds and is particularly useful for measurements involving chemical bond angles, bond lengths and the presence of adsorbates. The technique employs the fundamental phenomenon of absorption of an x-ray by a core level of an atom in the solid and the subsequent excitation/ionization of the core electron. The resulting core hole then is filled via electron capture from another shell followed by emission of a fluorescent photon or via Auger decay. Core excitation involves the excitation of deeply bound electronic shells (i.e. K- or –L shells) corresponding to the excitation of electrons in 1s-, 2s-, and 2p-orbitals. A core hole is a spatially well-defined charge vacancy with a very short (1-10 fs

in low Z atoms) lifetime. The excitation of core levels of an atom requires considerably higher photon energies than the energies needed to excite electrons in the outer shells. As a result photon excitation in the soft or hard X-ray regime or inelastic collisions with high kinetic energy electrons are requite in order to achieve core excitation. The binding energies of core electrons in an atom appear to be element-specific (Jolly *et al*, 1984). Slight changes may occur in excitation energies due to the local surrounding of the excited atom, which may in turn alter the properties of the initial and final states (Stöhr,1992). Core excitations very efficiently induce dissociation and desorption. Often core hole decay gives rise to doubly or even multiply (by cascade) excited valence states which are well localized and , if a hole in bonding valence state is encountered, strongly anti-bonding.

Synchrotron radiation has a natural polarization which can be used for surface studies with NEXAFS. Chemisorbed/Physisorbed molecules possess anti-bonding sigma (σ^*) and pi (π^*) bonds with particular orientations on the surface of the sample to be studied. Being and angle dependent phenomenon, SR x-ray absorption detects the orientation of the resonant bonds due to dipole selection rules. The structure of organic molecules at interfaces has been studied by means of Synchrotron X-ray scattering. Utilizing the chemical shift in chemically non-equivalent atoms or the difference in core electron binding energies we can selectively create core holes in individual atoms within a molecule by tuning the photon energy. Thus, here we measure NEXAFS spectra by detecting the Auger electron yields (measured by an electron spectrometer) which is emitted from the films as we scan the SR photon energy across a specific core edge energy, e.g. C(1s), N(1s), or O(1s).

XPS. (X-ray Photoelectron Spectroscopy) is an electron spectroscopy method often utilized to perform quantitative analysis of the elemental composition of electronic state of specific elements on surfaces of thin coverage. Ionization of the core electrons of particular elements of the molecules results in ejection of these electrons from the surface of the material. The kinetic energy and the yield of these emitted electrons give rise to an XPS spectrum. Form the photoelectric equation, the binding energy of the detected electrons is calculated by measuring their kinetic energies.

2.5 The Soft X-ray Absorption Spectroscopy at Beam line I511

Beam line (BL) I511 is an undulator based soft X-ray beam line (Figure 5) for XPS and NEXAFS, an analytical method that allows the study of chemical composition of molecular films. Yet NEXAFS is a bulk sensitive method which provides information on the site-specific nature of the chemical bonds in a molecule while XPS is a surface grazing method and allows analysis of the chemical composition of the atoms in the molecular films. Because of the availability of monochromatized synchrotron beam with high photon flux BL I511 is regularly used for surface analysis studies. The 511 beam line uses an undulator and, a Monochromator to produce monochromatic SR. The end station is equipped with an electron energy analyzers for XPS and NEXAFS on clean and adsorbate covered surfaces under UHV. The photon energy ranges from 50 to 1500 eV and the photon flux on sample is ~ 10^{11} -10^{13} ph.s^{-1}.

The electron energy analyzer (spectrometer) is combined with monochromatic arrangements in order to sharpen out the excitation energy distribution and/or to filter out

the satellite transitions in the excitation spectrum. Central to the beam line is a modified SX-700 monochromator with a 1220 $I.mm^{-1}$ grating which covers the 50-1500 eV SR range and delivers a photon energy resolution of 3 meV. Both the XPS and NEXAFS methods were utilized here to investigate solid surfaces of DNA bases e.g. Adenine.

In our experiments at BL I511, thin films of adenine were investigated. Molecular films (10-20 nm thickness) of adenine in UHV were evaporated *in vacuo* to a Si (100) substrate (Figure 6) held at room temperature using a custom made calibrated molecular evaporator (oven) identical to the one used for ion studies. Adenine films were prepared by evaporation at room temperature from this oven at ca. 110-150°C, well below the decomposition temperature of the molecule (~350°C).

Adenine sample was purchased form Sigma-Aldrich with a stated purity of 99% and was subsequently loaded in the miniature oven. The evaporation rates were measured using a QCMB. Upon evaporation, adenine molecules were adsorbed (physisorbed) on Si (100) wafers (CrysTec) (Figure 6) located as substrate in the load-lock chamber and then mounted on the transfer rod which carries the substrate into the main chamber. During the experiments the silicon substrate was frequently electrically heated to 1000°C in order to clean the surface from residual materials and oxides before preparation of new films. The cleanness of the substrate was also checked and monitored by running XPS spectra at the C, N and O (1s) edges and Si (2p) spectral line shape for residual oxide formation. Adenine films were prepared with an estimated thickness of 10-20 nm.

NEXAFS and time resolved XPS spectra were first taken on the unirradiated Films of adenine. The films were then irradiated by monochromatic SR in pure form and NEXAFS and XPS spectra at carbon C(1s) and nitrogen N(1s) edge energies were

performed. The first aim of this study was to investigate (a) the morphology of adenine films by taking NEXAFS spectra for C (1s) and N (1s) edges of films of adenine at different orientations relative to the SR polarization vector (Electric field vector) , and (b) the degradation of DNA bases in the condensed phase.

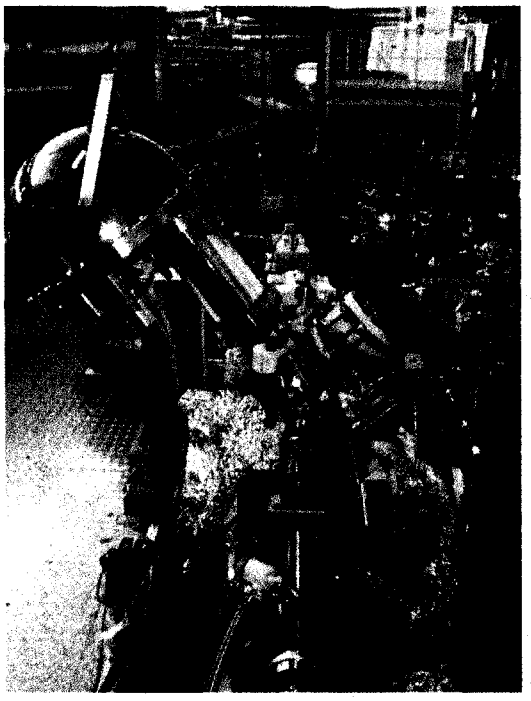

Figure 5. Beam line I511 at Max-Lab, Lund, Sweden.

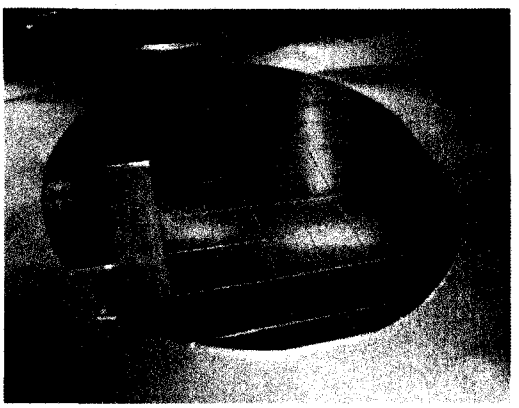

Figure 6. Silicon Si(100) wafer substrate.

The experimental set up for these measurements consists of an X-ray light source, a UHV stainless steel chamber with UHV pumps, a Scienta (R4000) electron energy analyzer (Mårtensson *et al*, 1994) able to rotate around the incoming beam axis (Figure 5) with an energy resolution of 60 meV for N K-edge and 40 meV for C K-edge for analyzing photoelectrons in XPS, and 2 eV for measuring partial Auger electron yields in NEXAFS. The Scienta is utilized for X-ray photoelectron spectroscopy of the sample where the energy of the electron is analyzed.

2.6 VUV Photochemistry of DNA & RNA sugars at Beam line 52

Studies on VUV photophysics and photochemistry of biomolecules such as DNA and RNA is of immense importance from an exobiological point of view because of the possible transport of these building blocks of life from space to the early Earth, and the remarkable role that they may have played in the development and origin of life on this planet, and possibly on other planets. Here we have performed experiments and recorded the cracking pattern of DNA and RNA sugar. Both molecules dissociate yielding various

fragments by mechanisms of ionization, fragmentation and concerted bond rearrangement with nuclear motion (atom scrambling) during dissociation.

Beam line (BL) 52 at Max-Lab utilises a normal incidence (1m NIM with 1200 l/mm grating) Monochromator, operating with a photon beam of 5-30 eV energy range, a bending magnet source, spherical mirrors forming pre-focusing optics, and a photon flux of ~10^{10} ph.s^{-1}. A Wiley-McLaren (Wiley and McLaren, 1955) type ion Time of Flight (TOF) mass spectrometer (Kukk *et al*, 2007) was used in a cross-beam configuration to investigate photofragmentation of, 2-deoxy-D-Ribose and D-Ribose (Figure 7), by means of photoionization mass spectroscopy (PIMS). Perpendicular to the synchrotron beam plane and to the TOF (Figure 8) is the source region consisting of a miniature oven to evaporate the sample into the gas phase and close to the source a liquid nitrogen cooling system is placed to protect the target chamber from extra condensation from the vaporized sugar compound. Absorption of VUV photons may induce various significant photo-processes, such as direct ionization, autoionization (resonant excitation of an excited state beyond ionization energies with subsequent coupling to the ionization continuum releasing the ionized species), dissociative photoionization as well as ion pair formation which can occur below and beyond the first ionization energy.

In the present experiments, VUV-induced fragmentation of DNA sugar molecule, deoxyribose ($C_5H_{10}O_4$), and RNA sugar molecule, d-Ribose ($C_5H_{10}O_5$), is investigated at various photon energies (5-30 eV). The molecular structure of the two sugar molecules is given in Figure 7. In the gas phase the pyranose from dominates.

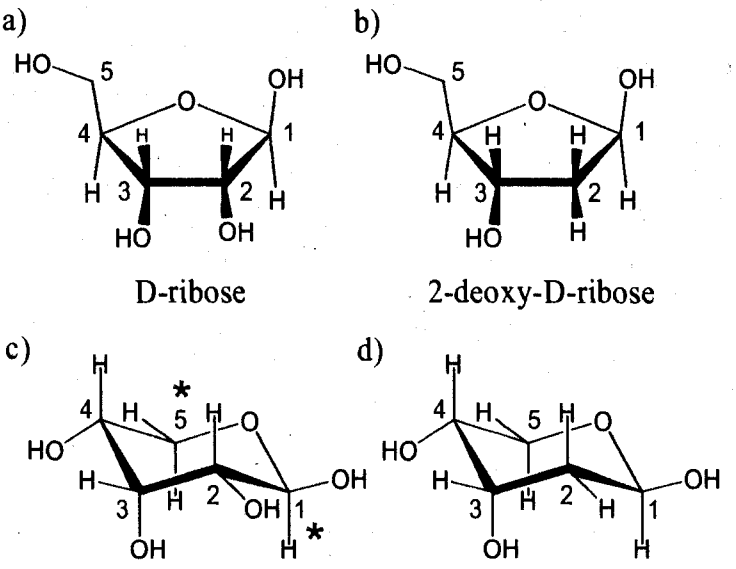

Figure 7. The Molecular Structure of 2-deoxy-D-ribose ($C_5O_4H_{10}$), and D-ribose ($C_5O_5H_{10}$) in the furanose (a and b) and pyranose forms (c and d) (Guler *et al*, 2002). These two molecules link via the furanose form to phosphate groups (*via* C3 and C5) to form the backbone of the RNA or DNA chain and provides the linkage (*via* C1) between the backbone and the nucleobases.

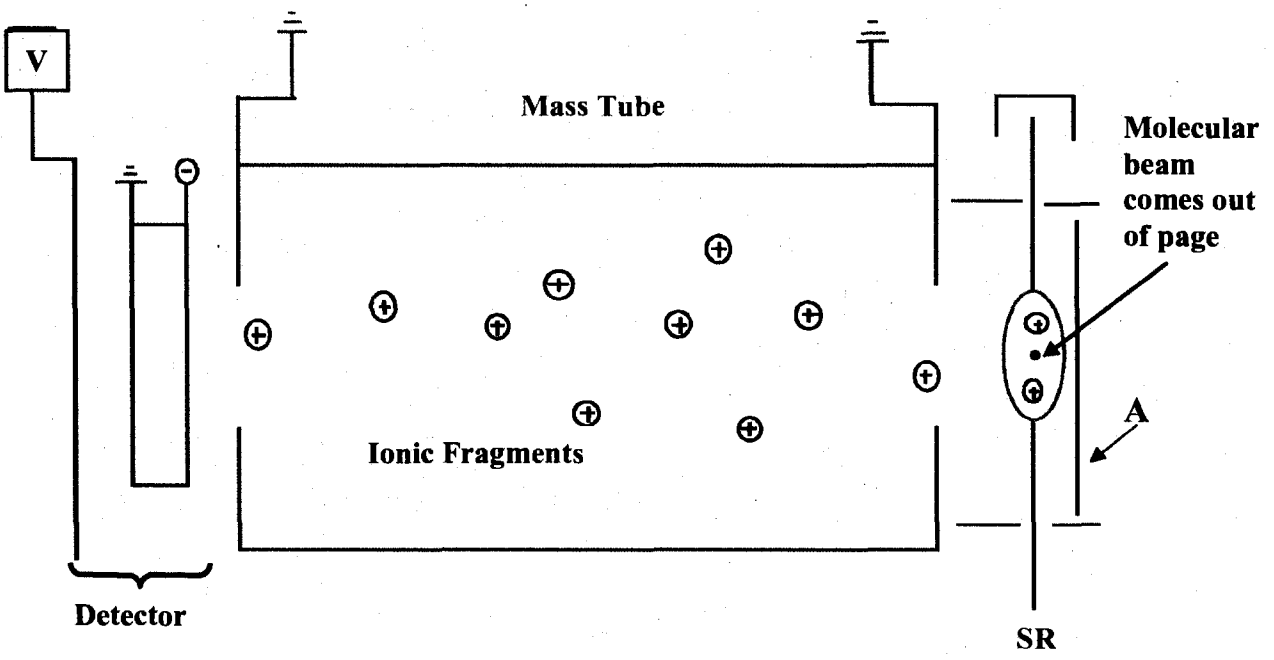

Figure 8. The working principle of a linear time of flight mass spectrometer (ultra high vacuum). In the typical vacuum inside a time-of-flight mass spectrometer an ion can fly on average 600 metres (mean free path) before it will hit an air molecule. Plate **A** is pulsed to a few kV, the molecular beam comes out of the page perpendicular to the photon beam (SR).

Figure 9. The Beam Line 52 at Max-Lab, Lund, Sweden.

Chapter 3. Results & Discussion

3.1 Deamination of DNA bases by hyperthermal heavy ion impact,

Article submitted to (June 2008) the *Journal of American Chemical Society.*

Résumé

Les ions secondaires hyperthermiques d'énergies inférieures à une centaine d'électronvolts sont produits abondamment le long de leur trajet dans les cellules, dans lesquelles la thermalisation s'opère via des événements de perte d'énergie ultra-rapides par diffusion multiple.

Nous montrons ici que les dommages à l'ADN sur les bases azotées, induits précisément par de faibles énergies (10 à 100 eV), peuvent survenir dans la phase condensée à travers des réactions concertées sites spécifiques impliquant des transferts de proton intra et intermoléculaires ainsi que l'effet tunnel. Ces réactions aboutissent à la déamination, par formation d'ions ammonium (NH_4^+) à partir de toutes les bases azotées et le 5-amino-uracile, et à la formation d'ions CH_3^+ à partir de la cytosine et le 5-amino-uracile, exclusivement par clivage du cycle en C5 ou C6 et en C6 sur le 5-amino-uracile. L'inexistence de cette voie pour l'uracile (ou la thymine, l'adénine et la guanine) suggère que c'est la présence du groupement amino donneur d'hydrogène (ou H^+) qui détermine l'élimination directe du groupement CH_3^+ des liaisons aromatiques C=C retrouvées dans les bases pyrimidiques aminées. De plus, dans les cellules vivantes, la déamination chimiquement induite est associée aux mutations[†], et nos résultats montrent que cette

[†] Caulfield J.L; Wishnk, J.S; and Tannenbaum S.R, *Journal of Biological Chemistry*, **1998**, *273*, 12689.

déamination des bases de l'ADN est également un processus physique induit par les ions secondaires hyperthermiques générés le long de la trajectoire des ions primaires dans les cellules.

J'ai personnellement contribué à 60% de la partie expérimentale de ces travaux, 100% en ce qui concerne l'analyse des données incluant la préparation des figures, et 65% de la rédaction (de cet article).

Abstract

Hyperthermal secondary ions with energies up to a few 100 eV are produced abundantly along ion tracks in cells, where they thermalize via ultra-fast multiple-scattering energy-loss events. Here we show that damage to the amino-bases of DNA by precisely such low energy (10 – 100 eV) ions can proceed in the condensed phase via site-specific concerted reaction pathways involving intra- and inter-molecular hydrogen transfer and proton tunneling; this leads to deamination, via the formation of NH_4^+, from all of the amino-bases as well as 5-amino-uracil, and to CH_3^+ formation from cytosine and 5-amino-uracil, exclusively via ring cleavage at C5 or C6, and C6 in 5-amino-uracil. The lack of this latter channel in uracil (or thymine, adenine, and guanine) suggests that it is the presence of the H (or H^+) donating amino group that mediates the direct CH_3^+ elimination from the aromatic C=C bond sites in aminated pyrimidines. Moreover, in living cells, *chemically* induced deamination is associated with mutations[1], and our results show that along primary ion tracks in cells a process of *physically* induced deamination of DNA bases can be mediated by the hyperthermal secondary ions created along the tracks.

I have contributed to 60% of the experimental work, 100 % of the data analysis including preparation of all figures and 65 % writing of this work.

Introduction

Proton or heavy ion-beam cancer therapy has made rapid progress to become a highly successful clinical treatment method; however, an absence of the underlying fundamental knowledge of their nascent damage mechanisms continues to exist, which prevents optimization of therapy methods. A vast number of investigations in the past decade have been dedicated to the study of damage induced by high-energy (MeV and higher) heavy particle beams in cells, and in particular in the DNA molecule and its components. Ion and electron bombardment of the DNA components, e.g. nucleobases and sugars, causes significant change in the chemical structure of these molecules, and hence in the genetic code. When part of the genetic code is lost by fragmentation due to ionizing radiation, the cell loses its ability to produce the necessary proteins and particularly enzymes. Hence the study of the damage induced in the pyrimidine and purine bases of DNA is of significant importance in biology and medicine. Irradiation of cells with energetic heavy particles causes mutagenesis due to the production of abundant excited neutrals or radicals, as well as secondary electrons and ions with kinetic energies below a few 100eV[2,3,4]. For example De vries *et al.* have shown that multiply charged heavy ion collisions with nucleobases leads to multiple ionization and fragmentations and the formation of singly or multiply charged atomic ion fragments with kinetic energies ranging up to a few 100 eV[5]. Thus, understanding the nascent processes that occur between the radiation energy absorption and the much slower, diffusion limited chemical damage at much later times will allow for the exploitation and control of these processes to maximize the damage to the cancerous cells, while minimizing the damage induced in the healthy tissue. While damage to the phosphate-sugar backbone of DNA will lead to

single and double strand breaks and likely cell death, more subtle damage to the DNA bases can lead to mutations, and higher risk of carcinogenesis, for example chemically induced deamination[6,7].

Here we have focused on such damage to DNA bases induced by heavy ions with precisely those hyperthermal energies as the secondary ions produced by high energy multiply charged ion impact on DNA bases[5,8,9]. Figure 1 shows the molecular structure of the DNA bases. In DNA, purine bases hydrogen bond to pyrimidine bases, with adenine and thymine bases sharing two hydrogens, while guanine and cytosine share three hydrogens, forming the more stable CG pair than the AT pair. Here ion irradiation is used to study the secondary ion induced damage pathways in the condensed phase, which more closely resembles the DNA state impacted in the nucleosome than DNA in solution, and where adjacent molecules can participate in or mediate the damage induced by secondary particles. At the same time, we also have investigated individual biomolecules via electron impact in the gas phase due to our need to distinguish between intrinsic and extrinsic properties of a specific dissociation pathway, e.g., dissociations involving intra-molecular versus inter-molecular hydrogen/proton transfer in DNA bases. Moreover unlike heavy ions, electrons do not transmit momentum in a collision, but rather interact with the electrons in the biomolecule leading to ionizations and dissociations; this allows us to directly compare the electron induced cracking patterns of various DNA bases in the gas phase to those induced by ion impact in the solid phase, where both are measured with the same mass spectrometer and detector system.

Here we report measurements of ion induced fragmentation of DNA bases adenine, guanine and cytosine (Fig.1) in the condensed phase for 1-100 eV ion impact,

and 70 eV electron impact of the same bases in the gas phase. Our measurements show that: (1) for both electron and ion energies well below 100 eV formation of NH_4^+ from adenine, guanine and cytosine is the result of an efficient deamination mechanism (detachment of amino- group from these bases) assisted by concerted intra- and inter-molecular hydrogen transfer or proton tunneling in the films, or by similar intra-molecular processes in the gas phase. Moreover in cytosine and 5-aminouracil a concerted ring cleavage channel accompanied by hydrogen/proton transfer is observed to result in the formation of CH_3^+ almost exclusively from the C5 and C6 sites in cytosine, or C6 in 5-aminouracil. Our experiments show that there exist several previously unknown physically induced pathways of low energy heavy ion induced damage to DNA, at least one of which has been observed in chemically induced DNA cleavage reactions[6]. This latter deamination channel, can not be repaired when present in the cellular DNA. Thus our present results show that aside the obvious kinetic fragmentations, and reactive scattering damage by secondary ions, more subtle damage to the genetic code of ion irradiated DNA can be induced by the secondary ballistic ions created along heavy ion tracks.

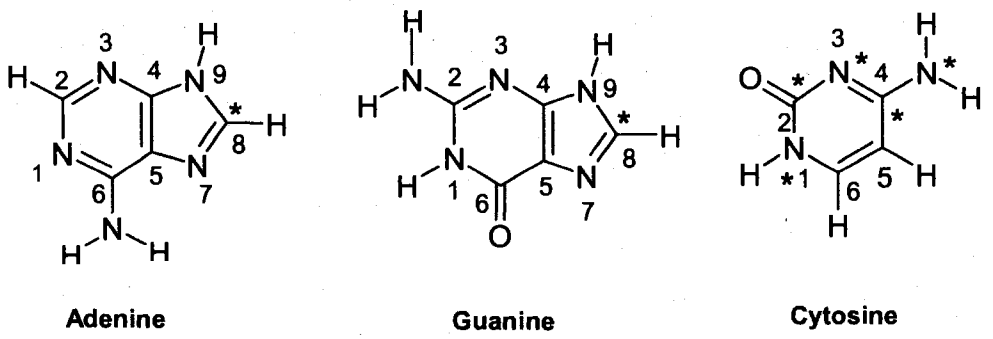

Figure 1: Molecular structures of Adenine, Guanine and Cytosine. The asterisks indicates where ^{13}C or ^{15}N isotopes were substituted in the present studies to aid in fragment identification. (color online)

Experimental Methods

The experiments were carried out on an ultra high vacuum (UHV) ion-beam system which will be described comprehensively elsewhere. Here we only give a brief description of the general experimental method. The system carries a focused, mass and energy selected positive ion beam in the 1-500 eV energy range into a UHV reaction chamber for irradiation of biomolecular sample films. The measured energy spread of the cation beams is ~ 1 eV full width at half maximum over the entire ion energy range. In the reaction chamber a quadrupole mass spectrometer (QMS) is installed perpendicularly to the ion-beam axis to monitor desorbing positive and negative ions during primary ion impact. The QMS measures desorbed ions with *in vacuo* energies between 0 and 5 eV. During the experiments the sample surface is oriented at 30° with respect to the incident ion-beam axis, and at 60° relative to the QMS.

The ion-beam apparatus[10] is loosely based on a previous design for low-energy gas phase ion scattering[11]. It consists of a low-energy ion source and beam line, biomolecular film preparation system and a reaction chamber with high-resolution mass spectrometer to monitor the desorbing ion yields. An electron-impact gas-discharge ion source (colutron type) is employed to produce positive ions which are extracted and directed by a series of focusing and deflecting lenses into a custom designed 90° magnetic mass analyzer. Subsequently the mass-selected ion beam is decelerated and focused onto a target. The full diameter of the beam at the target is 2-4 mm for ion energies between 1 to 500 eV. The base pressure in the differentially pumped vacuum system is 10^{-9} Torr. The pressure in the ion source chamber increases to near 10^{-5} Torr during the

experiments, while the pressure in the reaction chamber remains at 10^{-9} Torr with the assistance of four differential pumping stages.

Adenine, Guanine and Cytosine purchased from Aldrich (99% purity) are loaded without further purification into a miniature oven contained in a load-lock chamber, and degassed by heating for several hours near 40° C well below the evaporation onset (ca. 100° C for cytosine, ca. 150° C for adenine and guanine; these temperatures are well below their typical decomposition temperatures[12]). Multilayer films of Adenine, Guanine and Cytosine are prepared by *in vacuo* evaporation onto an electrically isolated, atomically clean polycrystalline Pt substrate, held on a manipulator at room temperature (22-25°C). The evaporation rate is calibrated in the load-lock chamber by a quartz-crystal microbalance with an active crystal area of about 0.5 cm^2 (0.8 cm diameter) positioned at 1 cm from the oven exit aperture, and the film desorption rate is characterized in 100 ng min^{-1} cm^{-2}, with an accuracy of 0.5 ng cm^{-2}. Here, given the density of the bases studied, the film thickness is estimated to be about 4 monolayers (4 ML) for a film mass of 200 ng cm^{-2}. The polycrystalline Pt substrate was cleaned by flash heating to 1000°C prior to each experiment, as determined by a thermocouple spot welded to the edge of the substrate.

As discussed elsewhere[13], for gas phase measurements, the low profile electron impact ionizer of QMS (turned off during the condensed phase ion impact measurements) was used to obtain standard electron impact cracking patterns of the unirradiated films from which the molecules where slowly evaporated into the ionizer of the QMS.

Results and Discussion

We have performed an extensive study of Ar^+ irradiation of 4 ML (200 ng cm^{-2}) films of Adenine (A), Guanine (G) and Cytosine(C). In general we find that Ar^+ irradiation of these molecules in the condensed phase yields the following major cation fragments assigned to, from low m/e (mass/charge) ratio to high m/e to NH_4^+, $HNCH^+$, $HCN_2H_2^+$, $C_2N_2H_2^+$, $C_3N_3H_3^+$, $[A\text{-}C_2N_2H_2]^+$, $[A\text{-}CHN_2]^+$, $[A\text{-}HCN]^+$, $[A\text{-}NH_2]^+$, $[A+H]^+$ for Adenine, NH_4^+, $HNCH^+$, CH_3O^+, $C_2H_3O^+$, $C_3H_3O^+$, $[G\text{-}C_3H_xO]^+$, $[G\text{-}HCN]^+$, $[G+H]^+$ for Guanine, and CH_3^+, NH_4^+, $HNCH^+$, $CN_2H_3^+$, $C_3NH_2^+$, $C_3NOH_3^+$, $C_2N_3OH^+$, $[Cyt\text{-}NH_2]^+$, $[Cyt+H]^+$ for Cytosine. The chemical fragment identification was performed by comparison of the mass spectra for isotope labeled compounds, namely Cytosine-2,4-$^{13}C_2$,$^{15}N_3$ (98+ % ^{15}N and 99% ^{13}C isotopic purity), Guanine-8-^{13}C and Adenine-8-^{13}C (all from Cambridge Isotopes), with unlabeled cytosine, guanine and adenine during both electron impact in gas phase and ion irradiation in the condensed phase. The formation of most of these fragments is mainly attributed to kinetic and potential scattering effects and will be discussed in detail elsewhere. Here we focus on the more remarkable and salient observation of NH_4^+ and CH_3^+ formation by hyperthermal ion impact in films. Since $HNCH^+$ is the common and most intense fragment for all the bases studied here, for the following discussion we compare all peak intensities relative to the 28 amu $HNCH^+$ peak in a particular molecule. Since all the measurements from the different films where obtained with the same QMS under identical mass spectrometric conditions, *ceteris paribus*, the peak ratio of a specific mass fragment (e.g. 18 amu NH_4^+) relative to the 28 amu peak for the different molecules should be independent of

transmission detection efficiency of the QMS, and thus can be compared between molecules.

Figure 2 shows the 12-19 amu mass patterns of positive fragments produced by 70 eV electron impact in gas phase (a, c, e) and 100-eV Ar^+ -ion irradiation (b, d, f) of 4 ML (200-ng/cm^2) films of Adenine (A), Guanine (G) and Cytosine(C). The close up view of the mass spectra for the three bases each depicts a rather strong peak at 18 amu assigned here to NH_4^+ fragment originating from the amino group in all three bases, as well as minor contributions from H_2O^+ from the oxygen site in cytosine and guanine, in both ion impact in condensed phase and electron impact in the gas phase experiments. The NH_4^+ fragment has not been observed in the studies of fragmentation pattern of thymine, deuterated thymine[13], uracil and bromouracil[14], , indicating that this fragment exclusively originates from an amino group in DNA amino-bases (adenine, guanine and cytosine), and not the ring nitrogens. As we will show here, the formation of NH_4^+ cation is the result of inter-molecular and intra-molecular proton/hydrogen tunneling in adenine, guanine and cytosine. In the cytosine mass spectrum the mass 15 peak is stronger than for all the other bases, and is assigned here mainly to CH_3^+; it is formed almost exclusively from the C5 and C6 positions in cytosine, as will be shown below.

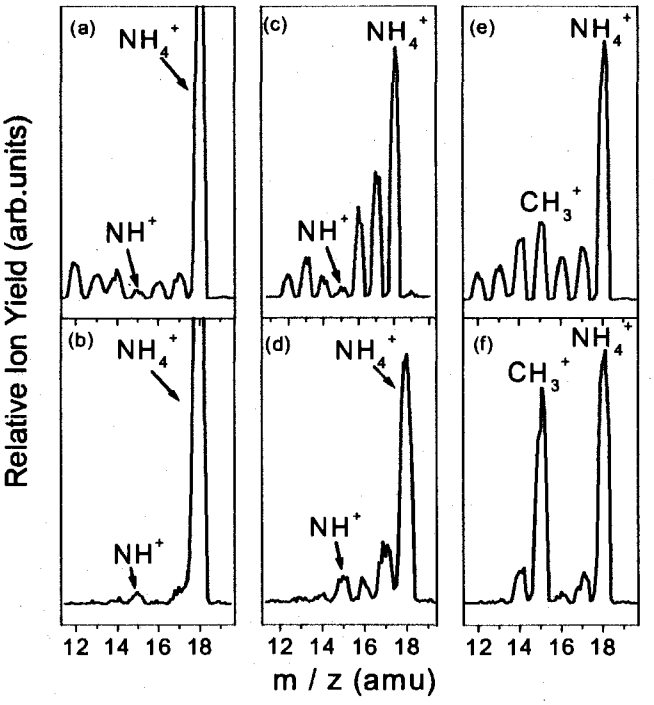

Figure 2: Cation fragmentation patterns for (a) Adenine, (c) Guanine, (e) Cytosine during 70 eV electron impact in the gas phase (blue curves – color online), and (b) Adenine, (d) Guanine, (f) Cytosine for ion stimulated desorption from ca. 4 ML (200 ng/cm^2) films during 100 eV Ar^+ irradiation (red curves – color online).

Looking more closely at the spectra for electron impact measurements, positive fragments are observed at most masses in the 12 – 19 amu range, with the 18 amu fragment having the highest relative intensity compared to the other fragments. The 16 and 17 amu fragments are observed at much higher intensities in guanine and cytosine (particularly in gas phase spectra) compared to adenine. In cytosine the hydrogen atoms (protons) available for abstraction are relatively close to the amino group, compared to guanine where the hydrogen atoms are located farther apart (Fig.1). Relative to $HNCH^+$, the fragment 18 amu has the highest relative intensity in adenine, followed by guanine and cytosine. This observation can be associated to the fact that in guanine and cytosine molecules there are other competing channels for hydrogen abstraction by dissociating

fragments, namely by the oxygen atom in guanine and cytosine, and the C5 and C6 C-H groups in cytosine. In guanine and adenine the C5 and C6 atoms are geometrically more difficult to access and form strong multiple bonds with adjacent atoms, hence are much more difficult to cleave from the molecule (Fig.1). In gas phase guanine, Fig. 2(c), peak 17 and then 16 amu has the highest relative intensity after peak 18, amu while in gas phase cytosine, Fig. 2(e), peak 15 and then 14 amu has the highest relative intensity after peak 18 amu. Similarly in the condensed phase, peak 18 amu is the major peak in the 12-19 amu range for all three molecules. In cytosine films, Fig. 2(f), peak 15 amu has much higher relative intensity compared to peak 15 amu in gas phase electron impact measurements, Fig. 2(e).

Figure 3 shows a close up of mass spectra for labeled and unlabeled cytosine in the 12-20 amu mass range from ion irradiation measurements in the condensed phase (a and b, respectively), as well as electron impact in the gas phase (c and d, respectively). Comparing the two spectra, we observe that most of the intensity of the 15 amu peak, which is mostly attributed to $^{12}CH_3^+$ cation in Fig. 3(a), does indeed <u>not</u> shift to 16 amu ($^{13}CH_3^+$ or $^{15}NH^+$) in Fig. 3(b); this suggests that (i) the 15 amu peak in <u>unlabeled</u> cytosine is <u>not</u> due to large amounts of NH^+, but is largely attributed to $^{12}CH_3^+$, and (ii) since in <u>labeled</u> cytosine the C2 and C4 positions are ^{13}C, this $^{12}CH_3^+$ necessarily originates from the C5 and C6 positions in cytosine, both labeled and unlabeled. While we note a slight increase of the 16 amu peak in the <u>labeled</u> cytosine, some of this signal may be indeed be attributed to a minor presence of $^{15}NH^+$ fragment, but it is clear that $^{14}NH^+$ contributes only negligibly to the 15 amu peak in <u>unlabeled</u> cytosine. Moreover, here the production of CH_3^+ caused by an endocyclic cleavage at C5 and C6 site is surprising, since in

previous studies performed with bases containing an exocyclic methyl group, such as thymine and partially deuterated thymine[13], the CH_3^+ fragment was not observed as intensely as here, and was shown to originate exclusively from the exocyclic methyl group.

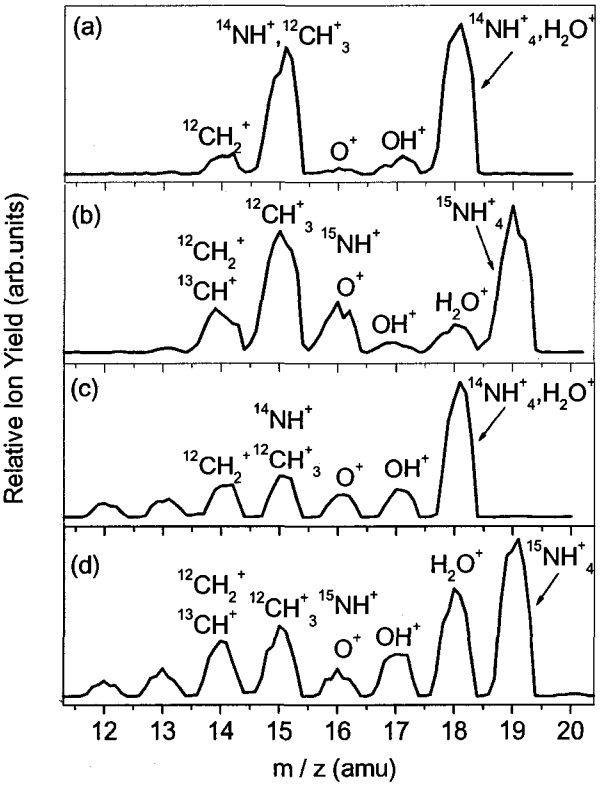

Figure 3. Mass spectra produced from 100 eV ion irradiation experiments for 4 ML films of (a) unlabeled cytosine (b) labeled cytosine, and gas phase electron impact on (c) unlabeled cytosine and (d) labeled cytosine. See figure 1 for the atomic positions in cytosine labeled with ^{13}C (C2, C4) and ^{15}N (all three N).

Looking again at the ion irradiation measurements, Figure 3(a) and (b), it can be seen that the 18 amu peak does almost completely shift to mass 19 amu, however some small signal remains at 18 amu. This suggests that the 18 amu fragment produced by ion impact in unlabeled cytosine films is predominantly $^{14}NH_4^+$, with a small contribution from

H_2O^+, while in labeled cytosine the 19 amu peak is exclusively due to $^{15}NH_4^+$. The same phenomenon can be observed in electron impact measurements in gas phase cytosine, Figures 3(c) and (d), however with the H_2O^+ fragments constituting a much more significant fraction of the mass 18 amu peak (higher intensity of peak 18 amu in labeled cytosine spectrum). The relatively high intensity of the H_2O^+ fragment in the gas phase electron impact mass spectrum of labeled cytosine (Fig. 3(d)) is believed to contain only a very minor contribution of water from the residual background gas in the baked-out UHV chamber, since here a residual gas mass spectrum has already been subtracted from the electron impact mass spectra obtained from gas phase cytosine. Thus, for electron impact on labeled gas phase cytosine, most of this 18 amu fragment is believed to originate from an oxygen atom (cation) in cytosine abstracting a hydrogen atom and/or protons from within the molecule, during its dissociation; i.e. elimination of water, which is often observed from organic molecules in electron impact mass spectrometry. Clearly, this H_2O^+ fragment can not be formed in adenine, at least not by ion impact in the adenine films, while in gas phase adenine mass spectra contributions from residual water have already been subtracted. These results show that the peak at 18 amu in adenine (Fig. 2, gas or condensed phase) is solely due to the NH_4^+ fragment, while only in the gas phase cytosine mass spectra up to fifty percent of the mass 18 amu fragment may consists of H_2O^+ originating from the oxygen atom in that molecule. In summary, the 18 amu cation fragment in the aminated bases studies here is attributed to the formation of NH_4^+ by either 70 eV electron impact in the gas phase, or ion impact in condensed films, while the strong 15 amu peak, observed exclusively in cytosine, is mainly attributed to the formation of CH_3^+ from the C5 and C6 positions exclusively.

Figure 4 shows the desorption energy thresholds of the major positive fragments in the 12-19 amu mass range as a function of the incident Ar^+ ion energy on adenine, guanine and cytosine films. Most of the cation fragments appear at energies near 15-45 eV in all three bases. In adenine, Fig. 4(a), it can be seen that the NH_4^+ fragment appears at 15eV - 20eV, while 15 amu fragments, i.e. NH^+, appear at much higher energies near 40eV. Similarly, for guanine, Fig. 4(b), the NH_4^+ threshold (20eV-25eV) is lower than that for either the 15, 16, or 17 amu fragments (approximately 30 – 40 eV), while for cytosine, Fig. 4(c), the thresholds for both CH_3^+

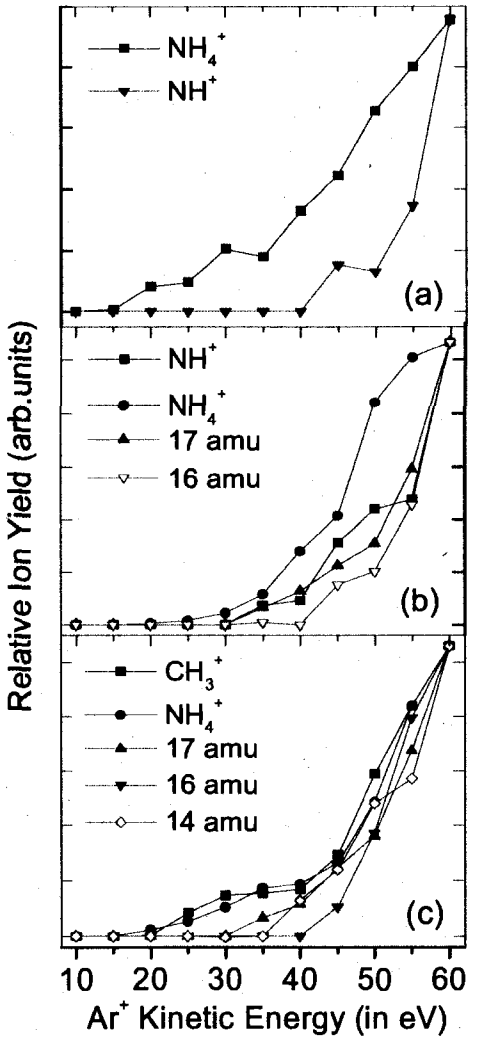

Figure 4. Deposition energy thresholds of positive fragments during Ar^+ ion irradiation of 4 ML (200 ng/cm^2) films of (a) Adenine, (b) Guanine and (c) Cytosine on a Pt substrate. All yields have been normalized in intensity at 60 eV to aid comparison; it is noted that in (a) and (b) the NH_4^+ yields are significantly larger than those of all fragments below 20 amu, while in (c) both the CH_3^+ and NH_4^+ yields greatly exceed those of the other fragments below 20 amu. This is seen in Figure 2.

and NH_4^+ are both near 20eV, while those of the 14, 16, and 17 amu fragments, *viz.* NH_3^+ / OH^+, NH_2^+ / O^+, or CH_2^+ are all at much higher energies near 30 – 40 eV.

The observation that for all condensed phase bases the ion impact threshold for NH_4^+ fragments is much lower than the threshold for NH^+ (or the other) fragments suggests that NH_4^+ is formed independently in a concerted dissociation reaction, rather

than a series of scattering events of lower mass fragments, e.g. free energetic NH^+, that "pick up" H atoms in successive scattering events from adjacent molecules in the film prior to desorption. Similarly, the low threshold for CH_3^+ from cytosine also suggests a one step concerted dissociation mechanism, rather than a secondary CH^+ fragment scattering event in the film. This is also suggested by the fact that NH_4^+ is seen very strongly from all bases, and CH_3^+ from cytosine, by electron impact in the gas phase, where H abstraction by smaller fragments from adjacent molecules obviously can not occur, and thus the formation of both NH_4^+ and CH_3^+ must involve a concerted dissociation pathway of the parent cation that involves H abstraction from within the molecule.

To interpret the chain of events which may lead to the observed fragmentation patterns in the adenine, guanine and cytosine mass spectra observed here, a number of physiochemical mechanisms are expected to be involved in the production of NH_4^+ and CH_3^+, either by electron impact in the gas phase, or ion impact in the condensed phase. These are briefly discussed below.

Formation of NH_4^+ (H_2O^+) and CH_3^+ by electron impact in gas phase adenine, guanine and cytosine.

Comparing the present fragmentation patterns of adenine, guanine and cytosine with previous studies on uracil[14] and thymine[13] bases shows that here the NH_4^+ fragment is only a fragmentation product of nucleobases containing amino groups. This observation demonstrates the fact that NH_4^+ cation originates from the NH_2 group in adenine, guanine and cytosine, and does not involve the ring N atoms, present in all DNA/RNA bases. In

the present gas phase experiments, there are two thermal procedures which occur prior to electron impact, and which may possibly influence the formation of NH_4^+ from isolated molecules during electron impact. The first process is the heating of the molecules to 100°C to evaporate and condense the sample nucleobases onto the substrate to form the film of biomolecules. Thus the first heating event may induce tautomerization to a minor extent. This tautomerization may involve movement of protons/hydrogen atoms within the molecules. The second event is the thermal heating of the substrate to 200 - 250°C (well below the decomposition temperature of cytosine ~320°C , ~337°C for adenine and guanine) in order to evaporate the condensed film into the gas phase to perform the gas phase electron impact measurements. As the molecules evaporate into the QMS in this last step, two phenomena may occur: one is the further tautomerization of the base molecules, and the second is vibrational/rotational excitations of the molecules. The increased internal energy of the molecules increases H atom movement within the molecule, i.e. will favor H abstraction by a "leaving" NH_2^+ moiety, and will also increase the dissociation cross section during electron impact.

Chemical experience shows that a hydrogen atom attached to an electronegative atom in a molecule may also be attracted to another electronegative atom in the same molecule. In the three nucleobases discussed in the present work, the electronegativity of nitrogen atoms is ~3.0 while the electronegativity of oxygen atoms is ~ 3.5, causing the proton to be shared between these two atoms. Sometimes there also exists an internal hydrogen bond between two electronegative atoms in the same molecule[15]. Here, during the second heating event, the biomolecules in the heating film, and once in the gas phase, will be vibrationally and rotationally excited, and may also form intra-molecular

tautomeric forms. The intra-molecular tautomers are formed by proton/hydrogen transfer within the individual molecules (occurs in gas phase and condensed phase), while inter-molecular tautomers, as a result of proton transfer and hydrogen abstraction processes between adjacent molecules in the heated condensed film, may occur while the film is being heated. Adenine has only keto-enol tautomerization, while cytosine and guanine can experience both keto-enol and amino-imine tautomerisation. By the time the evaporation occurs from condensed phase to gas phase, some of the H atoms from adjacent base molecules in the films may have been rearranged, and extra hydrogen atoms and protons may be accompanying a specific base molecule into the gas phase. Hence during electron impact, the amino group may already have a proton attached to it or close by, in addition to the intra-molecular transfer of protons/hydrogen atoms, which can attach to the dissociating amino group forming NH_4^+ fragment during electron impact. Similarly at the oxygen site in guanine and cytosine molecules, hydrogen atoms/protons may move during the first and the second heating events, and which may assist electron impact formation of H_2O^+ fragment in gas phase nucleobases containing oxygen. Likewise, the dissociating CH^+ moiety (from the C5 or C6 site) may abstract two hydrogens from within the molecule to form the CH_3^+ fragment. These intra-molecular proton transfer processes will be assisted by the ro-vibrationally excited geometry of the base molecule during electron impact in the gas phase.

The accessibility of hydrogen atoms to the amino group in all three bases (or the oxygen atoms in guanine and cytosine) and the probability of the amino group abstracting these mobile protons/hydrogen atoms depends on the geometry and structural properties of the DNA bases. Calculations have demonstrated that the amino-groups of adenine,

guanine and cytosine are very flexible, and intrinsically non-planar, allowing hydrogen-bond-like interactions within the molecule which are oriented out of the plane of the nucleobases[41]. Theoretical studies have demonstrated that nucleobases do not have a planar and conformationally rigid structure[16,17,18,19] and intermolecular vibrations and out of plane pyrimidine ring deformation are main sources of deviation from planarity of A-T and C-G base pairs. Two sources of intrinsic nonplanarity of isolated DNA bases have been revealed. The first one originates from a partial sp^3 hybridization of the bases' amino groups[20]. The second source of nonplanarity has a dynamic nature. Due to high flexibility of bases pairs originating from a number of intermolecular vibrations with low lying frequencies, some excited vibrational levels are populated at room temperature. Therefore at every moment of time a significant fraction of isolated DNA base pairs will possess a nonplanar geometry[15]. At the higher temperatures which the base molecules posses here during the first and second heating events, these deformations may amplify leading to higher inter/intra-molecular vibrations, and hence higher probabilities and rates of tautomerisation. Amino group nonplanarity and deformability are essential for the explanation of many base-base interactions observed in DNA crystal structure; close amino group contacts between neighboring bases may involve a large degree of nonplanarity[21]. Therefore, in the present studies the abundant production of NH_4^+ fragments from the amino group during electron impact on the gas phase bases may be assisted by (a) the presence of thermally produced amino tautomers in the film, and/or (b) enhance H atom/proton mobility within the molecules due to ro-vibrational excitation during the second heating, which will facilitate NH_4^+ production via concerted bond reactions during the electron impact ionization/dissociation process. Similar mechanisms

will be involved in the formation of minor quantities of H_2O^+ by electron impact to gas phase guanine and cytosine, or the pronounced CH_3^+ formation from cytosine, and the relative intensities between these products will be determined by the competition for concerted H abstraction/ proton tunneling between the CH/CH^+, NH_2/NH_2^+, and O/O^+ moieties that may dissociate from the ionized molecule.

An estimation of the total energy required to ionize a cytosine molecule, dissociate bonds between a specific atom and its neighbors, and/or to abstract H atoms or protons from the molecule, shows that process of formation of NH_4^+, H_2O^+ and CH_3^+ species from tautomers of cytosine favors a particular pathway. For the formation of NH_4^+ from cytosine the total energy required is ~13 eV when it involves abstraction of two hydrogen atoms by an NH_2^+ radical that dissociates from the singly ionized cytosine, i.e. after electron impact ionization creating a parent cation, the valence hole localizes on the amino group, which then abstracts two H atoms as it dissociates from the molecule, forming an NH_4^+. Alternatively, it would be less energetically favorable if the neutral NH_2 radical, during dissociation from the ionized cytosine, abstracts a proton and a hydrogen to form NH_4^+ (~18.6 eV). Similarly, formation of NH_4^+ by electron impact in gas phase adenine and guanine via concerted double hydrogen abstraction from the molecule by the "leaving" NH_2^+ is more energetically favorable. However, for H_2O^+ formation from cytosine the opposite is estimated, i.e. it seems energetically more favorable that after electron impact ionization the neutral O radical abstracts a hydrogen and proton from within the ionized cytosine during the dissociation process (~9.3 eV) compared to a "leaving" O^+ abstracting two hydrogen (~13.1 eV) from within the molecule. For guanine, likewise, intra-molecular proton abstraction by a "leaving" O is

more energetically favorable (~8.17 eV) compared to the hydrogen abstraction by O^+ (~12.2 eV). In the case of CH_3^+ formation during gas phase electron impact to cytosine, double hydrogen abstraction by a "leaving" CH^+ moiety is more favorable (~ 18.7eV) compared to ~ 23.1 eV for hydrogen plus proton abstraction by a leaving CH.

Formation of NH_4^+ (H_2O^+) and CH_3^+ by ion impact in films of adenine, guanine and cytosine.

In the present condensed phase experiments on the other hand, there is only one thermal step involved in film formation, namely the sample heating to evaporate the sample onto the substrate, which occurs at a much lower temperature, below 100 C, than when the films are evaporated into the QMS ionizer for gas phase electron impact ionization. Thus, the ion irradiated films are believed to contain significantly less *thermally* produced tautomers, than the vapor of nucleobases irradiated in the gas phase experiments. However, unlike in gas phase electron impact, in the ion irradiated films formation of NH_4^+ and CH_3^+ by H atom or proton transfer will occur via two possible mechanisms, namely intra-molecular proton/hydrogen transfer (as in the gas phase), and inter-molecular proton/hydrogen transfer processes from adjacent molecules. Proton transfers upon input of energy by irradiation goes into displacement of atoms and ionization. Proton transfer (PT) processes in condensed phase have been extensively studied by a number of groups[22,23,24,25,26,27] and single/double proton tunneling has been suggested as the predominant phenomena in many chemical and biological reactions even at room temperature[28] These events occur in solid condensed phase as well as solutions[29]. Experimental studies have confirmed a proton transfer / tautomerization rate of less than

5.0 ps in condensed phase for hydrogen bonded Watson-Crick base-pairs[29] at room temperatures.

Actually, it is likely that there are additional tautomerisation pathways in the present films upon condensation, since in the condensed phase the molecules may form H-bonded base-pair networks, assisted by sharing of H atoms/protons. During the inter-molecular proton transfer between two base molecules in the room temperature film, the heavy atoms move first to bring the two molecules closer together with the minimum distance corresponding to the saddle point, therefore decreasing the barrier for proton transfer. The activation energy of tunneling reactions does not arise from the barrier along the proton's reaction coordinate, but it comes from the reorganization energy of the medium required to approximately equalize the proton's energy in the initial and final states[30]. As a consequence in irradiation induced proton-transfer reactions, the rate is influenced by the properties of the medium which in our experiments are the solid condensed films of Adenine-Adenine, Guanine-Guanine and Cytosine-Cytosine base pairs[31]. The proton transfer events can also be assisted by the impact induced excitations of the medium (here the film), such that the ion impact induced excitation of the skeleton motion of the base molecules in our films may lead to a vibrationally enhanced proton transfer mechanism[32]. Localized excitation, i.e. by ion impact here, breaks the symmetry of the proton potential[32] as well as changes the electrostatic properties of the base molecules in the film[33]. Irradiating our films with energetic Ar^+ ions amplifies these excitations and hence increases the proton transfer rate. Figure 5 shows the type of base pairing which may occur in solid condensed films of identical base molecules.

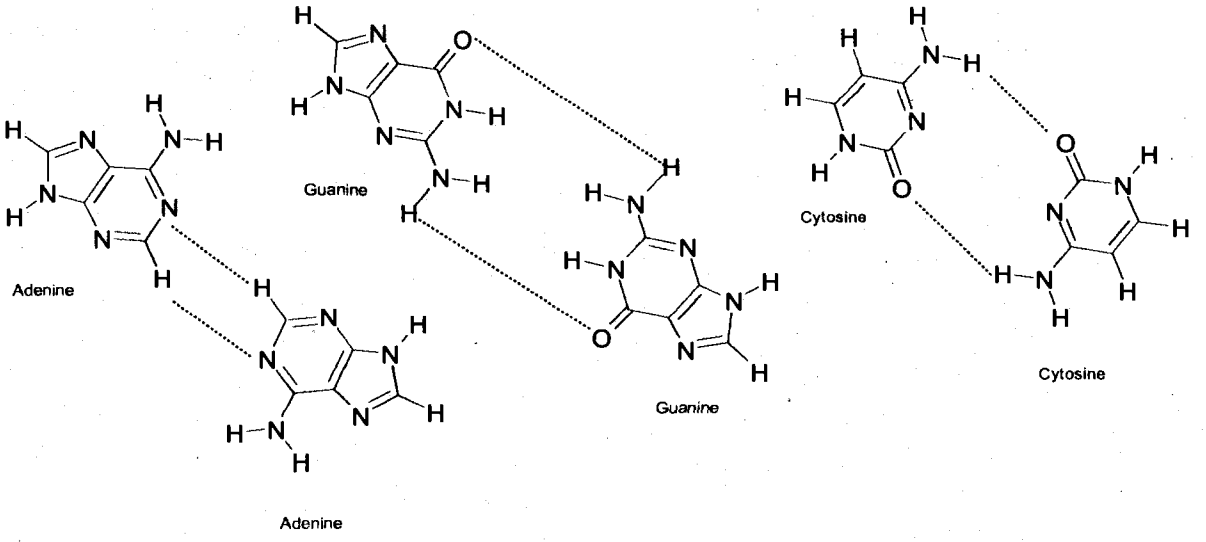

Figure 5. The bases in solid condensed films form intermolecular hydrogen bonded networks with adjacent molecules.

Complementary base pairing exists in DNA molecule and is responsible for keeping the genetic information in the DNA. Simultaneous existence of all four tautomers of Guanine has been demonstrated in gas phase[34,35]. Moreover, multiple-(double)-proton transfer reaction can occur where the bases in the base pair assist each other in proton transfer[36]. Double proton transfer reaction in DNA base pairs has been studied comprehensively and has been hypothesized as a possible source of spontaneous mutation[31,37,38]. In molecular spectroscopy, the tunnel effect is quite well known as causing the phenomenon of pre-dissociation. The tunneling time is also temperature dependent. In molecules which are damaged by irradiation or certain chemical processes, the proton tunneling may turn into a fast process. Here, once a heavy ion hits a base molecule in the present films, a single charge may be added or removed from the molecule. When one of the bases in the H-bonded base pair becomes charged, one of the two double well potentials in the hydrogen bond loses part of its symmetry and the probability for a single proton transfer via tunneling increases dramatically[31]. A tunneling frequency of 6.3×10^{11} Hz in the

vibrational ground state has been measured for hydrogen transfer in vapor phase which can be understood in terms of the intra-molecular potential surface[39]. Moreover a tunneling oscillation period of 1.6 ps has been measure for proton oscillation between symmetrically equivalent wells[39]. The process of proton tunneling has been studied in water[40], and for many compounds involving nitrogen, where the tunneling frequencies have been found to be of the order 10^{11} sec[39].

Moreover, in DNA the bases are associated to each other not only by hydrogen bonding but also base stacking (π stacking) which contributes to the stability of the DNA double helix[21]. The π-stacked bases are stabilized by dispersion attraction and the mutual orientation of the stacked bases is determined by the electrostatic energy[41]. Similarly, here, in films of DNA base molecules, both of these interactions may play a role in linking the base molecules to each other. These two phenomena interact since the base-base stacking coupling is modified by the H-bonded base-pair. This modification is maximum for the closer bases and decreases for the farther bases. While here we may have somewhat disordered physisorbed films, it is noted that at least adenine and guanine films at room temperature actually form π stacked multilayer films, with molecules lying flat on top of each other, even for films of many 100 nm thickness[42], while cytosine films are less ordered. Thus, here base stacking phenomena may still occur because of the multilayer property of the films. The base molecules in the film are likely to interact not only with the molecules in their own plane but also with the ones in the layers underneath and above. The hydrogen atoms in a particular molecule in one layer are shared with the atoms of another molecule in the upper/lower layer in particular due to non-planarity of

NH_2 group the hydrogen atoms attached to N may be shared with other atoms in the layer above and below.

Thus, here in the condensed phase, we propose that formation of NH_4^+ and CH_3^+ by ion impact are the result of both intra- and inter-molecular H-atom/proton transfer, and not successive scattering, i.e. pick up reactions of NH^+, or CH^+ precursor fragments in the film prior to desorption. This is clearly evidenced by either the complete absence of these precursors in the ion desorption spectra, or by their extremely low intensity, relative to the NH_4^+ and CH_3^+. Thus, ion impact induced ionization and excitation (ro-vibrational, and translational) of the target molecules lead to ionization, localization of the valence hole on a dissociating (i.e. "leaving") moiety, e.g. NH_2^+ and CH^+, which will abstract H atoms from within the dissociating molecule, or an adjacent neighbor, to form the final desorbing NH_4^+ and CH_3^+ products. Again, the absence of desorbing precursor fragments, suggests that this mechanism is a concerted reaction pathway.

The formation of desorbing NH_4^+ and CH_3^+ products likely depends on film morphology, e.g. H-bonding between identical bases which promotes H-atom/proton mobility in the films, as well as π-stacking between bases, or other molecular interactions between the individual molecular layers. Both will affect the proton affinities of the molecules or their fragments, and the films electronic structure, or flexibility of the physical structure of the film.

Summary and Conclusions

We have shown that the fragmentation of three amino bases of DNA, Adenine (A), Guanine (G), and Cytosine (C) by hyperthermal (1-100 eV) Ar^+ ions in condensed

phase leads to abundant formation and desorption of NH_4^+, which implies efficient de-amination of these DNA bases; this is also evidenced by desorption of de-aminated base cations, *viz.* $[M\text{-}16amu]^+$ where M= G, C, A (data not shown). The formation of NH_4^+ is not observed in the other bases, i.e. thymine, or uracil, and thus must involve the amino group in A, G, C.

To conclusively verify this, we have performed similar experiments on 5-amino-uracil. The results are shown in Figure 6 below, for ion impact on films, or electron impact in the gas phase. Here we clearly see formation of NH_4^+ and CH_3^+ from films of Ar^+ irradiated 5-amino-uracil, neither of which is observed in uracil films[14] irradiated with Ar^+ of identical energies. This clearly shows that (a) ion impact induced NH_4^+ formation occurs via the amino group in the amino bases, and moreover (b) CH_3^+ formation by ion impact from pyrimidine bases that contain no exocyclic methyl groups requires the presence of an amino group in the molecule. The amino group is believed to be not only a good H/proton abstractor, but also a good H/proton donor, during impact induced excitation/ionization, and thus facilitates the formation of CH_3^+. The formation of either NH_4^+ or CH_3^+ from these aminated molecules involves concerted bond rearrangements, and nuclear motion, i.e. intra- and inter-molecular H/proton transfer, and can occur by ion impact in films, as well as electron impact in the gas phase.

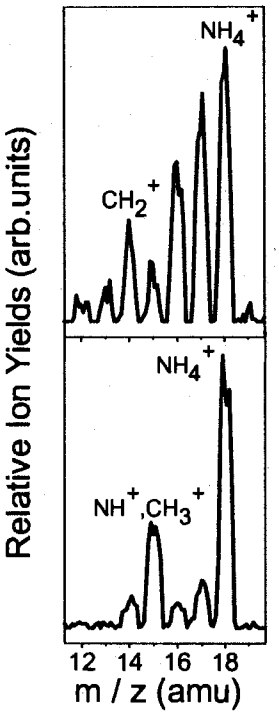

Figure 6: Cation fragment formation from 5-amino-uracil by 70 eV electron impact in the gas phase (top – blue, color online), and 100 eV Ar^+ impact in films of ca 20 ML thickness (bottom – red, color online)

From a biological perspective, deamination is an important damage process. In cells, deamination of cytosine in a single strand of DNA has been observed at a range of temperatures at a biologically significant rate[43]. Incidents of cytosine deamination and eventually cytosine to thymine mutations in nontranscribed strands of DNA have been observed in genes of mammalian bacteria cells[44]. Deamination phenomena have also been observed in oxidative damage to various forms of DNA and RNA by radical agents such as nitric oxide thereby leading to mutations[45]. Several processes involving deamination have been proposed in single strands of DNA, i.e. Cytosine (C) into Uracil (U), and adenine (A) into hypoxanthine (hX), which would imply a transformation of G into A in one strand of DNA and T into C in the complementary strand [44]. Moreover deamination

has been found to be the dominant process behind asymmetrical base composition in human DNA and RNA[45]. The type of mutation that deamination of the three DNA nitrogen nucleobases can induce may be "Transition" in which a purine changes to another purine, or a pyrimidine to a pyrimidine.

Thus, our experiments for the first time demonstrate the possibility of producing a deaminated bases via a *physical mechanism* of deamination by either low energy ion impact at energies down to 15-20 eV, or by electron impact at 70 eV. These ion energies are those of the abundant secondary ions that are produced along heavy ion tracks, while 70 eV electrons can be produced by some core excitation/ionization events along soft X-ray tracks. Thus, physical deamination of a DNA base along a radiation track may occur much earlier than the slow, diffusion limited chemical or biological deamination occurs at later times.

Acknowledgement

This work is continuously supported by grants from Canadian Space Agency and National Science and Engineering Research Council of Canada.

References

(1) Caulfield J.L; Wishnk, J.S; and Tannenbaum S.R, *Journal of Biological Chemistry*, **1998**, *273*, 12689.

(2) *ICRU Report 31*, International Commission on Radiation Units and Measurements, Washington, DC **1979**, and ICRU Report 55, **1995**.

(3) Pimblott, S.M.; LaVerne, J.A. In *Radiation Damage in DNA: Structure/Function Relationship at Early Times*, Fuciarelli, A.F., Zimbrick, J.D., Eds., Battelle Press: Columbus, OH. **1995**; Chapter 1. LaVerne, J.A.; Pimblott, S.M. *Radiat.Res.* **1995**,*141*, 208.

(4) Cobut, V.; Frongillo, Y.; Patau, J.P.; Goulet, T.; Fraser, M.-J.; Jay-Gerin,J.-P. *Rad.Phys.Chem.* **1998**, *51*, 229.

(5) De Vries. J.; Hoekstra. R.; Morgenstern. R.; and Schlathölter. T., *Physica Scripta.* **2004**, *T110*, 336.

(6) Burger, A.; Fix, D; Liu, H; Hays, J.; Bockrath, R.; *Mutat Res.* Jan **2003**, *522*,145.

(7) Privat, E.; and Sowers, L.C.; *Chem Res Toxicol.* **1996**, *9*, 745.

(8) De Vries, J.; Hoekstra, R.; Morgenstern, R.; and Schlathölter, T.; *Phys. Rev. Lett.* **2003**, *91*, 053401.

(9) Tappe; W.; Flesch, R.; Ruhl, E.; Hoekstra, R.; and Schlathölter, T. ;*Phys. Rev. Lett*, **2002**, *88*,143401 .

(10) Deng, Z.; Bald. I.; Illenberger, E.; and Huels, M. A.; *Phys. Rev. Letters.* **2005**, *95*, 153201.

(11) Huels, M.A; Champion, R.L.; Doverspike, L.D.; and Wang. Y.; *Phys. Rev.* **1990**, *A41*, 4809.

(12)Yang, Z.; and Rodgers, M.T.; *Phys. Chem. Chem. Phys.* **2004,** *6*, 2749.

(13) Imhoff, M.; Deng, Z.; Huels, M.A.; *Int. J. Mass. Spec.* **2005,** *245*, 68.

(14) Imhoff, M.; Deng, Z.; Huels, M.A.; *Int. J. Mass. Spec.* **2007**, *262*, 154.

(15) Gorb, L.; Podolyan, Y.; Dziekonski, P.; Sokalski, W. A.; and Leszczynski, J.; *J. Am. Chem. Soc.* **2004**, 126, 10119.

(16) Ferenezy, G.; Harsanyi, L.; Rozsondai, B.; Hargittai, I.; *J.Mol.Struct.* **1986**, 140, 71.

(17) Clowney, L.; Jain, S.C.; Srinivasan, A.R.; Westbrook, J.; Olson, W.K.; Berman.H.M.; *J.Am.Chem.Soc.* **1996**, 118, 509.

(18) Poltev, I.V.; Shulyupina N.V.; *J.Biomol.Struc.Dyn.* **1986**, 3, 739.

(19) Hobza, P.; Sandrofy, C.; *J.Am.Chem.Soc.* **1987**, 109, 1301.

(20) Šponer, J.; Florian, J.; Hobza, P.; and Leszczynski, J.; *J.Biomol.Struc.Dyn.* **1996**, 13, 827.

(21) Šponer, J.; and Hobza, P.; *J.Am.Chem.Soc.* **1994**, 116, 709.

(22) Bell, R.P.; "*The Tunnel Effect in Chemistry*", (Chapman and Hall, London, **1980**).

(23) German, E.D.; Kuznetzov, A.M.; and Dogonadze, R.R.; *J.Chem.Soc.Faraday Tran.* **1980**, 2, 76, 1128.

(24) Brunische-Olsen, N.; and Ultrup, J.; *J.Chem.Soc.Faraday Trans.* **1979,** 1, 75, 205, Ulstrup, J.; Charge Transfer Processes in Condensed Media, Vol.10 in Lecture Notes in Chemistry (Springer,Berlin,**1979**).

(25) Kasha, M.; *J.Chem.Soc.Faraday Trans.* **1986,** 2 82, 2379.

(26) Barbara, P.F.; and Jarzeba, W.; *Acc.Chem.Res.* **1998,** 21, 195.

(27) Goldanski, V.I.; Fleurev, V.N.; and Trakhtenberg, L.I.; *Sov.Sci.Rev.B.Chem.* **1987,** 9, 59.

(28) Meyer, R.; Ernst, R.R.; *J.Chem.Phys.* **1990,** 93, 5518.

(29) Chachisvilis, M.; Fiebig, T.; Douhal, A.; and Zewail, A.H.; *J.Phys.Chem.A.* **1998,** 102, 4.

(30) Morillo, M.; and Cukier, R.I.; *J.Chem.Phys.* 15 march **1993**, 98 (6).

(31) Löwdin, Per-Olov.; *Rev.Mod.Phys.* **1963,** 35, 723.

(32) Remmers, K.; Meerts, W.L.; and Ozier, I.; *J.Chem.Phys.* **2000,** 112, 24.

(33) Lobaugh, J.; and Voth, G.A.; *J.Chem.Phys.* (Febuary **1994**), 100 (4), 15.

(34) Mons, M.; Dimicoli.I.; Piuzzi, F.; Tardivel, B.; and Elhanine, M.; *J.Phys.Chem.A.* **2002**, 106, 5088.

(35) Nir, E.; Plützer, Ch.; Kleinermanns, K.; and de Vries, M.; *Eur.Phys.J.D.* **2002**, 20, 317.

(36) Gorb, L.; Podolyan.Y.; Dziekonski, P.; Sokalski, W.A.; and Leszczynski, J.; *J.Am.Chem.Soc.* **2004**, 126, 10119.

(37) Florian, J.; Hrouda, V.; and Hobza, P.; *J.Am.Chem.Soc.* **1994**, 116, 1457.

(38) Marañón, J.; Fantoni, A.; and Grigera, J.R.; *J.Theor.Biol.* **1999**, 201, 93.

(39) Meyer, R.; and Ernst, R.R.; *J.Chem.Phys.* **1987,** 86, 2.

(40) Pauling, L.; "*The Nature of the Chemical Bond*", (Cornell Univ. Press, Ithaca **1939**).

(41) Šponer, J.; Leszczynski, J.; and Hobza, P.; *J.Biomol.Struc.Dyn.* **1996,** 14, 1.

(42) Fujii, K.; Akamatsu, K.; and Yokoya, A.; *J. Phys. Chem. B.* **2004,** *108,* 8031.

(43) Frederico, L.A.; Kunkel, T.A.; and Shaw, B.R.; *Biochemistry.* **1990,** 29, 2532-2537.

(44) Reyes, A.; Gissi, C.; Pesole, G.; and Saccone, C.; *Mol.Biol.Evol.* **1998,** 15(8), 957-966.

(45) DeRojas-Walker, T.; Tamir, S.; Ji, H.; Wishnok, J.S.; and Tannenbaum, S.S.; *Chem.Res.Toxicol.* **1995,** 8, 473-477.

Table of contents graphic (TOC)

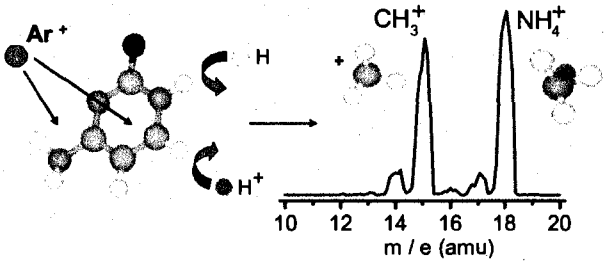

TOC text: Physical deamination of DNA amino-bases by hyperthermal ion impact involves concerted bond reactions involving intra- and inter-molecular H and proton transfer.

3.2 Fragmentation pathways of Cytosine by hyperthermal (10-100 eV) Ar^+ ion impact in the condensed phase, Article In preparation for submission to *Journal of Analytical Atomic Spectroscopy.*

Résumé

Nous présentons ici des mesures de la formation de fragments positifs et négatifs induite par une irradiation de faible énergie (10-100 eV) aux ions Ar^+ sur des films de cytosine (C) évaporés sur une surface de platine polycristalline. Différents types de fragmentation spécifique ont été observés, en particulier la déamination (détachement d'un groupement amino), l'ouverture de cycle et l'amination.

Les espèces cationiques majeures générées sont les ions H^+, NH_4^+, CH_3^+, $HNCH^+$, $C_2NH_4^+$, $C_3NH_2^+$, $C_2N_2OH^+$, $C_3N_2OH_4^+$, $[Cyt\text{-}NH_2]^+$, $[Cyt+H]^+$, et les anions, H^-, O^-, CN^- ,et OCN^-. Les fragments cationiques se désorbent à des énergies variant de 15 à 25 eV et suivent toutes le même modèle. L'utilisation d'isotopes radiomarqués de Cytosine-2, 4-^{13}C2, ^{15}N3 révèle le site spécifique de l'origine de certains fragments, et donc la nature chimique du clivage de liaison. En plus de l'ionisation et la fragmentation moléculaires, des mesures antérieures ont montré que certaines réactions chimiques telles que l'effet tunnel et le transfert de proton sont observés lorsqu'un groupement amino (-NH_2) de la cytosine arrache un proton pour se désorber sous forme NH_4^+ tel que retrouvé dans le spectre de désorption ionique de la molécule.

Il a également été montré que la formation d'ions CH_3^+ est exclusivement due à un transfert de proton sur les sites C5 et C6 et donc au dommage endocyclique sur la cytosine. Enfin, des voies de clivage des liaisons chimiques communes aux pyrimidines (clivage axial et planaire) ont été identifiées par comparaison des résultats obtenus pour la

cytosine avec les données déjà publiées relatives à l'irradiation aux ions Ar^+ de films de thymine, uracile, et 5-bromouracile.

Mots-clés : pyrimidine, impact électronique et ionique, phase condensée, phase gazeuse

J'ai personnellement contribué à 60% de la partie expérimentale de ces travaux, 100% en ce qui concerne l'analyse des données incluant la préparation des figures, et 100% de la rédaction (de cet article).

nature of the bond cleavage. In addition to ionization and molecular fragmentation, in previous measurements[14] some chemical reactions such as proton tunneling and hydrogen transfer are also observed when amine group ($-NH_2$) in the cytosine donates/abstracts a hydrogen/proton to desorb as NH_4^+ in the ion desorption mass spectrum of this molecule. It is also found that the formation of CH_3^+ ion is exclusively due to proton transfer at C5,C6 sites and thus endocyclic damage to the cytosine. Furthermore common bond cleavage pathways in pyrimidines (cleavage axis, cleavage plane) has been identified by comparing the results obtained for cytosine with previously published results on Ar^+ ion irradiation on films of thymine, uracil and 5-bromouracil.

Keywords: Pyrimidine, Electron & Ion impact, Condensed phase, Gas phase

I have contributed to 60% of the experimental work, 100 % of the data analysis including preparation of all figures and 100% writing of this work up to present version.

Introduction

Ionization and fragmentation of DNA and its components is a key step in radiation damage to biological tissue. All types of ionizing radiation heavy ions and protons in particular induce mutagenic effects and lethal damage in DNA such as single and double strand breaks, base loss and clustered damage[1]. At high energies which is used in radiation therapy modalities such as proton and heavy ion therapy, most of this damage is not induced by direct effect of radiation i.e. primary particles but is caused by abundant secondary ions and electrons produced along the ionization track in the tissue. In their pioneering study, Schlathölter *et al* demonstrated that multiply charged secondary ions with energies starting from 10 eV to few hundreds of eV are produced as a result of interaction of heavy, highly charged 0.5 MeV $^{129}Xe^{25+}$ with thymine and uracil molecules[2]. These low energy (1-500 eV) projectiles induce sever fragmentation of DNA and RNA by electron attachment processes before they are thermalized [3,4,5,6,7,8]. As well as these secondary particles, damage to DNA and RNA can also be induced by the subsequent interactions of the latter with the surrounding DNA and RNA. These reactions may lead to significant physical and chemical alterations of the cell medium and determine the eventual biological fate of the cell.

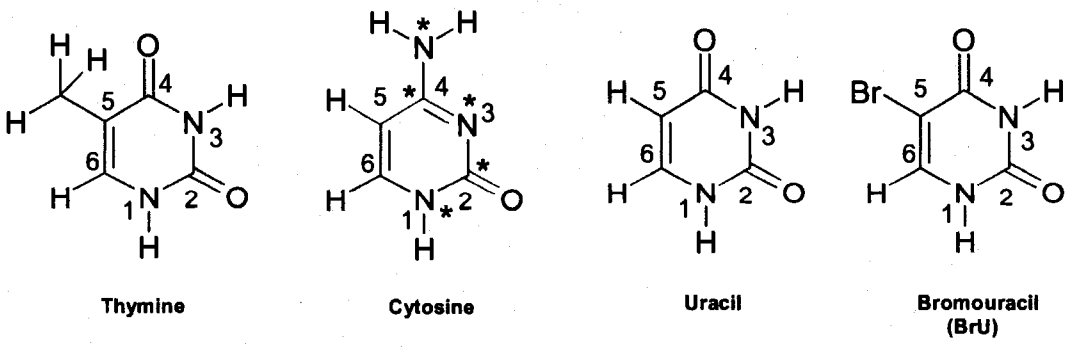

Fig. 1 Molecular Structure of thymine, cytosine, uracil and 5-bromouracil.

Fig.1 shows the molecular structure of DNA and RNA pyrimidine bases and 5-bromourail (BrU) studied in the current work. DNA and RNA nucleobase structures differ in one base, thymine in DNA and uracil in RNA. BrU is a derivative of uracil, acting as a base analog and substituting for thymine in DNA. Integration of 5-BrU into DNA may lead to point mutations via base substitution and hence has significant biological implications [9].

In the present study we focus on heavy ion induced fragmentation of DNA base, cytosine, in the condensed phase by 1-100 eV Ar^+ ions, the desorption energy threshold of the products, and the 70 eV electron impact in the gas phase. The fragmentation patterns and mechanisms of cytosine are investigated as a function of incident ion energy and are compared to those of other pyrimidines such as thymine, uracil and 5-bromouracil [10].

Experimental Procedure

The experiments were conducted on an ultrahigh-vacuum (UHV) ion-beam apparatus developed in- house [11] which is to be described in details elsewhere. The experimental setup briefly consists of a low-energy ion beam system, delivering a highly focused energy- and mass- resolved positive ion beams in the 1-500 eV energy range into the UHV($\sim 10^{-9}$ Torr) reaction chamber for the film irradiation. In order to monitor the desorbing positive and negative fragments *in vacuo* during ion and electron impact, a high resolution quadrupole mass spectrometer (QMS) (Hiden Analytical Ltd.) is installed perpendicular to the ion beam line. The QMS is optimized to detect ions which have

kinetic energy of up to 5 eV. The base pressure of the system is 10^{-9} Torr. The pressure in the reaction chamber remains at 10^{-9} Torr, while the pressure in the ion source increases to ~10^{-5} Torr during the experiments.

Films of cytosine were prepared *in vacuo* by evaporation from an oven onto an atomically clean, Pt substrate held at room temperature (22-25° C). Cytosine purchased from Aldrich (99%) was loaded into an oven inside a load-lock chamber. A quartz-crystal microbalance with an active area of about 0.5 cm^2 positioned at 1 cm from the oven was used to calibrate the evaporation and condensation rates in $ng.min^{-1}.cm^{-2}$.

In the present work, we concentrate mainly on 10-100 eV Ar^+ ion irradiation of 200 ng/cm^2 cytosine (C) films on Pt substrate, corresponding to roughly 3-4 nominal monolayers of cytosine assuming no clustering of the molecules during sample evaporation on the substrate[12]. The Pt substrate is repeatedly cleaned by 200 eV Ar^+ sputtering as well as resistive heating to 1000°C prior to film deposition. The evaporation temperature (≤100° C) is well below the cytosine decomposition temperature (~ 325°C)[13]. The sample film is positioned in the center of reaction chamber, 2 cm away from the QMS, with an angle of 30° with respect to incident beam and 60° with respect to the QMS. The QMS is programmed to operate with an ionizer and mass filter, as well as the residual gas analyzer (RGA) mode in order to fragment and ionize neutral molecules in the gas phase. The results of electron impact in the gas phase, presented in this paper, were collected in this mode with the electron impact energy of 70 eV. The electron impact experiments were performed after baking of the UHV system and degassing of the cytosine sample in the load-lock chamber in order to reduce the background RGA signal (in particular the H^+ and H_2O^+) to minimum. A background spectrum is taken

immediately prior to sample evaporation and is subtracted from the cytosine electron impact spectra presented here. Relatively large amounts (2-6 μg) of cytosine molecule are evaporated to the Pt substrate, placed in front of the QMS. The mass spectra obtained for the electron impact on cytosine in gas phase is comparable to the ion desorption spectra of Ar^+ irradiation on cytosine due to the fact that the QMS filter and the detection system were the same for both types of measurements.

To assist chemical identification of the fragments, all the experiments were repeated with Cytosine-2, 4-$^{13}C_2$, $^{15}N_3$ (from ISOTEC 98+ % ^{15}N and 99% ^{13}C isotopic purity). To remove impurities in the compound prior to sample evaporation, both labeled and unlabeled compounds were slowly degassed in the load-lock chamber to near 60°C, well below the evaporation onset of cytosine (ca. 150°C).

Results and Discussions

Fig.2 shows the desorption mass spectrum of positive and negative ions generated by (a)100 eV Ar^+ -ion irradiation of 200 ng/cm^2 cytosine (C) films (3-4 ~ nominal ML) on Pt and (b) 70 eV electron impact in the gas phase. Major cation fragments are identified from low to high mass-to-charge ratio to H^+, CH_3^+ , NH_4^+ , $HNCH^+$, $C_2NH_4^+$,$CN_2H_2^+$,CNO^+, $C_3NH_2^+$, $C_2N_2OH^+$,$C_3NOH_3^+$, $C_3N_2OH_4^+$, $[Cyt\text{-}NH_2]^+$, $[Cyt+H]^+$, $[Cyt+NH_2]^+$ for the condensed phase measurements and H^+ , H_2^+, NH_4^+ , CH_3^+ , $HNCH^+$, $CN_2H_3^+$,CN_2H^+, $C_2NOH_2^+$,$C_3NOH_3^+$, $C_2N_2OH^+$, $C_2N_3OH^+$, $[Cyt\text{-}NH_2]^+$, $[Cyt]^+$ for the gas phase measurements. Major anions desorbed in the condensed phase measurements include H^-, O^-, CN^-, and OCN^-.

Here we focus on the results of Cytosine but shall frequently cite the results on thymine, uracil and 5-bromouracil. In order to assist fragment identification, close ups of labeled and unlabeled cytosine spectra is shown for electron impact in Fig.3 and ion impact in Fig.4.

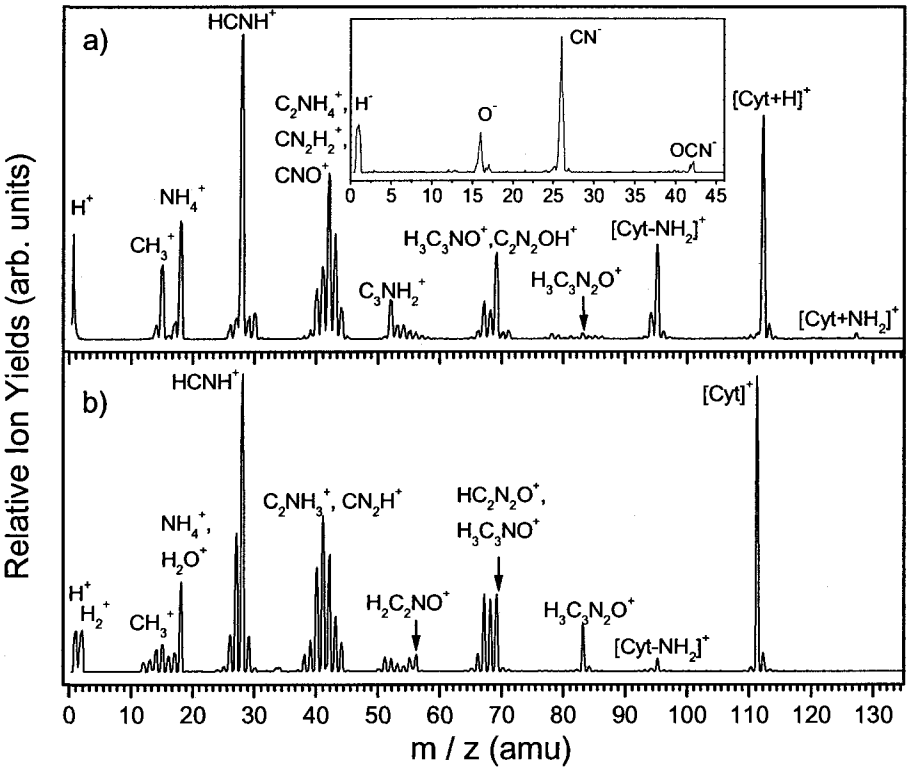

Fig. 2 Typical positive (top panel) and negative (bottom panel) ion stimulated desorption (ISD) mass spectra from a 200 ng/cm^2 cytosine (C) film on Pt, produced by (a)100-eV Ar^+ ion irradiation, (b) 70 eV electron impact.

First, in Fig.2 we can easily identify the molecular parent cation for cytosine $[Cyt]^+$ at 111 amu during electron impact, and the protonated parent cation $[Cyt + H]^+$ at 112 amu during ion irradiation. When cytosine is labeled as Cytosine-2, 4-$^{13}C_2$, $^{15}N_3$, these

parent cations both shift 5 amu to 116 amu during electron impact and 117 amu during ion impact, respectively (Fig. 3 and Fig.4).

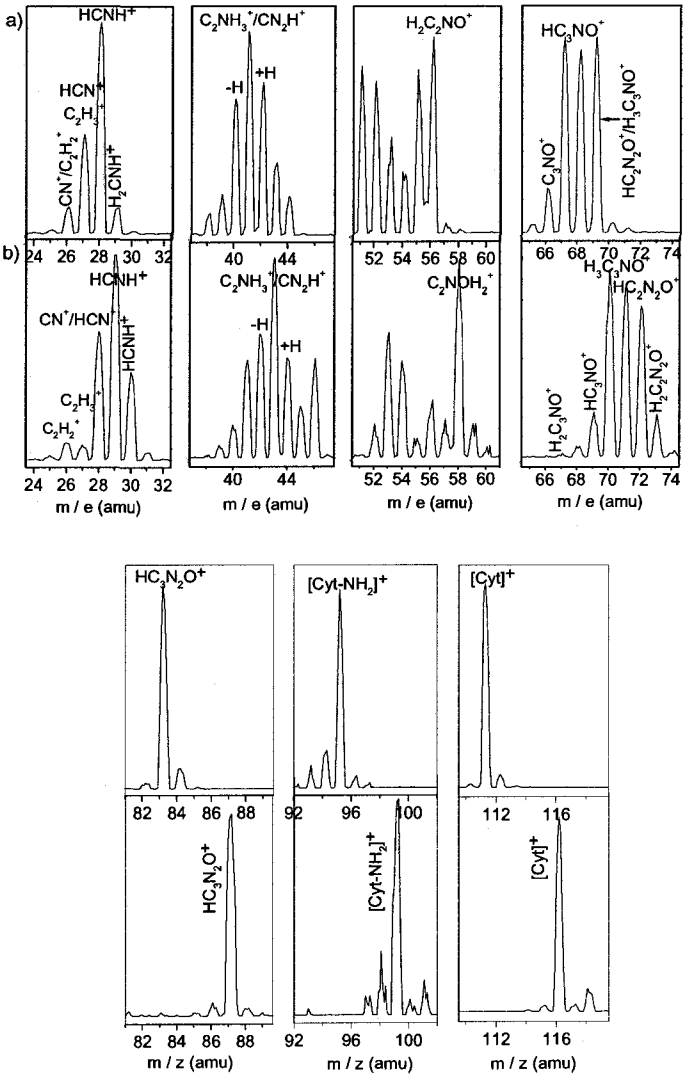

Fig. 3 Electron impact measurements on (a) unlabeled cytosine (b) labeled cytosine.

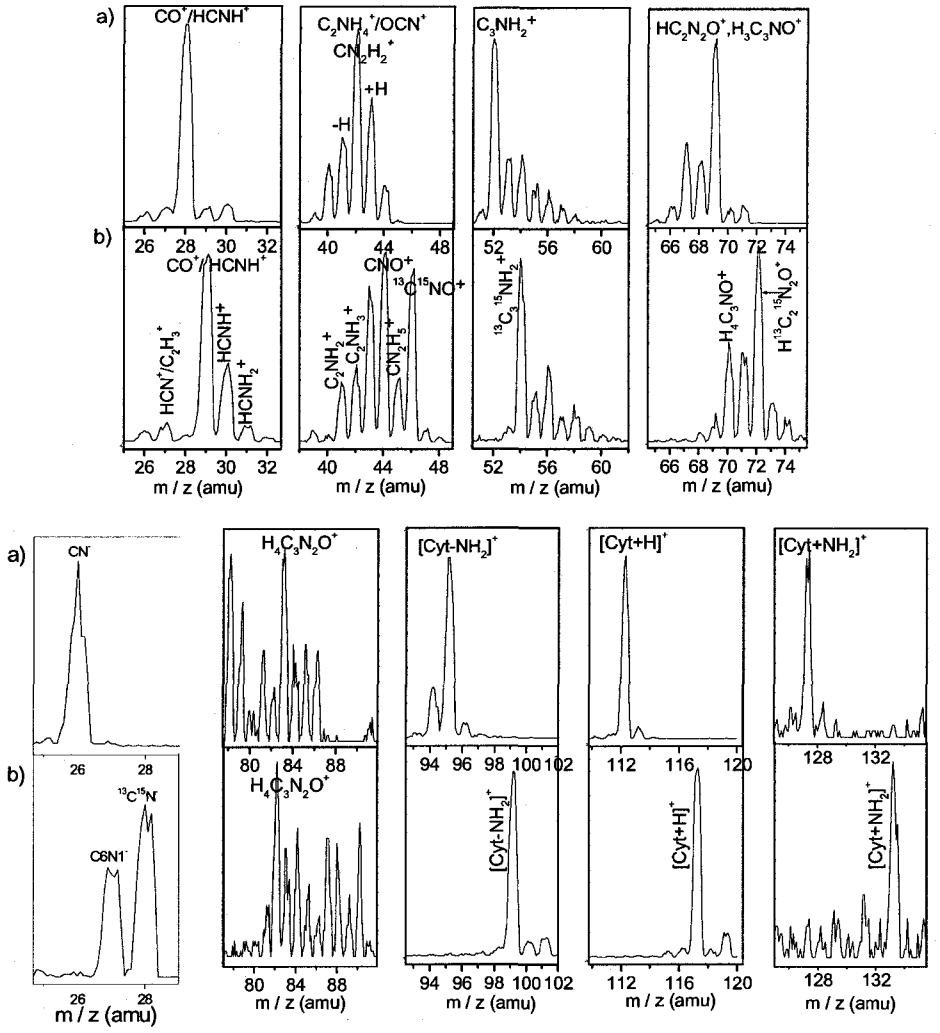

Fig. 4 Ion irradiation measurement for (a) Unlabeled Cytosine and (b) labeled Cytosine.

Now looking at the fragments, in the 10 -20 amu mass range, fragment peak 15 and 18 appear prominent both in electron and ion impact spectra and are assigned to CH_3^+ and NH_4^+/H_2O^+, respectively. As discussed comprehensively in [14], the CH_3^+ fragment originates from ring fragmentation at the C5 and C6 sites while the NH_4^+ fragment exclusively arises from the amine group (exocyclic fragmentation of the cytosine molecule). Elimination of the amino group also leads to the formation of $[Cyt - NH_2]^+$ at

95 amu during both electron impact (Fig.3) and ion irradiation (Fig. 4). These fragments shift 4 amu to 99 amu when Cytosine-2, 4-$^{13}C_2$, $^{15}N_3$ is irradiated.

In addition, the eliminated amino group can also combine with another cytosine molecule and desorb as $[Cyt + NH_2]^+$ at 127 amu during ion irradiation, which is negligible during electron impact in the gas phase. This claim is also supported by the fact that the fragment $[Cyt + NH_2]^+$ at 127 amu shifts 6 amu to 133 amu during ion irradiation (Fig. 4). It is likely a result of the formation of cytosine dimers via hydrogen bonds in the condensed phase.

In the mass range of 20 to 30 amu, 26-29 amu peak fragments are common in both electron and ion impact with the peak 28 amu having the highest relative intensity. Peak 30 amu (29 amu + H) is only observed in the ion irradiation spectrum since hydrogen/proton are more abundantly available by proton transfer processes in condensed phase as compared to the gas phase. Based on our published data on thymine and thymine-methyl-d3-6-d1, we concluded that (1) cation at 28 amu is assigned to $HCNH^+$ during ion irradiation and $HCNH^+/CO^+$ during electron impact, respectively; (2) the contribution to $HCNH^+$ is mainly from N1-C6 of thymine, contribution from the O=C-N groups to the formation of $HCNH^+$ is negligible. Here during ion irradiation of Cytosine-2, 4-$^{13}C_2$, $^{15}N_3$, it is found that the 28 amu peak of cytosine shifts partly to 29 amu and partly to 30 amu (Fig. 4). The 29 amu peak is indicative of contribution from N1-C6 of cytosine, and the 30 amu peak is indicative of contribution from C4-N4 and C4-N3. Contribution from C2-N1 or C2-N3 to the formation of $HCNH^+$ is believed to be negligible according to the results of thymine. Then given the partial ratio between 29 amu to 30 amu, it can be concluded that the formation probability of $HCNH^+$ from N1-C6

is nearly 4-fold higher than from C4-N3 or C4-N4, suggesting that the N1-C6 site is weaker than the N4-N3 site.

During electron impact of cytosine, similar mass pattern is observed, but the relative intensity of fragments at 26 and 27 amu is much higher. During electron impact of Cytosine-2, 4-$^{13}C_2$, $^{15}N_3$, the major difference is the remaining of a partial peak at 28 amu. Because the $HCNH^+$ fragment shifts to 29 and 30 amu, and the CO^+ fragment if any shift to 29 amu with C2 replaced with ^{13}C, the peak at 28 amu clearly indicates the contribution of HCN^+ originated from the N1-C6 site, the remaining peaks at 26 and 27 amu indicate the intensity of $C_2H_2^+$ and $C_2H_3^+$ without mass shift.

Loss of a HCNH group also leads to the formation of several fragments in the 80-90 amu mass range. However, the electron impact spectrum is much simpler than the ion impact spectrum. The 83 amu fragment appears as the most intense peak in the group, indicating loss of 28 amu from cytosine, i.e. a HCNH group. This fragment shifts 4 amu to 87 amu during electron impact of Cytosine-2, 4-$^{13}C_2$, $^{15}N_3$, indicating that the lost HCNH group contains only one isotope-labeled atom and thus is originated from the N1-C6 site. This suggests a bond cleavage plane along C5-C6, C2-N1 as the responsible pathway for the fragmentation. Ion impact produces a cluster of fragments in this mass range as a result of the condensed phase effect, but they can still be attributed to the loss of a HCNH group from the N1-C6 site as the fragment cluster shifts 4 amu during ion impact of Cytosine-2, 4-$^{13}C_2$, $^{15}N_3$. It is also likely that loss of HCNH group from the C4-N4 or C4-N3 sites also contributes to this fragment cluster. The fragments at 78 and 79 amu are slightly difficult to recognize.

In the 36-45 amu mass range in the electron impact, the most significant peak is 41 amu which is assigned mostly to $C_2NH_3^+/CN_2H^+$. In the ion impact spectrum, 42 amu (peak 41 amu cation with an extra H) is the most significant peak in this range.

The peaks observed in the 50-60 amu range appear numerous, with the peak fragment $C_2NOH_2^+$ (56 amu) and $C_3NH_2^+$ (52 amu) having the highest intensity in the electron and ion impact spectra respectively. As observed in the ion irradiation spectrum (Fig.4), peak 52 amu in the unlabeled cytosine measurements mostly shifts to 54 amu in the labeled cytosine spectrum, indicating that this peak is to a major part due to bond cleavage at C6-N1 and C4-N3 sites resulting in $C_3NH_2^+$. The electron impact results (Fig.3) demonstrates a shift for the major peak 56 amu in unlabeled cytosine to 58 amu in labeled cytosine spectrum suggesting $C_2NOH_2^+$ assignment and implying involvement of C2, C6, N1 and O2 (C5-C6 and C2-N3 bond cleavage plane).

The fragment 41 amu in the electron impact spectrum of unlabeled cytosine (Fig. 3.a) shifts to 43 amu in the spectrum of labeled cytosine (Fig.3.b) indicating that this fragment is mostly initiated from C4,N4,C5 site and hence is $C_2NH_3^+$, and less originates from N3,C4,N4/ N1,C2,N3/ N1,C5,C6 sites. Fragment 52 amu in ion impact (Fig.4.a) is assigned to $C_3NH_2^+$ as it shifts to 54 amu in the labeled spectrum (Fig.4.b) signifying that this cation originates from N4,C4,C5,C6 sites in the cytosine molecule. The rich fragment pattern in 50-60 amu of the electron impact spectrum is slightly harder to assign.

For the next mass range of fragments between 64-72 amu, we observe peaks of 67-69 amu with cation peak at 69 amu as the most intense fragment. These fragments are a result of loss of a OCNH (±H) group. During ion irradiation measurements (Fig.4) all the peaks shift 3 amu to 70-72 amu, respectively, indicating that the lost OCNH (±H)

group contains two isotope-labeled atoms, i.e. the N1-C2-O2 group. This suggests bond cleavage plane along N1-C6, C2-N3 as the most probable pathway.

Negative ion formation is measured only during Ar^+ ion irradiation of cytosine (Fig.2.a), and the major anions are H^-, O^-, CN^- and OCN^-. The CN^- fragment at 26 amu (closeup shown in Fig.4.a) shifts to 27 and 28 amu in the spectrum of labeled cytosine (Fig.4.b), to some extent manifesting the contribution to its formation from different possible sites of cytosine molecule. The peak at 27 amu is an indicative of contribution from N1-C6 site, whereas the peak at 28 amu indicates contribution from C4-N4, C4-N3, C2-N3 and C2-N1 sites with the latter two likely negligible. Given a partial ratio of ~ 40%, it also suggest a more facile fragmentation at the N1-C6 site to form CN^-, in agreement with the formation of $HCNH^+$ where its favorite origin is also the N1-C6 site. Fig.5 shows the relative yields of cation and anion fragment desorption as a function of incident energy during Ar^+ ion irradiation of a 200 ng/cm^2 cytosine film. The desorption threshold of major fragments from cytosine can be approximated from this graph. Most cation fragments from cytosine start to desorb at energies between 15 eV ($C_2NH_2^+$, $C_2NH_4^+$) and 25 eV($[Cyt\text{-}NH_2]^+$). These desorption energies closely resemble those of major cation fragments desorbed from thymine, uracil and 5-bromouracil for films of similar thicknesses.

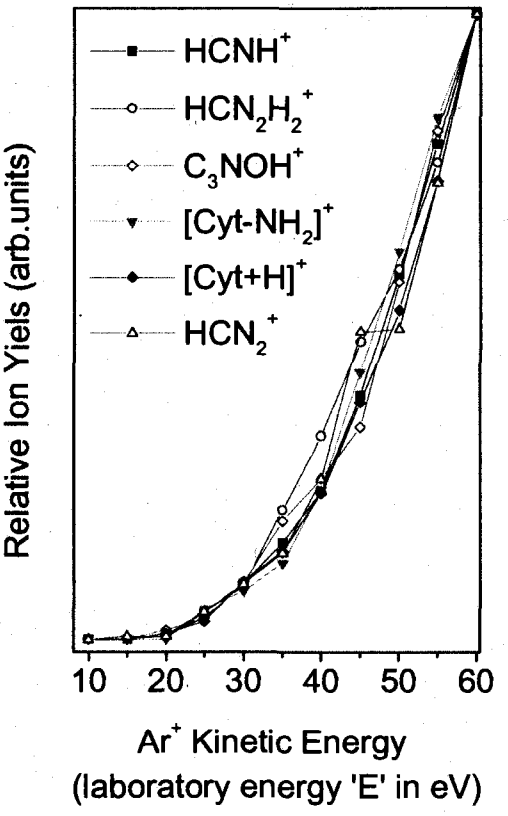

Fig. 5 Desorption energy threshold for cation and anion fragments by Ar^+ ion impact on films of cytosine (3-4 ML).

Complementary fragments induced by Ar^+ -ion irradiation of cytosine:

As already manifested in the above discussion, both electron and ion impact of cytosine exhibit several complementary fragmentation pathways, e.g., the formation of NH_4^+ and the loss of NH_2 leading to the formation of $[Cyt\text{-}NH_2]^+$, the formation of $HCNH^+$ from the N1-C6 site and the loss of HCNH from this site leading to the formation of cation fragments at 83 amu, etc. Nonetheless, despite the equivalent relative intensity of NH_4^+ and $HCNH^+$ with regard to the parent cation during ion and electron impact, ion impact exhibits a more significant $[Cyt\text{-}NH_2]^+$ cation fragment whereas electron impact

leads to a more significant $[Cyt\text{-}HCNH]^+$ cation fragment. Fig.6 summarizes the main bond cleavage axis upon ion irradiation of cytosine. Similar complementary patterns have been observed for CNO^+ (42 amu) and $C_3N_2H_5^+$ (69 amu), $C_2N_2H_3^+$ (55 amu) and $C_2NOH_2^+$ (56 amu).

Cleavage pathways in Cytosine compared to Thymine, Uracil and 5-bromouracil:

Fragments $C_2H_2^+$ (26 amu) and $C_2H_3^+$ (27 amu) is observed in the cation desorption spectrum of all studied bases –Cyt, U and 5-bromouracil, signifying the C5-C6 cleavage plane as the common important pathway responsible for these fragments in pyrimidine. $HCNH^+$ (28 amu) is the most intense fragment relative to other peaks in the ion impact cation desorption spectrum of all four molecules in the condensed phase with the N1-C6 site as the major contribution.

The formation of $[M\text{-}OCNH]^+$ fragment (M=C,T,U or 5-BrU) as a result of loss of an OCNH group is another common fragment pathway, leading to fragments at 69 amu for cytosine and uracil, 82, 83 amu for thymine, and 147, 149 amu for 5-bromouracil. The complementary fragment is also observed as OCN^+, $OCNH^+$ and $HOCNH^+$ in the spectra of these bases contributing to peaks 42, 43 and 44 amu. There are two possible cleavage pathways in cytosine and three in T, U and BrU which are not resolvable by the studies performed.

Moreover bond cleavage plane N1-C2, C4-C5, appears common in these bases, producing fragments $HNC_2H_2^+$ [±H] (40-42 amu) from cytosine and uracil, $HNC_3H_3^+$[+H] (54,55 amu) from thymine, and $[HNC_2HBr+H]^+$ (120,122 amu) from 5-bromouracil.

A $[M-O]^+$ fragment is observed during ion impact of thymine, uracil and 5-bromouracil, but it is not observed during ion impact of cytosine. This fragment is absent in electron impact of the all studied four base molecules.

Instead, the loss of amino group $[M-NH_2]^+$ from C4 is observed as a relatively intense peak (95 amu) in the spectrum of cytosine (Fig.2). The possible pathways and consequences of C4-NH2 bond cleavage in cytosine is discussed in some details. Breaking this bond results in deamination of cytosine and is evident in ion irradiation of this prymidine in the condensed phase as well as electron impact of the molecule in the gas phase. NH_4^+ (18 amu) fragment desorbs abundantly as a result of this deamination, and its formation is believed to be assisted by proton/hydrogen tunneling processes which aid tautomerization of cytosine molecules in the condensed film. Unimolecular tautomerization of cytosine in the gas phase can not occur by evaporation of solid cytosine under its decomposition rate (~325°C), since below this temperature sufficient energy is not provided to overcome the unimolecular tautomerization barrier[15]. In contrast, proton tunneling processes which take place between two cytosine molecules stabilized by intermolecular hydrogen bonds in the condensed film of cytosine (i.e. Ar^+ irradiation experiments), exhibit much lower energy barriers to tautomerization, specially when dual hydrogen bonds are present between the each two cytosine molecules in the condensed film, where one molecule acts as proton donor and the other as proton acceptor in one hydrogen bonding interaction, and each play the reverse role in the second hydrogen bond[13, 16, 17].

Equally interesting is the observation of the addition of an $-NH_2$ group to the cytosine molecule in the ion irradiation mass spectrum of this molecule (Fig.2) by a

process known as amination. The corresponding peak for this fragment, $[Cyt+NH_2]^+$, is observed after the parent peak at 127 amu and shifts to 133 amu in the labeled cytosine spectrum. This phenomenon is expected from addition of an $-NH_2$ group and completely rules out the other possible assignment, $[Cyt+O]^+$.

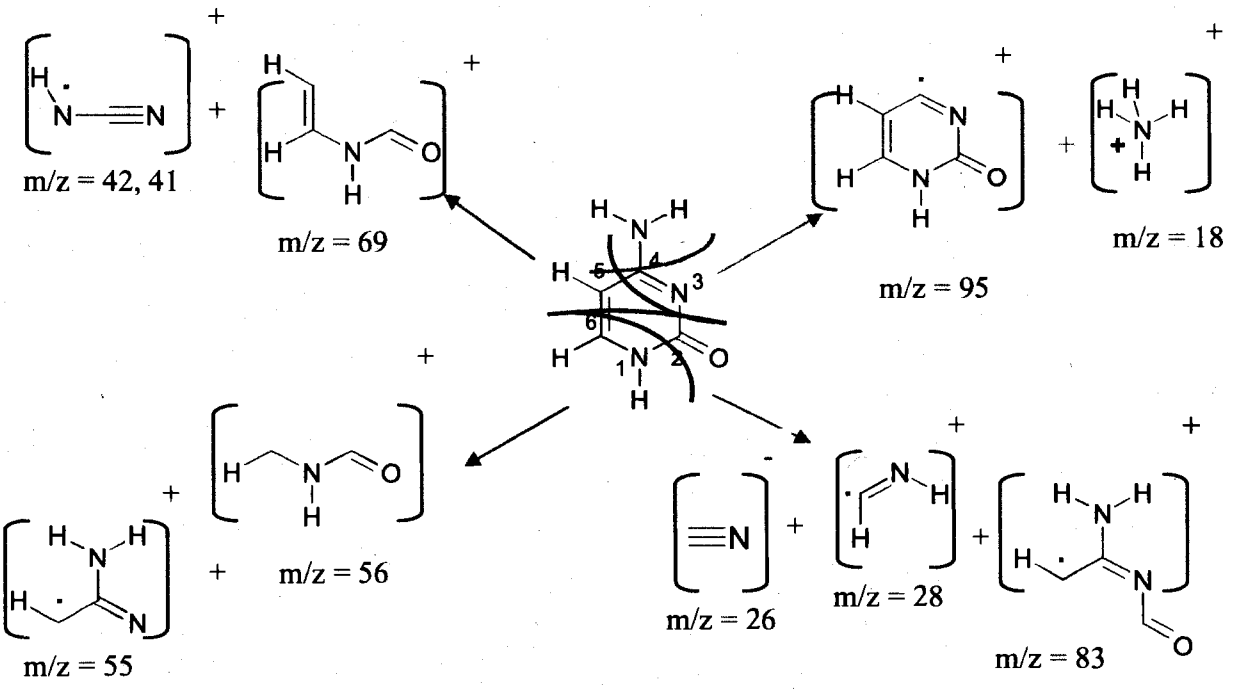

Fig. 6 Most common fragmentation pathways by electron and Ar^+ ion impact on cytosine.

Summary and Conclusion

In order to unravel the possible fragmentation pathways of DNA pyrimidine bases by primary track-end or secondary heavy ions, we have performed a set of experiments on ionization and fragmentation of cytosine by 1-100 eV Ar^+ ions in the condensed phase in connection with investigations performed on ion induced damage on other pyrimidine

bases such as uracil, thymine and 5-bromouracil by our group. The fragmentation pathways and cleavage planes were then compared to 70 eV electron impact measurements in conducted the gas phase. Abundant ionic fragments are produced by ion irradiation and electron impact on cytosine molecule in the condensed and gas phase respectively, demonstrating a rich fragmentation pattern, to some extent similar to the pathways observed in other DNA and RNA pyrimidine nucleobases.

Acknowledgements

This work is continuously supported by the Natural Science and Engineering Research Council of Canada and the Canadian Space Agency.

[1] C.von Sonntag, *The Chemical Basis for Radiation Biology* (Taylor & Francis, London, UK, 1987).
[2] T. Schlathölter *et al.* Int. J. Mass Spectr. **233**, 173 (2004).
[3] B.Boudaiffa, P.Cloutier, D.Hunting, M.A.Huels, and L.Sanche, Science **287**, 1658 (2000).
[4] M.A.Huels, I.Hahndrof, E.Illenbergher, and L.Sanche, J.Chem.Phys. **108**, 1309 (1998).
[5] D.Antic, L.Parenteau, M.Lepage, and L.Sanche, J.Chem.Phys.B **103**, 6611 (1999).
[6] M.-A.Hervé du Penhoat, M.A.Huels, P.Cloutier, J.-P.Jay-Gerin, and L.Sanche, J.Chem.Phys. **114**, 5755 (2001).
[7] H.Abdoul-Carime, M.A.Huels, E.Illenberger, and L.Sanche, J.Am.Chem.Soc. **123**,5354 (2001).
[8] L.Sanche, Mass Spectrom.Rev. **21**,349 (2002).
[9] X.Hu, H.Li, J.Ding, S.Han Biochemistry. **43**, 6361, (2004).
[10] M.Imhoff, Z.-W.Deng, and M.A.Huels, Int.J.Mass.Spectr. **262**, 154-160, (2007).
[11] Z.-W.Deng, M.Imhoff, M.A.Huels, J.Phys.Chem.Phys. **123**, 144509, (2005).
[12] M.A.Huels, I.Hahndoff, E.Illenberger, L.Sanche, J.Chem Phys. **108**, 1309 (1998).
[13] Z.Yang and M.T.Rodgers, Phys.Chem.Chem.Phys. **6**, 2749-2757, (2004).
[14] S.Sarabipour, Z.-W.Deng, M.Michaud, M.A.Huels, submitted to J.Am.Chem.Soc. (2008).
[15] N.Russo, M.Toscano, and A.Grand, J.Am.Chem.Soc. **123**, 10272, (2001).
[16] K.C.Ingham and M.A.El-Bayoumi, J.Am.Chem.Soc. **93**, 5023, (1971).
[17] P.-T.Chou, C.-Y.Wei, C.P.Chang, and M.S.Kuo, J.Phys.Chem B, **101**, 9119, (1997).

3.3 Adenine and Guanine fragmentation by hyperthermal Ar^+ ion irradiation in the condensed phase, and gas phase electron impact,

Article In preparation for submission to *International Journal of Mass Spectrometry.*

Résumé

Des dommages à l'ADN, sur les deux bases puriques Adénine (A) et Guanine (G), ont été observés sous l'impact hyperthermique (10-100 eV) des ions Ar^+ dans la phase condensée. Les voies de dommages à l'ADN incluent l'amination, la déamination, l'ionisation et la fragmentation des bases nucléiques. L'impact ionique sur ces bases dans la phase condensée aboutit à la formation des fragments suivants : H^+, NH_4^+, $HNCH^+$, HC_2NH^+/CN_2^+ , $HC_2NH_4^+/HCN_2H_2^+$, $HC_2N_2H_2^+$, $HC_3N_2H_2^+$, $HC_3N_3H_3^+$, $HC_4N_3H^+$, $HC_4N_3H_3^+$, $H_5C_4N_4^+/H_3N_5C_3^+$, $[A\text{-}NH_2]^+$, $[A+H]^+$, et $[A+NH_2]^+$ pour l'adénine, et H^+, NH_4^+, $HNCH^+$, $HCN_2H_2^+/HNCO^+$, HC_2NO^+, $C_2N_2O^+$, $H_2C_3N_2O^+/HC_3N_3H_2^+$, $C_3N_3O^+/H_2C_4N_2O^+$, $H_4C_4N_3O^+$, $[G\text{-}NH_2]^+$, et $[G+H]^+$ pour la guanine.

Pour l'adénine, seuls les fragments anioniques H^- et CN^- sont désorbés, bien que les fragments H^-, O^- et CN^- soient générés sous irradiation ionique de la guanine. De plus, pour l'adénine, le fragment anionique principal, CN^-, se désorbe avec une énergie ionique de plus faible incidence que celle des fragments positifs formés par irradiation.

L'utilisation d'isotopes radiomarqués (Guanine-8-^{13}C et Adenine-8-^{13}C) a révélé la spécificité du site de clivage de la liaison chimique sur le site C8. Il apparaît de ces résultats que le site C8 est très sensible dans les deux types de fragments générés et constitue une cible privilégiée de l'impact électronique et ionique, dans le cas d'une irradiation ionique d'énergie faible de 150 eV, et particulièrement au niveau des liaisons endocycliques C8-N7 et C8-N9.

Mots-clés : bases puriques, faible énergie, impact ionique, phase condensée, impact électronique, phase gazeuse

J'ai personnellement contribué à 60% de la partie expérimentale de ces travaux, 100% en ce qui concerne l'analyse des données incluant la préparation des figures, et 100% de la rédaction (de cet article).

Abstract

We have observed damage to Adenine and Guanine, two purine nucleobases of DNA, by hyperthermal (10-100 eV) heavy Ar^+ ion impact in the condensed phase. Damage pathways include amination, deamination, ionization and fragmentation of the nucleobases. Ion impact on these bases in the condensed phase results in the formation of the following fragments: H^+, NH_4^+, $HNCH^+$, HC_2NH^+/CN_2^+ , $HC_2NH_4^+/HCN_2H_2^+$, $HC_2N_2H_2^+$, $HC_3N_2H_2^+$, $HC_3N_3H_3^+$, $HC_4N_3H^+$, $HC_4N_3H_3^+$, $H_5C_4N_4^+/H_3N_5C_3^+$, $[A\text{-}NH_2]^+$, $[A+H]^+$, and $[A+NH_2]^+$ for Adenine, and H^+, NH_4^+, $HNCH^+$, $HCN_2H_2^+/HNCO^+$, HC_2NO^+, $C_2N_2O^+$, $H_2C_3N_2O^+/HC_3N_3H_2^+$, $C_3N_3O^+/H_2C_4N_2O^+$, $H_4C_4N_3O^+$, $[G\text{-}NH_2]^+$, and $[G+H]^+$ for Guanine. For Adenine H^- and CN^- are the only anion fragments desorbed, however H^-, O^-, and CN^- are observed upon ion irradiation of Guanine. Moreover for adenine, the major negative fragment, CN^-, desorbs at much lower incident ion energy than the positive fragments formed by ion irradiation. Using isotopically labeled molecules (Guanine-8-^{13}C and Adenine-8-^{13}C) the site specificity of the fragments involving chemical bond cleavage at the C8 site has been revealed. From these results, it appears that the C8 site in both molecules is very sensitive and vulnerable to both ion and electron impact at energies as low as 15 eV in the ion irradiation case, in particular at the endocyclic C8-N7 and C8-N9 bonds.

Keywords: DNA purine bases, low energy, Ion impact, condensed phase, electron impact, gas phase

I have contributed to 60% of the experimental work, 100 % of the data analysis including preparation of all figures and 100% writing of this work up to present version.

Introduction

When ionizing radiation interacts with biological tissue, a nascent cascade of events unfolds leading to mutagenic effects in the DNA of the living cell[1]. As ionizing radiation traverses the cell, the primary particles induce ionization, excitation and fragmentation by loss of energy in multiple steps causing DNA and RNA lesions in the cell. It has been established that a large part of this damage is not the mere effect of the high energy incident particles (e.g. proton therapy or heavy ion therapy beam), but stems from secondary species, i.e. secondary ions, electrons and neutrals induced along the ionization track of the primary particles or near its track-end[1,2]. Since they occur abundantly and in close vicinity of each other, ionization and fragmentation of DNA components such as nucleobases and sugars can lead to more complex types of damage such as single strand breaks (SSB) and double strand breaks (DSB) and clusters of such lesions have been shown to be potentially lethal and extremely difficult to repair for the cell[3,4,5,6,7,8].

Therefore, hyperthermal heavy ions are of significant importance in the study of radiobiological damage since these particles (either as primary at the end of ionization track or as secondary) are known to be capable of inducing the most severe damage to the cell nucleus. For particles beams of such kinetic energies, the linear energy transfer to the biological medium is the highest, and hence the maximum damage is induced. Such low energy ions can be produced via different mechanisms during exposure to ionizing radiation. Auger decay of core ionization, e.g. by soft X-rays, can result in production of positive fragments with energies up to 15 eV[9,10]. Moreover, during hadron therapy, singly or multiply charged secondary atomic cations such as N^+, C^+, or O^+ are abundantly

produced with energies ranging form 10 to hundreds of eV as a consequence of high energy primary ion impact on nucleobases[11,12]. It has been demonstrated in previous studies that these hyperthermal heavy ions have the potential to induce severe damage in DNA and RNA subunits (e.g. sugars) by physical and physico-chemical mechanisms, such as reactive scattering over short distances[13], and hence are of significant biological importance.

The present work investigates ionization and fragmentation pathways of the two DNA purine bases, Adenine (A) and Guanine (G) (Figure 1) by low energy (1-100 eV) Ar^+ ion interaction with films of these molecules. In DNA, each purine base is attached to a sugar molecule and phosphate unit and is complemented with a pyrimidine base (cytosine with guanine and thymine with adenine). Here, detailed mass spectroscopy measurements are presented, comparing the resulting ion stimulated desorption (ISD) spectra of the two purine molecules to each other. Moreover these spectra are compared to the fragmentation mass spectra obtained for these nucleobases by 70 eV electron impact in the gas phase, and the chemical fragment identification is performed using isotopically labeled purine bases.

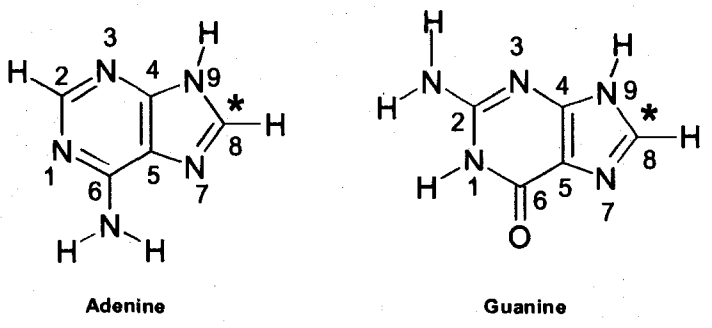

Figure 1. *Molecular Structure of Guanine and Adenine. The asterisk indicates where the molecules were labeled with ^{13}C. (color online)*

Experimental Methods

The experiments were performed on an ion beam apparatus developed in-house[14], to be described in details elsewhere. A low energy ion source is used to generate positive ions with the energies of interest (1-500 eV). Using sets of electrostatic lenses, a highly focused mass and energy resolved beam is delivered into a UHV (10^{-9} Torr) reaction chamber, where sample films are irradiated. In order to monitor the desorbing positive and negative fragments upon ion irradiation, a high resolution quadrupole mass spectrometer (QMS) (Hiden Analytical Ltd.) is installed perpendicular to the ion beam system line. The QMS is optimized to detect desorbing ionic fragments with kinetic energies in the 0-5 eV range. The sample is placed 2 cm from both the mass spectrometer and the exit of the ion beam line, in the center of the reaction chamber, with the incident beam at 30°, and a 60° QMS collection angle both with respect to the sample surface.

In the current work, the focus in mainly on 10-100 eV Ar^+ ion irradiation of adenine (A) and guanine (G) films on a Pt substrate. Films of Ade and Gua are prepared by *in vacuo* evaporation from an oven onto an atomically clean polycrystalline Pt substrate held at room temperature (20-24 °C). The substrate is cleaned by resistive heating to 1000 °C prior to film deposition. Furthermore the condensation rates of the two purine bases are calibrated using a quartz crystal microbalance (QCMB) to within 0.5 ng. cm^{-2}. The evaporation temperatures of the purine compounds ($\leq$ 150°C) are kept well below their decomposition temperature of ~320 °C. The base pressure of the target chamber is kept at ~2 $\times 10^{-9}$ Torr during the experiments.

In order to perform the electron impact experiments, the QMS is operated in the residual gas analyzer (RGA) mode to ionize neutral molecules in the gas phase. The

results presented in this paper for gas phase adenine and guanine were taken in this mode, with electron collision energy set at 70 eV. Prior to these experiments, the UHV system was baked and the each sample was degassed in the load-lock chamber in order to minimize the RGA background signal (mostly consisting of H^+ and H_2O^+). A few micrograms of sample is deposited on the Pt substrate and is subsequently placed in front of the QMS entrance. The substrate is then heated up to 200°C so that the sample molecules evaporate from the Pt substrate into the mass spectrometer, to be subjected to electron impact. A background spectrum taken immediately before the film evaporation into the QMS, and is subtracted from the guanine and adenine mass spectra presented in this work.

To assist chemical identification of the fragment channels, Guanine-8-^{13}C and Adenine-8-^{13}C (from ISOTEC 99% ^{13}C isotopic purity) were also utilized in the current experiments.

Results and Discussion.

Both electrons and Ar^+ ions induce positive fragment formation upon bombardment of adenine and guanine. Figure 2.a and Figure 3.a show the mass spectra for positive ion stimulated desorption (ISD) produced by 100 eV Ar^+ -ion irradiation of 200-ng/cm^2 of unlabeled adenine and guanine respectively. The major cation fragments resulting from the guanine experiment are assigned as, H^+, NH_4^+, $HNCH^+$, $HCN_2H_2^+/HNCO^+$, HC_2NO^+, $C_2N_2O^+$, $H_2C_3N_2O^+/HC_3N_3H_2^+$, $C_3N_3O^+/H_2C_4N_2O^+$, $H_4C_4N_3O^+$, the deamination product $[G\text{-}NH_2]^+$, the parent cation $[G+H]^+$,and aminated guanine $[G\text{-}NH_2]^+$. Significant anion fragments produced are H^-, O^-, and CN^-. In order to chemically identify each fragment

and its site of origin, the mass spectra of guanine and that of labeled guanine (Guanine-8-^{13}C) have been compared during both ion irradiation in the condensed phase, and electron impact (70 eV) in the gas phase. For the electron impact measurements, a low-profile electron impact ionizer of the QMS is used to obtain the fragmentation pattern of unirradiated thermally desorbing films of guanine and adenine.

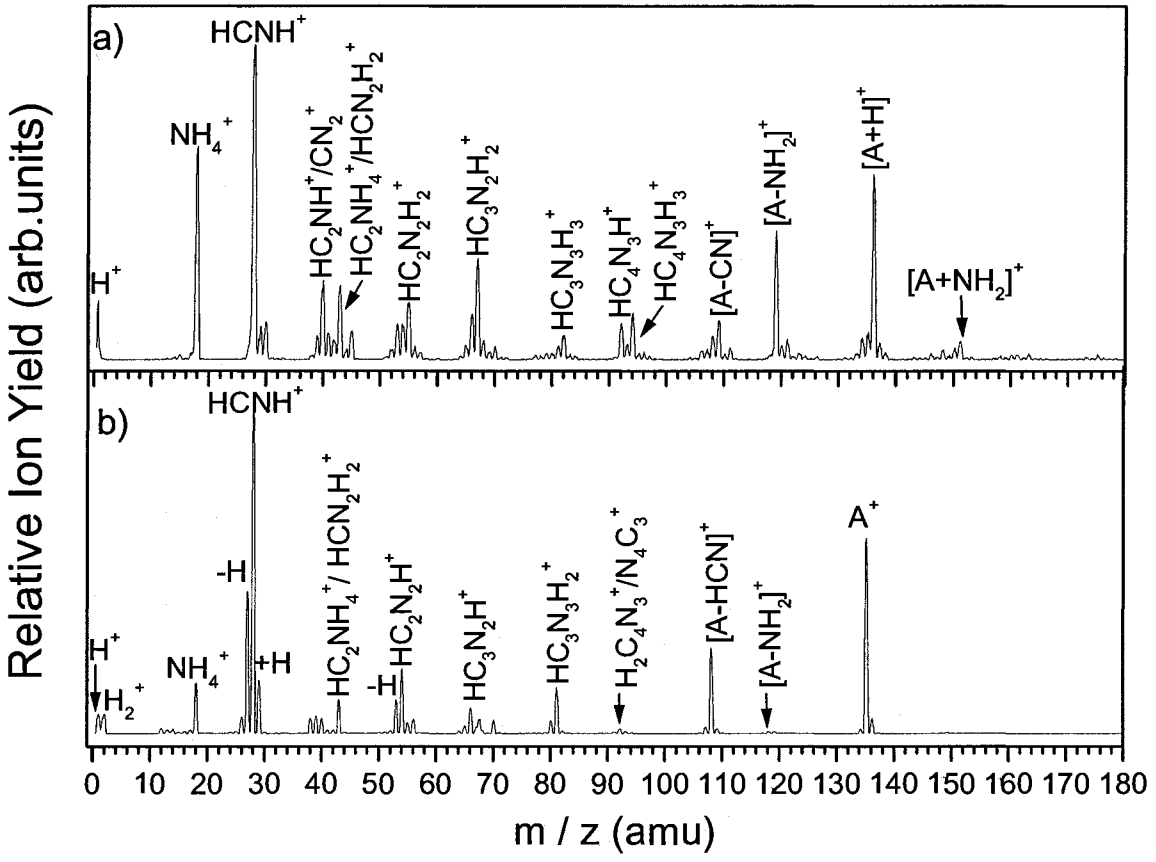

Figure 2: *Global positive ion fragmentation spectrum induced by (a) 100 eV Ar^+ ion irradiation of 200 ng.cm^{-2} adenine films on a Pt substrate and (b) 70 eV electron impact in the gas phase.*

For adenine irradiation by Ar^+ the major desorbing cation fragments as, H^+, NH_4^+, $HNCH^+$, HC_2NH^+/CN_2^+ , $HC_2NH_4^+/HCN_2H_2^+$, $HC_2N_2H_2^+$, $HC_3N_2H_2^+$, $HC_3N_3H_3^+$,

$HC_4N_3H^+$, $HC_4N_3H_3^+$, $H_5C_4N_4^+/H_3N_5C_3^+$, $[A\text{-}NH_2]^+$, $[A+H]^+$, and the amination product $[A+NH_2]^+$. Major negative ions desorbing are H^- and CN^-. Protonation of the parent cation is observed during ion irradiation of both adenine and guanine in the condensed phase.

Figure 2.b and Figure 3.b demonstrate the global positive ion fragmentation pattern produced by 70 eV electron impact in the gas phase from adenine and guanine respectively. Major fragments produced by 70 eV electron impact on adenine in the gas phase include: H^+, H_2^+, NH_4^+, $HNCH^+(\pm H)$, $HC_2NH_4^+/HCN_2H_2^+$, $HC_2N_2H^+(\pm H)$, $HC_3N_2H^+$, $HC_3N_3H^+$, $[A\text{-}HCN]^+$, $[A\text{-}NH_2]^+$, A^+, and similarly for Guanine.

Adenine fragmentation products by ion impact

Figure 6 shows the close ups for mass spectra of fragments produced by 100 eV Ar^+ ion irradiation of (a) unlabeled and (b) labeled adenine in the condensed phase. In the 20-30 mass range, the major peak (28 amu) assigned to $HCNH^+$ with a total of nine different arrangements of C-N sites available in the adenine molecule for the formation of this fragment. Looking at the close up of this fragment in the labeled adenine spectrum (Fig.6.b) this peak partly shifts to 29 amu indicating major contribution from $^{13}C8$, N7 or N9 sites in the molecule.

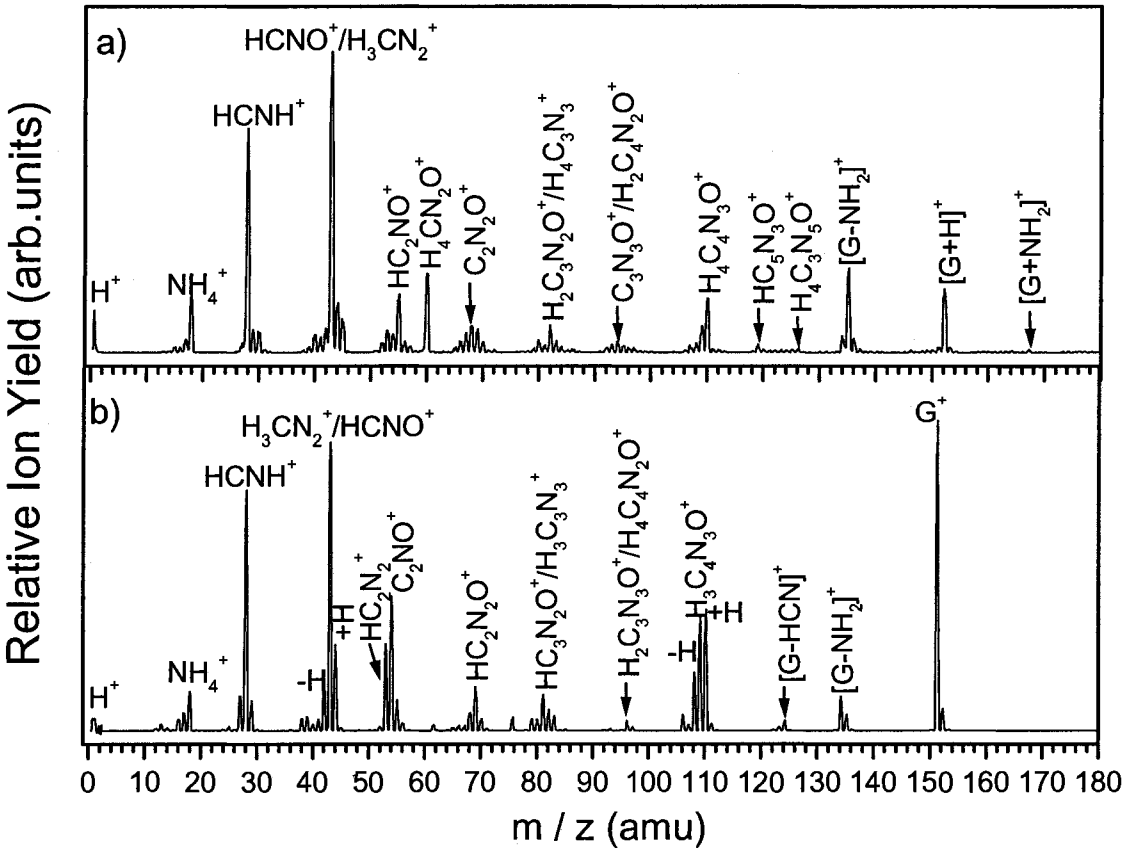

Figure 3: : *Global positive ion fragmentation spectrum induced by (a) 100 eV Ar^+ ion irradiation of 200 ng.cm^{-2} guanine films on a Pt substrate and (b) 70 eV electron impact in the gas phase.*

In the 35-45 amu mass range, fragments 40 amu, HC_2NH^+/CN_2^+ , and 43 amu, $HC_2NH_4^+/HCN_2H_2^+$, dominate the spectrum. Fragment 40 amu partly shifts to 41 amu ($H^{13}C_2NH^+/^{13}CN_2^+$), while fragment 43 amu stays nearly unchanged.

In the 50-60 amu range, fragment 55 amu ($HC_2N_2H_2^+$) appears as the most intense peak, slightly shifting to 56 amu ($H^{13}C_2N_2H_2^+$) in the labeled adenine spectrum.

Looking at the 60-70 amu mass range, the peak at 67 amu ($HC_3N_2H_2^+$) dominates as the major peak, moving to 68 amu ($H^{13}C8C_2N_2H_2^+$) in the labeled adenine spectrum, implying the involvement of the C8 site in the molecule, as well as bond cleavage

between C5 and C6 together with C4 and N3, resulting in liberation and desorption of the protonated five membered ring ($HC_3N_2H_2^+$). The complementary fragment, $HC_2N_2^+$ (53 amu), is also observed as a relatively small peak in the ion desoption mass spectra.

The formation of fragment 82 amu ($HC_3N_3H_3^+$) appears the most intense in the family of peaks at 70-85 amu, and shifts significantly to 83 amu ($H^{13}C_3N_3H_3^+$) in the labeled adenine spectrum.

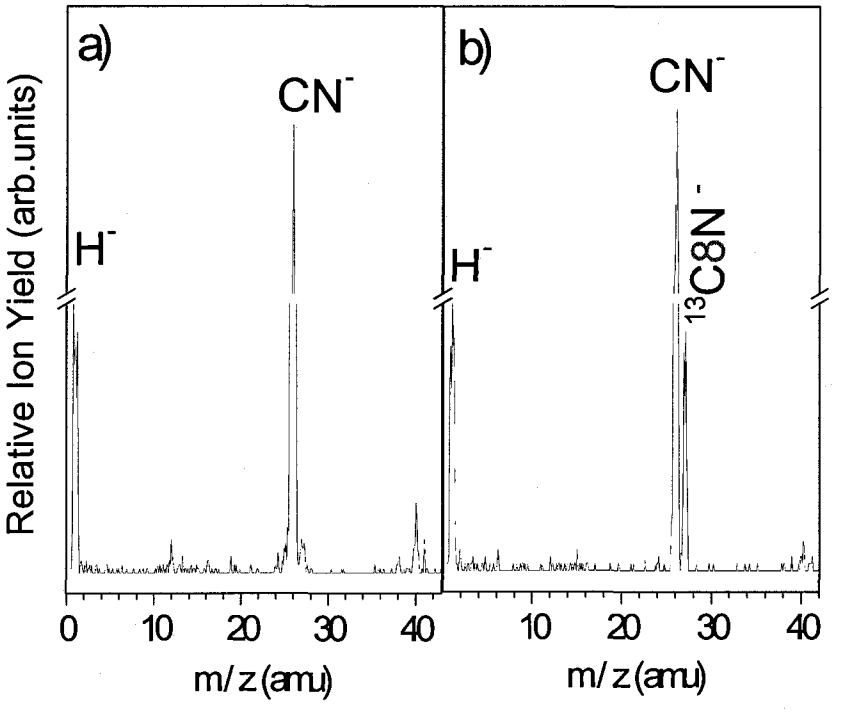

Figure 4: *Negative ion desorption spectrum of (a) Unlabeled and (b) Labeled adenine by 100 eV Ar^+ ion impact in the condensed phase.*

In the 90-100 amu range, fragments 92 amu ($H_2C_4N_3^+$) and 94 amu ($HC_4N_3H_3^+$) appear as the most intense, shifting to 93 amu ($H^{13}C_4N_3H^+$) and 95 amu ($H^{13}C_4N_3H_3^+$),

respectively, in the labeled adenine spectrum. Fragment 93 amu in the unlabeled adenine spectrum (Fig.6.a) corresponds to the six membered ring ($C_4N_3H_3^+$) of the adenine molecule. This peak appears to be small, suggesting high probability of desorption of this fragment as a neutral, with a possibility of fragment 43 amu ($HCN_2H_2^+$) being its protonated complementary fragment.

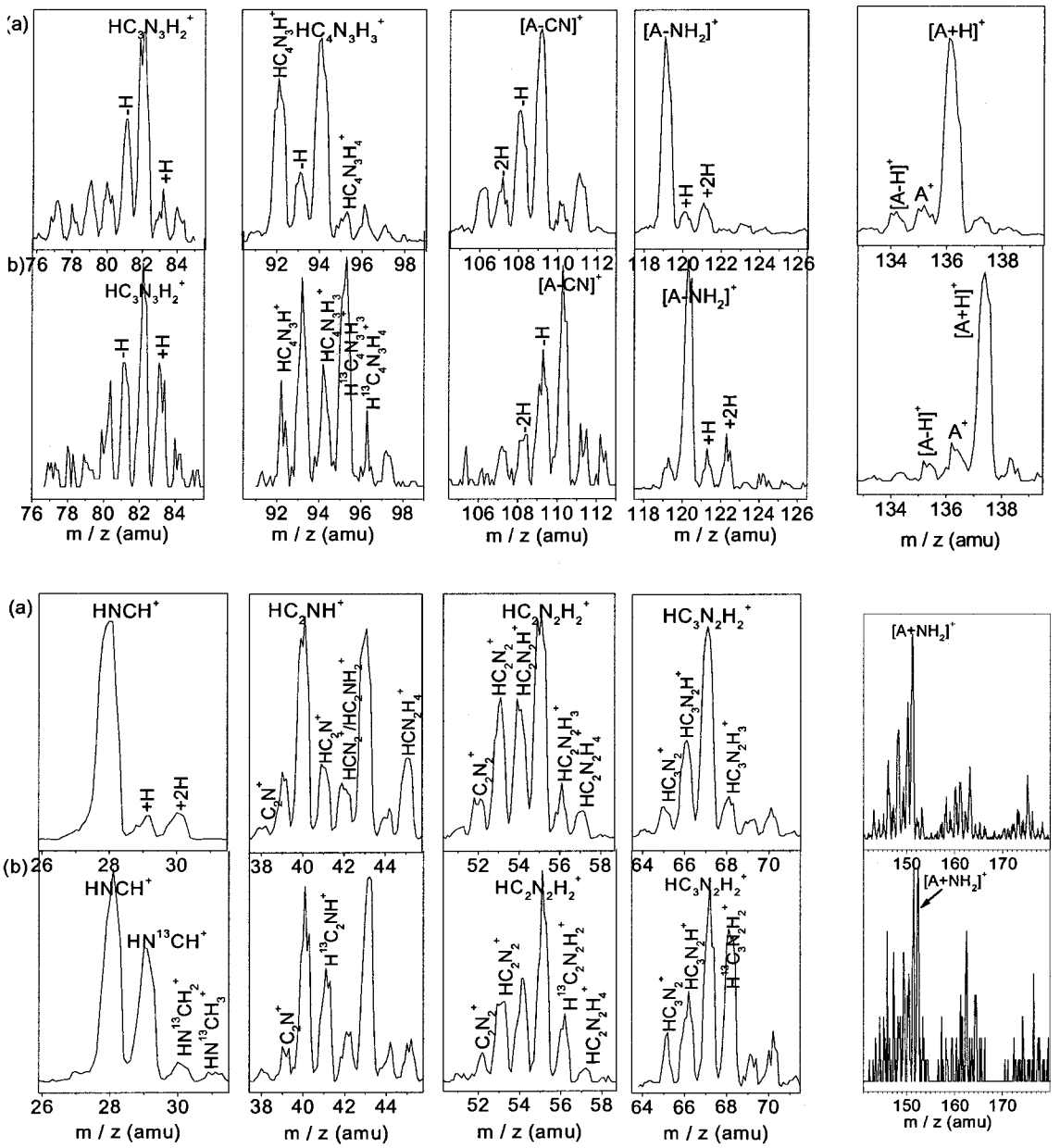

Figure 6: *Close up of positive fragment spectra induced by 100 eV Ar^+ ion impact on (a) Unlabeled and (b) Labeled adenine.*

In the 100-115 amu range, fragment 109 amu, $[A\text{-}CN]^+$, is most intense, and almost entirely shifts to 110 amu, implying that the loss of CN is not from the C8 site in the adenine molecule.

In the 115-125 amu range, fragment 119 amu, $[A\text{-}NH_2]^+$, is the most intense corresponding to deamination of adenine molecule by heavy ion impact. This fragment shifts to 120 amu in the labeled adenine spectrum as expected.

In the 130-140 amu range, fragment 135 amu, $[A+H]^+$, is the most intense peak, and the parent cation desorbs protonated, and shifts to 136 amu in the labeled adenine spectrum as expected.

Adenine fragmentation products by electron impact

Figure 7 demonstrates the close ups for cation mass spectrum for (a) unlabeled and (b) labeled adenine produced by electron impact in the gas phase. Major differences between the electron impact and ion impact spectra appears at mass 40 amu ($H_2C_2N^+$) which appears as a major fragment in the ion impact desorption spectrum. Moreover fragments 67 amu ($H_3C_3N_2^+$) and 92 amu ($H_2C_4N_3^+$), 94 amu ($H_4C_4N_3^+$), and 119 amu ($[A\text{-}NH_2]^+$) also emerge with much higher intensity in the ion impact spectrum (Fig.2a), as compared to the electron impact spectrum in the gas phase. The parent cation however appears most intense in the electron impact measurements (Fig.2b).

The most remarkable difference between the two spectra (Fig.2a and Fig.2b) is however the emergence of peaks after the parent cation in ion impact spectrum as $[A+NH_2]^+$ molecule which is synthesized from the adenine molecule and an amino group following ionization and fragmentation by ion impact in the condensed films.

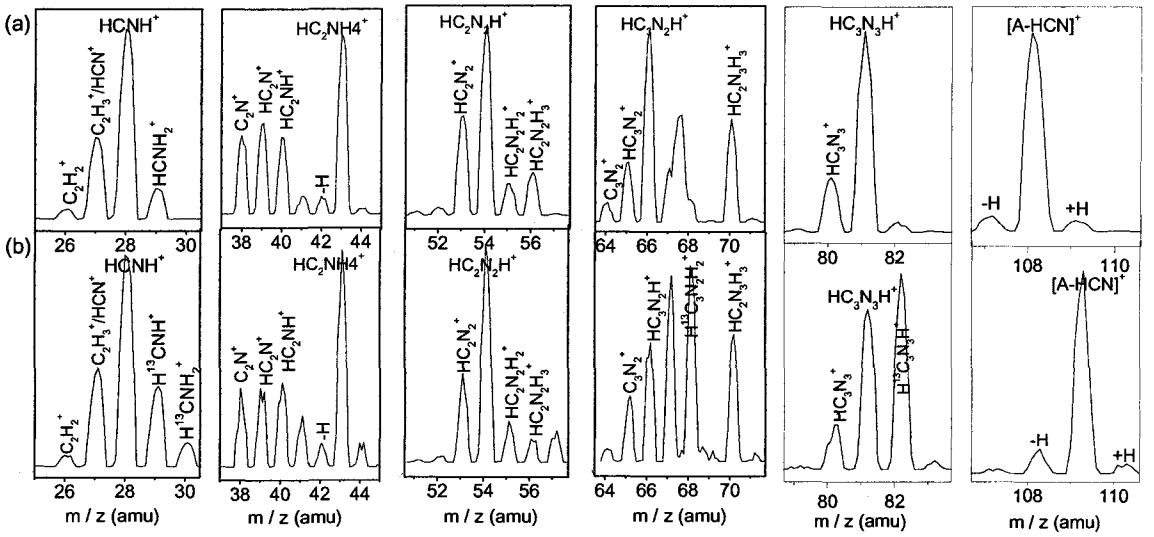

Figure 7: *Close ups of 70 eV electron impact measurements on (a) unlabeled and (b) labeled adenine.*

Guanine fragmentation products by ion impact

Figure 3.a shows the typical cation mass spectra of ion stimulated desorption of 200 ng.cm^{-2} films of unlabeled guanine by 100 eV Ar^+ ion irradiation.

Figure 5 demonstrates the negative fragments desorbed from guanine films as a result of ion irradiation. We observe the formation of H^-, O^- and CN^- ions as a result of 100 eV Ar^+ ion irradiation of films of unlabeled guanine spectrum (Fig 56.a), and a clear shift of CN^- fragment (26 amu) to $^{13}C8N^-$ (27 amu) in the labeled guanine spectrum (Fig.5.b). Fragment CN^-(26 amu) partly remains at 26 amu in the labeled guanine spectrum, indicating formation of the fragments from C, N sites other than the $^{13}C8$ position.

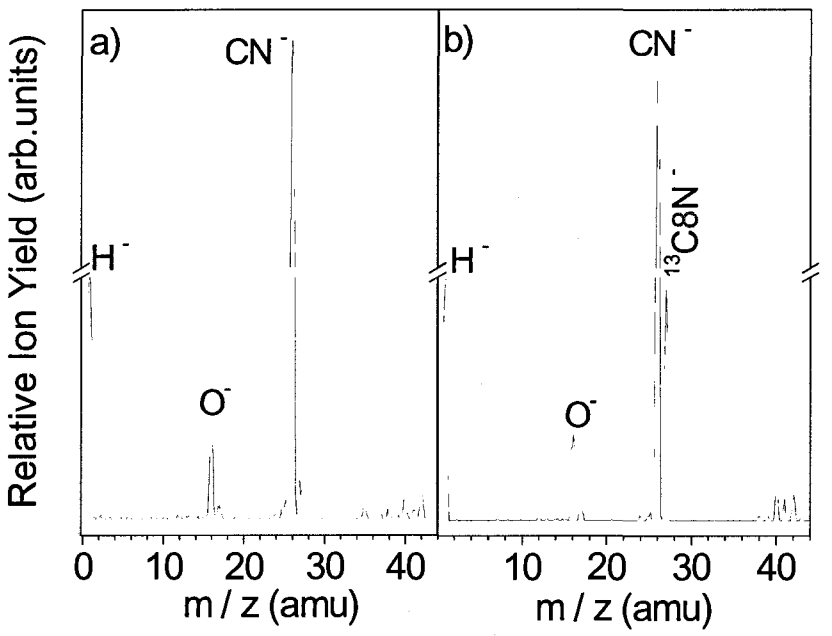

Figure 5: *Negative ISD spectrum of (a) Unlabeled and (b) Labeled guanine by 100 eV Ar^+ ion impact measurements.*

Looking at the close ups of the unlabeled and labeled guanine produced by ion impact in the condensed phase, Figure 9 (a) and (b) respectively, fragment 28 amu ($HCNH^+$) is the most intense peak, shifting mostly to 29 amu ($H^{13}CNH^+$), signifying the sensitivity of C8 in guanine molecule.

In the 30-40 amu mass range, fragment 41 amu, HCN_2^+, appears the most intense and remains almost unchanged in the labeled guanine spectrum, thus not involving the C8 position.

In the 50-60 amu range, fragments 55 amu and 60 amu are most prominent corresponding to $HC_2NOH_3^+$ and $HCN_2OH_3^+$ respectively.

Between 62 and 75 amu, fragment 68 amu is assigned to $C_2N_2O^+$ and appears with the highest intensity (Fig.9.a), remaining unchanged in the labeled guanine spectrum (Fig 9.b).

In the 75 to 90 amu range, $H_2C_3N_2O^+/HC_3N_3H_3^+$ (82 amu) is the most significant fragment and shifts to 83 amu revealing involvement of the $^{13}C8$ site in formation of this cation.

From 90 to 100 amu, $C_3N_3O^+/H_2C_4N_2O^+$ (94 amu) appears as the major cation fragment (Fig.9.a) and moves to 95 amu in Fig.9.b revealing the presence of $^{13}C8$ atom in the composition of this fragment.

Between 100 to 115 amu, the most intense fragment, $H_4C_4N_3O^+$ (110 amu), makes a clear shift to 111 amu due to the role of $^{13}C8$ in this fragment. Fragment 109 amu mostly remains unshifted corresponding to the entire six membered ring, $H_3C_4N_3O^+$, which does not contain the carbon position eight.

Peak 135 arises from deamination of Guanine by ion impact as a $[G\text{-}NH_2]^+$ (Fig.9.a) fragment, and shifts to 136 amu in labeled guanine spectrum (Fig.9.b) as expected.

Moreover Fig.9.a demonstrates the protonated parent peak for the guanine molecule, $[G+H]^+$ (152 amu), which expectedly makes a one amu shift in the labeled guanine spectrum (Fig.9.b).

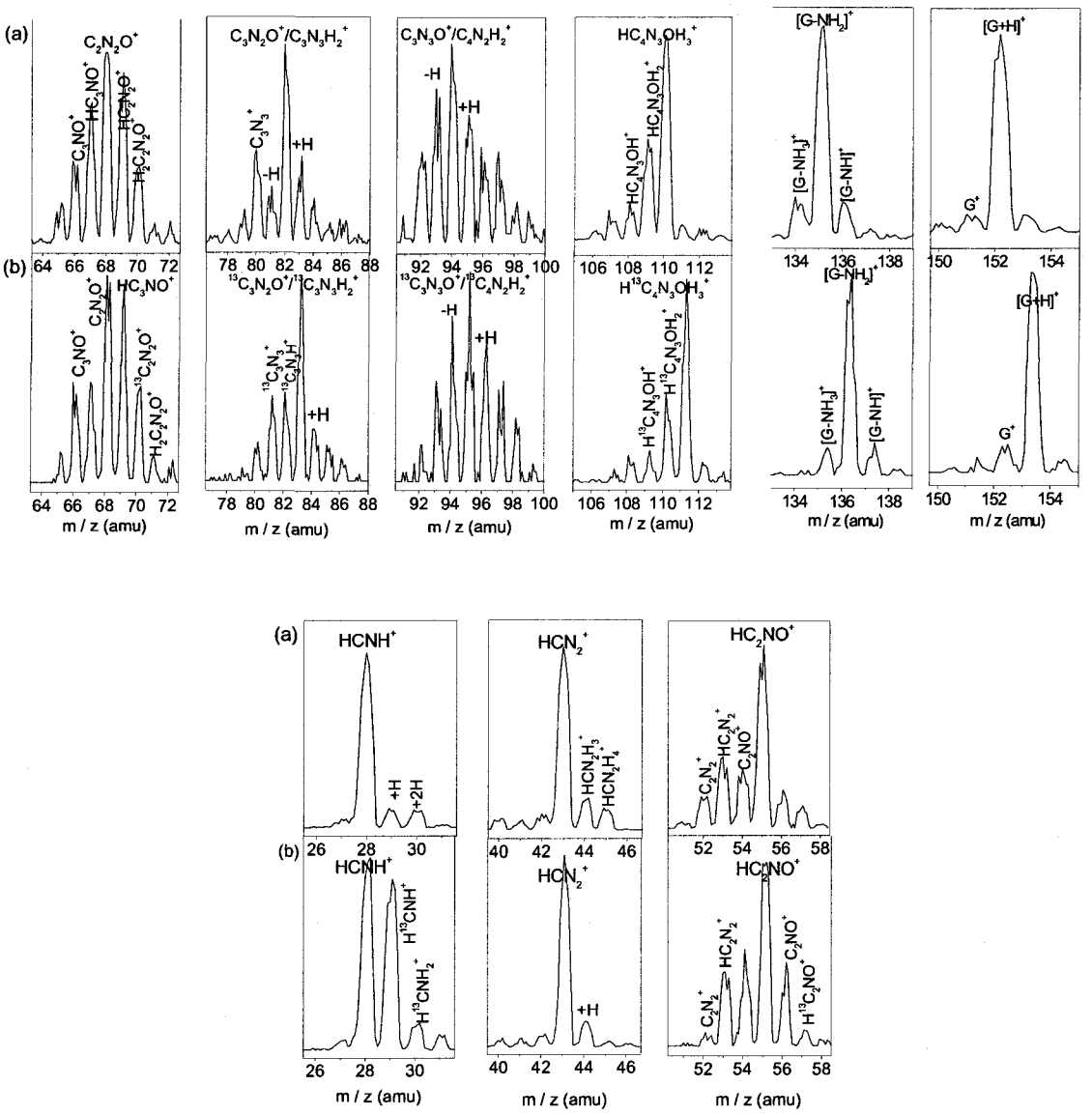

Figure 9: *Detailed positive ion fragment spectra induced by 100 eV Ar^+ ion impact on (a) Unlabeled and (b) Labeled guanine.*

Guanine fragmentation products by electron impact

As shown in Figure 8, the close ups for the fragmentation pattern induced by 70 eV electron impact of guanine molecules in the gas phase contains H^+, NH_4^+,

$HNCH^+(\pm H)$, $H_3CN_2^+/HCNO^+(\pm H)$, C_2NO^+, $HC_2N_2O^+$, $HC_3N_2O^+/HC_3N_3H_2^+$, $H_2C_3N_3O^+/H_4C_4N_2O^+$, $H_4C_4N_3O^+(\pm H)$, $[G\text{-}HCN]^+$, $[G\text{-}NH_3]^+$, G^+.

Overall, below 60 amu, the 70 eV electron impact mass spectrum of guanine is very similar to that of 100 eV Ar^+ ion impact of condensed films of this molecule. However the ion impact fragmentation pattern (Fig.3a) shows a major difference at 60 amu ($H_4CN_2O^+$). Fragments $[G\text{-}NH_2]^+$ and NH_4^+ appears more pronounced in the ion irradiation spectrum of guanine (Fig.3a) compared to the electron impact spectrum, while the parent cation, G^+, emerges with much higher intensity in the electron impact fragmentation pattern (Fig.3b).

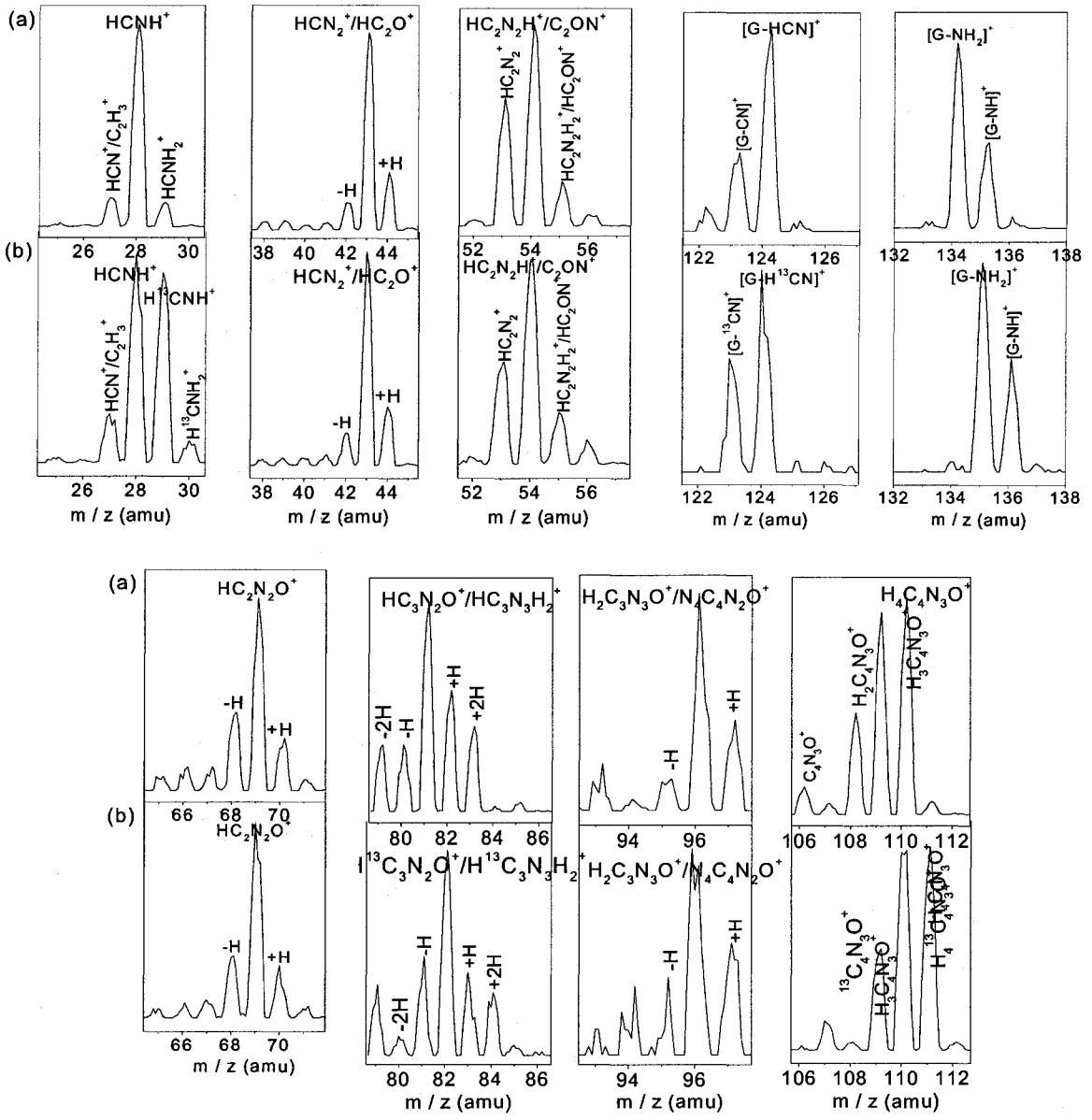

Figure 8: *Detailed presentation of positive fragment patterns induced by 70 eV electron impact on (a) Unlabeled and (b) Labeled guanine.*

Ion fragment formation and desorption thresholds

Figure 10.a shows the desorption energy thresholds for typical positive and negative ion fragments induced by Ar^+ ion irradiation of Adenine films. Major cation and

anion fragments in the mass spectrum induced by ion irradiation (Figure 2.a) up to 119 amu indicate endocyclic bond cleavage, while the fragments $[A\text{-}NH_2]^+$ and $[A+H]^+$ arise from exocyclic bond cleavage of adenine molecule. Most cation fragments appear at ~25 eV, except $HNCH^+$ and $[A+H]^+$ which appear at ~ 15 and 20 eV, respectively. The most intense anion fragment, CN^-, appears at ~15 eV.

Figure 10.b represents the desorption energy thresholds for ion induced fragments of films of guanine. Cation fragments $HCN_2H_2^+/HNCO^+$, $HCN_2OH_3^+$, $[G\text{-}H]^+$ appear at ~15 eV, $HNCH^+$, $[G\text{-}NH_2]^+$, and CN^- appear at ~20 eV, while HC_2NO^+ arises at ~25 eV and O^- appears much higher energy than the cation fragments (~30 eV).

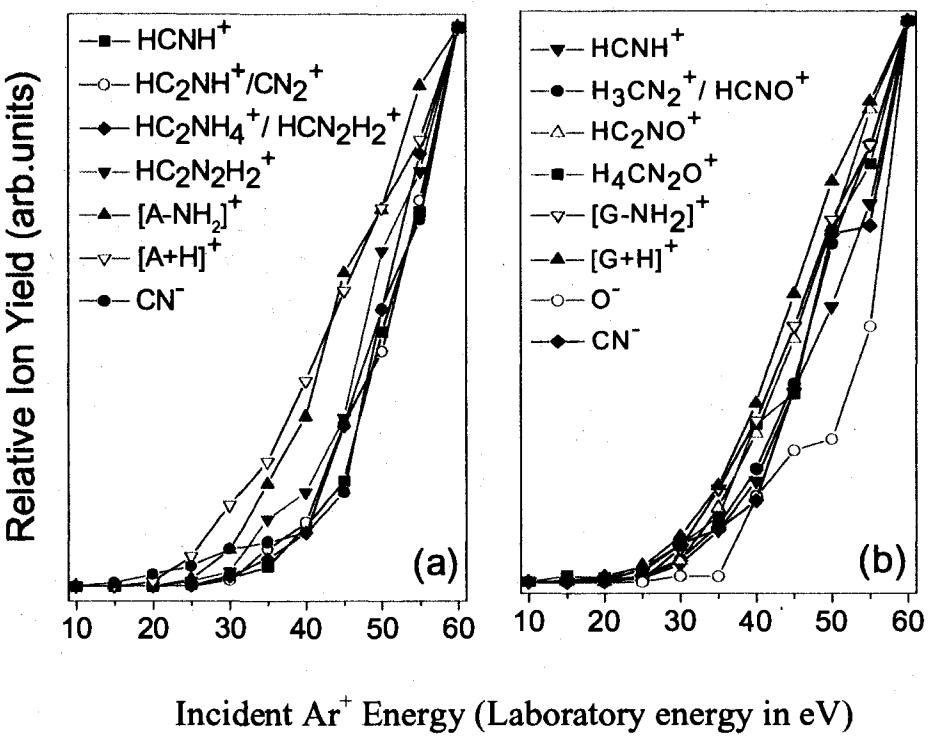

Figure 10: *Ion desorption energy thresholds for cation and anion fragments induced by Ar^+ ion irradiation of 200 ng.cm^{-2} films of (a) Adenine and (b) Guanine on a Pt substrate. Ion yields are normalized to the intensity at 60 eV.*

Summary and Conclusions

In order to investigate the radiation damage induced in DNA purine bases by heavy ions, with energies similar to those of secondary ions, or track-end ions, we have conducted a series of studies on ionization and fragmentation of adenine and guanine films in the condensed phase by very low-energy ions. The degradation of adenine and guanine films has been observed by monitoring the desorbing positive and negative fragments using mass spectroscopy. The most intense observed fragments include H^+, NH_4^+, $HNCH^+$, HC_2NH^+/CN_2^+ , $HC_2NH_4^+/HCN_2H_2^+$, $HC_2N_2H_2^+$, $HC_3N_2H_2^+$, $HC_3N_3H_3^+$, $HC_4N_3H^+$, $HC_4N_3H_3^+$, $H_5C_4N_4^+/H_3N_5C_3^+$, $[A\text{-}NH_2]^+$, $[A+H]^+$, and $[A+NH_2]^+$, H^- and CN^- for Adenine, and H^+, NH_4^+, $HNCH^+$, $HCN_2H_2^+/HNCO^+$, HC_2NO^+, $C_2N_2O^+$, $H_2C_3N_2O^+/HC_3N_3H_2^+$, $C_3N_3O^+/H_2C_4N_2O^+$, $H_4C_4N_3O^+$, $[G\text{-}NH_2]^+$, and $[G+H]^+$, H^-, O^-, and CN^- for Guanine. The desorbing ionic fragmentation products were collected using a quadrupole mass spectrometer.

Both in Adenine and Guanine, carbon position 8 (C8) was identified as a sensitive carbon site in these molecules, most evidently by observation of the fragment 28 amu ($HCNH^+$) fragment shifting to 29 amu ($H^{13}CNH^+$) in the ion stimulated desorption spectrum of the C8 labeled compounds.

Other interesting bond cleavage axes are those that yield five membered and six membered ring cleavage, which were identified in the cation desorption spectrum of both molecules as intense $H(C8)C_2N_2H_2^+$ (67 amu), and $C_4N_3H_3^+$ (93 amu) peaks respectively, indicating fragmentation of DNA purine bases by ions with energies below 1 eV/amu.

The protonated parent adenine and guanine molecules were also seen in the ion impact spectra, a phenomenon widely observed in previous ion impact measurements[15,16].

Acknowledgements.

This work has been continuously supported by the Natural Science and Engineering Research Council of Canada, and Canadian Space Agency.

References.

[1] Von Sonntag, C.; *The Chemical Basis for Radiation Biology* (London, Taylor and Francis, 1987).

[2] Cobout,V.; Frongillo,Y.; Patau, J.P.; Goulet, T.; Fraser, M.-J.; Jay-Gerin, J.-P.; *Radiat. Phys. Chem.* 1998, **51**, 229.

[3] Boudaiffa, B.; Cloutier, P.; Hunting, D.; Huels, M.A.; Sanche, L.; Science, 2000, **287**, 1658.

[4] Sanche, L.; *Mass Spectrom. Rev.* 2002, **21**, 349, and references therein.

[5] Huels, M.A.; Hahndorf, I.; Illenberger, E.; Sanche, L.; *J. Chem. Phys.* 1998, **108**, 1309.

[6] Antic, D.; Parentau, L.; Sanche, L.; *J. Phys. Chem.* 2000, B**104**, 4711.

[7] Abdoul-Carime, H.; Huels, M.A.; Illenberger, E.; Sanche, L.; *J. Am. Chem. Soc.* 2001, **123**, 5354.

[8] Antic, D.; Parentau, L.; Sanche, L.; *J. Phys. Chem.* 1999, B**103**, 6611.

[9] Eberhardt, W.; Plummer, E.W.; Lyo, I.-W.; Carr, R. and Dord, W.K.; *Phys. Rev. Lett.*1987, **58**, 207.

[10] LeBrun, T.; Lavollée, M.; Simon, M.; and Morin, P.; *J. Chem. Phys.* 1993, **98**, 2534.

[11] Schlathölter,T.; Hoekstra, R.; and Morgenstern, R.; *Int. J. Mass. Spectrom.* 2004, **233**, 173.

[12] De Vries, J.; Hoekstra, R.; Morgenstern, R.; and Schlathölter, T.; *Phys. Rev. Lett.* 2003, **91**, 053401.

[13] Bald, I.; Deng, Z.-W.; Illenberger, E.; and Huels, M.A.; *Phys. Chem. Chem. Phys.* 2006, **8**, 1215-1222.

[14] Deng, Z.-W.; Imhoff, M.; and Huels, M.A.; *J. Chem. Phys.* 2005, **123**, 144509.

[15] Imhoff, M.; Deng, Z.-W.; and Huels, M.A.; *Int. J. Mass. Spectrom.* 2005, **245**, 68-77.

[16] Deng, Z.-W.; Bald,I.; Illenberger, E.; and Huels, M.A.; *Phys. Rev. Lett.* 2005, **95**, 153201.

3.4. Ion Beam measurements

I. Ar^+ and Xe^+ ion and electron impact of 5-Aminouracil

Figure 10 shows the results for cation desorption mass spectrum, of 100 eV (a) Ar^+ (40 amu) (b) Xe^+(136 amu) irradiation of 800 ng.cm^{-2} films of 5-Aminourail and (c) 70 eV electron impact on 5-Aminouracil. Major fragmentation products of 5-Aminouracil molecular films in the condensed phase upon 100 eV Ar^+ ion irradiation include H^+, CH_3^+, NH_4^+, $HCNH^+$, H_2CNH^+, H_3CNH^+, $C_2NH_4^+$, $HCNO^+$, $H_2C_2NO^+$, $H_3C_3NO^+$, $H_3C_3N_2O^+$, $H_3C_4N_2O^+$, $[5\text{-AU-}NH_2]^+$, and the protonated parent cation $[5\text{-AU+H}]^+$. Significant cations desorbed upon 100 eV Xe^+ bombardment of 5-Aminouracil films are, H^+, CH_3^+, NH_4^+, $HCNH^+$, H_2CNH^+, H_3CNH^+, $C_2NH_3^+$, H_2CNO^+, $H_2C_2NO^+$, $H_3C_3NO^+$, $H_3C_3N_2O^+$, $H_3C_4N_2O^+$, $[5\text{-AU-}NH_2]^+$, $[5\text{-AU}]^+$ and $[5\text{-AU+H}]^+$. The fragments resulting from 70 eV electron impact measurements on 5-Aminouracil molecules in the gas phase are, H_2^+, NH_4^+, $HCNH^+$, H_2CNH^+, H_2CNO^+, $H_2C_2NO^+$, $H_3C_3NO^+$, $H_4C_3N_2O^+$, and the parent cation $[5\text{-AU}]^+$.

General fragmentation pattern shown in all three spectra indicate families of fragments induced by specific ionization channels. Some fragments such as the parent cation as seen in Figure 10.a and b partially abstracted a hydrogen/proton. Some other fragments desorb without hydrogen addition, e.g. HCN^+. These results demonstrate the difference in proton affinity of individual fragments, and their potential to induce further damage in the surrounding medium by hydrogen/proton transfer following their formation by ionizing radiation. The mass spectrum obtained for 100 eV Xe^+ irradiation of 5-Aminouracil films (Figure 10.b) shows a simpler pattern compared to the fragmentation

pattern induced by 100 eV Ar^+ ion illustrated in Figure 10.a, implying that the heavier the projectile ion, specific fragmentation channels of the molecule appear to be more pronounced. Of major fragmentation pathways, deamination of 5-Aminouracil is observed in all three spectra in Figure 10, as evidenced by the formation of NH_4^+ and $[5AU\text{-}NH_2]^+$ fragments only in Ar^+ and Xe^+ -ion impact of 5-Aminouracil films.

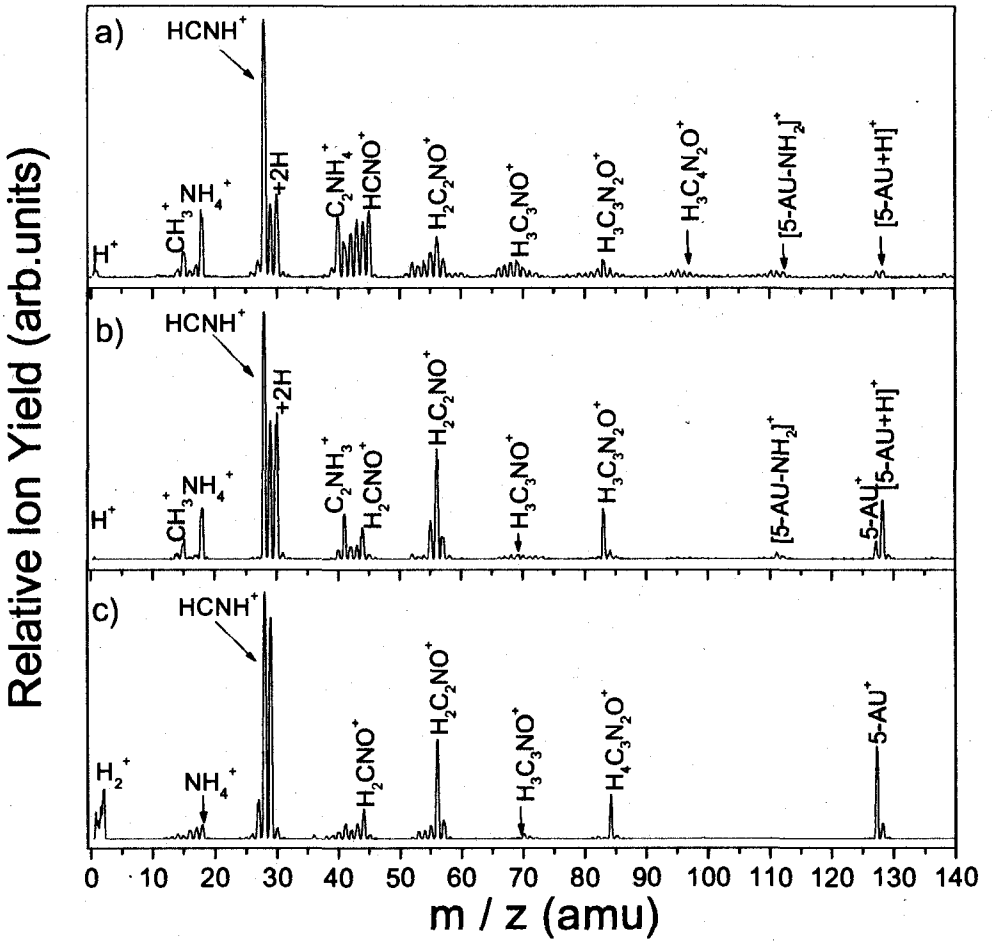

Figure 10. Cation desorption mass spectrum, of 100 eV (a) Ar^+ (40 amu) (b) Xe^+ (136 amu) irradiation of 800 $ng.cm^{-2}$ films of 5-Aminourail and (c) 70 eV electron impact on 5-Aminouracil (Sarabipour *et al*, paper in preparation 2008)

Other significant feature of the spectra presented in Figure 10 include intense emergence of peaks $HCNH^+$(28 amu), H_2CNH^+ (29 amu) in all three spectra and H_3CNH^+/H_2CO^+ (30 amu) in the case of Ar^+ and Xe^+ ion impact. The formation of these three fragments are attributed to bond cleavage at N1-C6 and N5-C5 sites in the 5-Aminouracil molecule (Structure in Figure 2).

Figure 11 demonstrates the mass spectrum of the negative ions desorbed as a result of 100 eV Ar^+ ion irradiation of 800 ng.cm^{-2} films of 5-Aminouracil. Formation of major peaks, H^-, O^-, CN^- (most intensely observed), and CNO^-, are evident from the figure with CN^- appearing as the most intense of negative ionic species. The desorption energy thresholds have been measured for a number of major fragments resulting from Ar^+ ion irradiation of 800 ng.cm^{-2} 5-Aminouracil films. Most cation and anion fragments appear at (15-20 eV) as demonstrated in Figure 12.

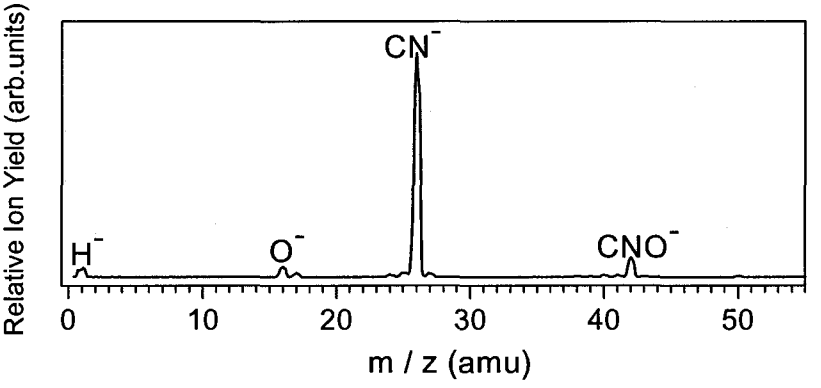

Figure 11. Negative fragmentation pattern induced by 100 eV Ar^+ ion impact on 800 ng.cm^{-2} films of 5-Aminouracil (Sarabipour *et al*, paper in preparation 2008).

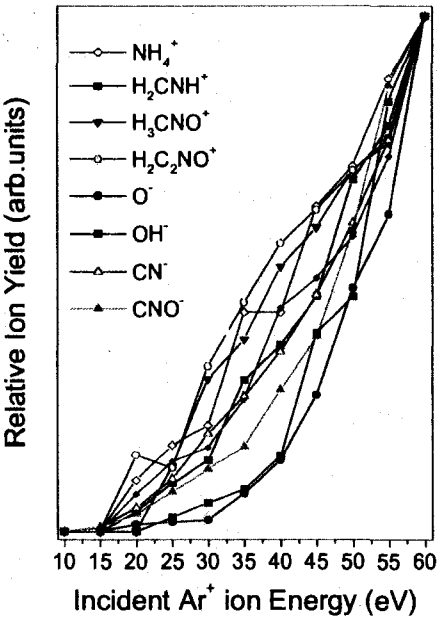

Figure 12. The desorption energy thresholds of typical positive and negative ion fragments produced by Ar^+-ion irradiation of 5-Aminouracil films. The relative ion yields are normalized at 60 eV incident Ar^+-ion energy for ease of comparison (Sarabipour et al, paper in preparation 2008).

Figure 13 demonstrates the close ups for cation desorption mass spectrum, of 100 eV (a) Ar^+ (40 amu) impact on Uracil (b) Ar^+ impact on 5-Aminouracil and (c) Xe^+ (136 amu) irradiation of 800 $ng.cm^{-2}$ films of 5-Aminourail. Fragment CH_3^+ (mass 15 amu) is most intensely observed in Figure 12.b and c (the fragmentation patterns of 5-Aminouracil) indicating a new fragmentation channel assisted by availability of hydrogens from $-NH_2$ group on C5 in 5-Aminouracil molecule (Structure on Figure 2). Moreover, fragment NH_4^+ (mass 18 amu) is only observed in fragmentation patterns of 5-Aminouracil and not in Uracil, indication the explicit involvement of the amino ($-NH_2$) group in the formation of this fragment. These results demonstrate that deamination, a major damage pathway leading to mutations in mammalian cells (Reyes *et al*, 1998), only occurs in nucleobases containing an amino group, namely, Adenine, Guanine and

Cytosine, and none of the ring nitrogens in DNA and RNA bases contribute to this type of damage.

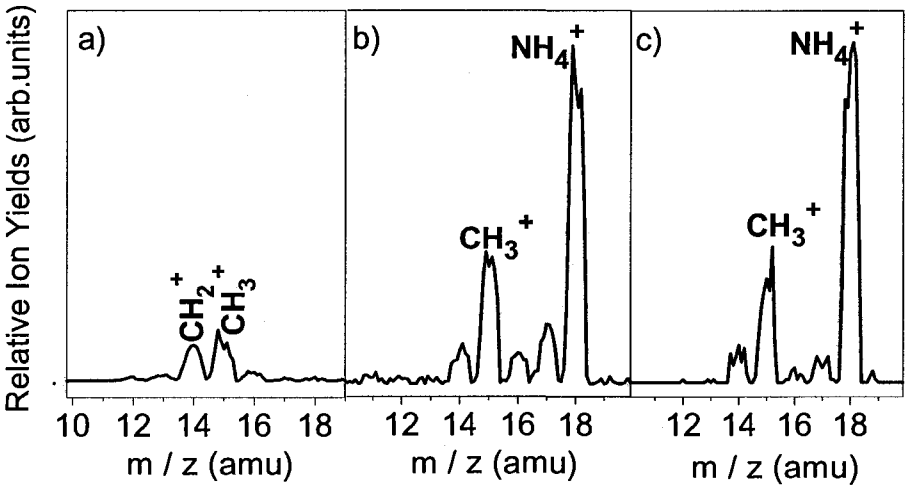

Figure 13. Close ups for cation desorption mass spectrum, of 100 eV (a) Ar^+ (40 amu) impact on Uracil (b) Ar^+ impact on 5-Aminouracil and (c) Xe^+ (136 amu) irradiation of 800 ng.cm^{-2} films of 5-Aminourail (Sarabipour *et al*, paper in preparation 2008).

3.5 Synchrotron measurements

I. Soft X-ray experiments at BL I511

I.1 Degradation-XPS Results

Figure 14 demonstrates the results of the time resolved C (1s) spectra of pure, dry adenine films. Moreover the time dependent C (1s) XPS measurements (Figure 14) demonstrate that contrary to previous published studies to date, films of adenine are extremely sensitive to degradation by core-specific ionizations. The C (1s) XPS

measurements are obtained at very low photon flux (20 μm mono-slit, detuned undulator gap) and high spectrometer sensitivity (Scienta slit at 480 μm) conditions. Comparing these experimental results in the condensed phase to gas phase results published by Plekan *et al.*, (Figure 15) show the low binding energy (high kinetic energy) structure which is associated with the C5 atom in adenine as observed in the gas phase (Plekan *et al,* 2007), is degraded rapidly during the first 10 scans (5.4 sec./scan), making C5 positions a sensitive cleavage site. Only after ~ 10-30 scans (depending on the beam photon flux), under these low flux conditions, the XPS spectra exhibit similar properties as the spectra found in the literature for measurements performed on supposedly undegraded films for extended time durations with SR (Seifert *et al,* 2007; Plekan *et al,* 2007). Figure 15 demonstrates the experimental and theoretical XPS spectrum of gas phase of adenine obtained with 382 eV SR (Plekan *et al,* 2007), the vertical lines demonstrate the energies for five non-equivalent carbon sites on adenine (Structure on Figure 2). According to the theoretical calculations performed by Plekan *et al,* the peak observed at 40.4 eV in our XPS spectra (Figure 14) of the adenine C (1s) spectrum mainly originates from C5 position in adenine molecule (Structure on Figure 2) , while the more intense peak observed at 39 eV in our spectra is a collective contribution of the carbon atoms in positions 2, 4, 6, and 8 in this molecule. Looking at the structure and geometry of adenine molecule (Figure 3), C5 occupies a unique position, bounded to a nitrogen and two carbon atoms. Such uniqueness is noticeable in the XPS spectra by the clearly separated peak observed at 40.4 eV (Figure 14). Notable also that the XPS spectra taken at different angles between the polarization axis of the beam and the surface normal did not show any differences (Vall-llosera *et al,* paper in preparation 2008).

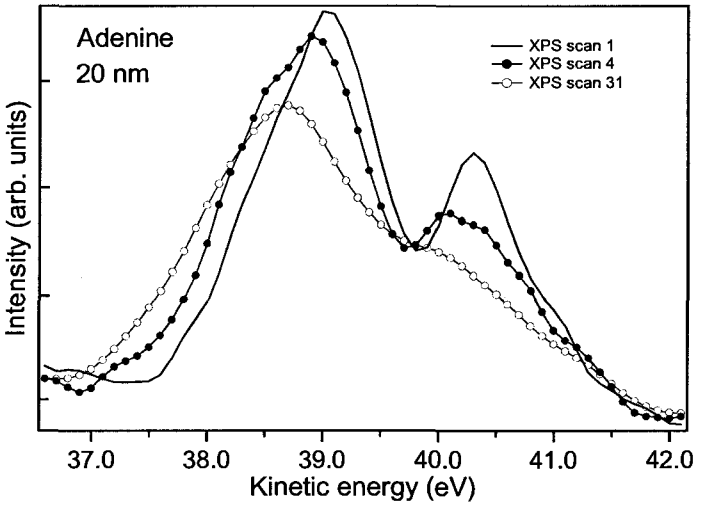

Figure 14. Carbon (1s) XPS spectra of 20 nm films of adenine. The time-evolution of successive scans obtained from a 20 nm adenine film on Si substrate during continuous irradiation with 330 eV SR, each scan takes 5.4 sec, obtained at very low SR flux conditions (Vall-llosera *et al*, paper in preparation 2008).

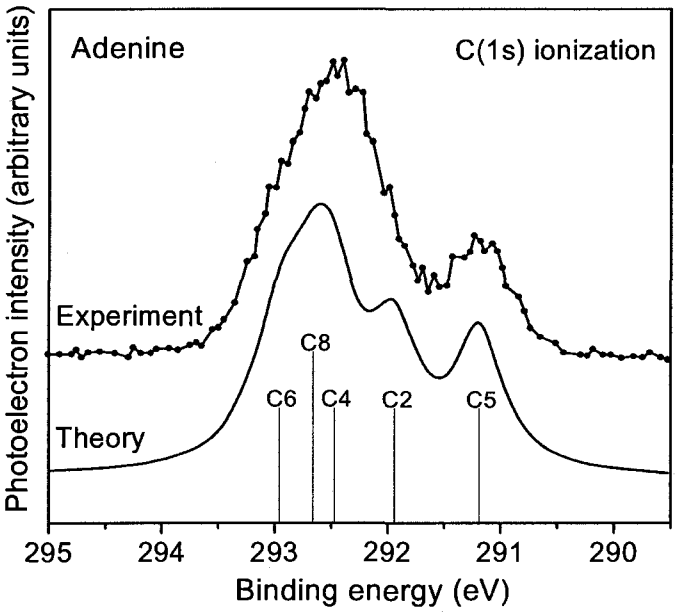

Figure 15. Experimental and theoretical C(1s) XPS spectrum of gas phase of adenine obtained with 382 eV SR (Plekan *et al*, 2007), the vertical lines demonstrate the energies for five non-equivalent carbon sites on adenine (Structure on Figure 2) (Vall-llosera *et al,* paper in preparation 2008).

I.2 Morphology-NEXAFS results

Figure 16 shows the NEXAFS spectra (Auger electron yield) obtained at C(1s) (Figure 16 top) and N(1s)(Figure 16 bottom) edges of adenine molecules upon soft X-ray irradiation of 20 nm adenine films. These observations demonstrate that as the relative intensity ratio between π^* and δ^* orbital resonances changes significantly with changing the orientation of the sample surface with respect to the polarization vector of the beam suggesting that films of adenine are ordered and lie flat/with a very small angle on monocrystalline Si(100) substrate. The polarization vector (Electric field vector) of synchrotron radiation possesses a specific orientation. If this electric field vector is

oriented parallel with respect to the orientation of sigma (σ) orbitals in the adenine molecule (the plane of the ring), the overlap between the wavefunction of the photon and these orbital reaches a maximum value while the overlap with the pi (π) orbitals is minimized, thus σ^* excitation will dominate over π^* excitation. The opposite occurs as the photon polarization angle reaches 90° with respect to the sigma orbitals, and is now parallel with respect to the pi (π) orbital in the molecule. Therefore the NEXAFS results displayed in Figure 16 show that (a) the molecules lie relatively flat on the substrate, and that (b) inter-molecular interaction i.e. π–stacking of adenine molecules at room temperature, lead to highly ordered film bulk even for multilayer films of 10-20 nm thickness. Since this molecular interaction seems to occur throughout the film, not only in the first few layers near the silicon substrate, our ion impact experiments on adenine films on platinum substrate may also involve similarly ordered films.

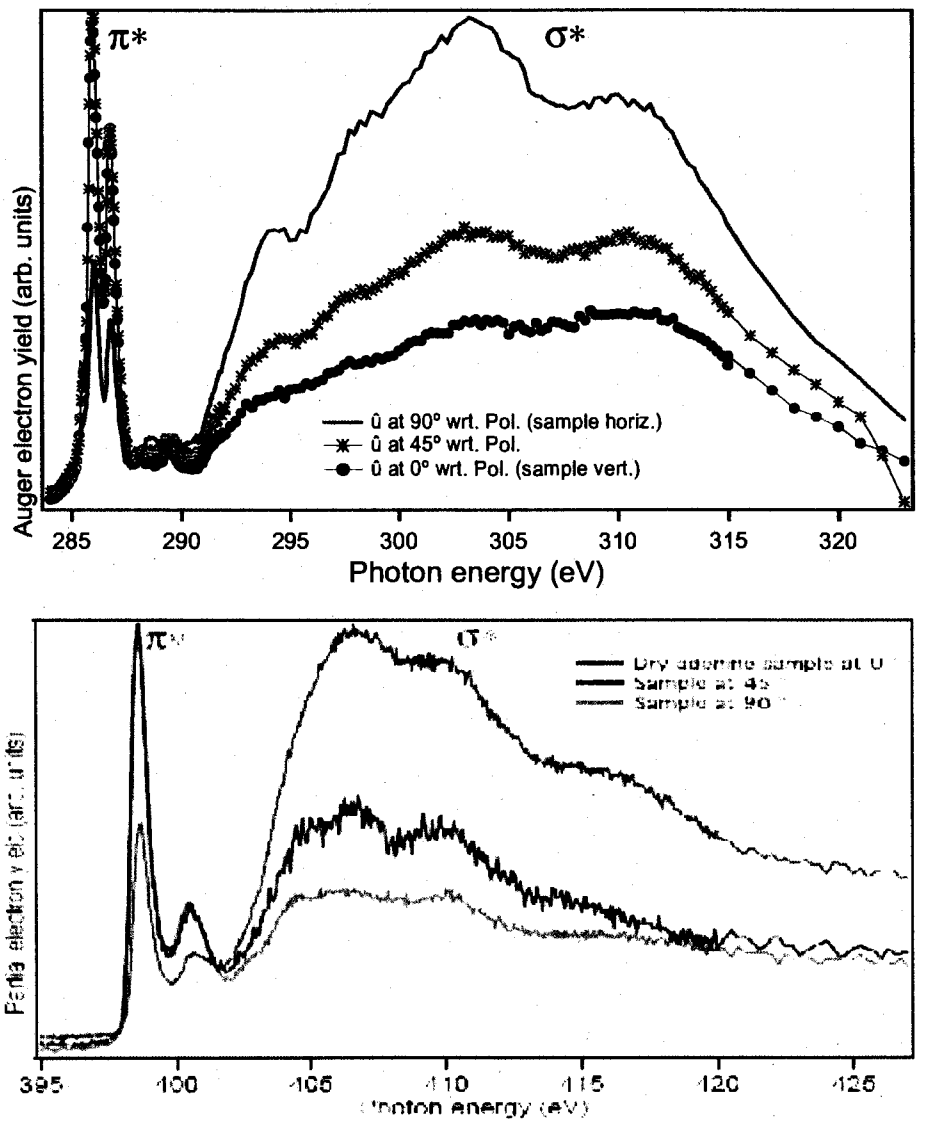

Figure 16. C(1s)(top) and N(1s)(below) NEXAFS spectra for a 15 nm adenine film on Si (100), obtained at three different angles between the surface normal (ŭ) and the SR polarization vector (Vall-llosera *et al*, paper in preparation 2008).

II. VUV photofragmentation experiments

The fragmentation pathways of genetic sugars, 2-deoxy-D-ribose and D-ribose (Structure in Figure 7), were determined by 5-30 eV photon impact in the gas phase.

Furthermore using partially deuterated 2-deoxy-D-ribose and D-ribose, and $^{13}C1$ and $^{13}C5$ labelled molecules, the origin of important fragments were identified in the two sugar molecules. Moreover using the excitation function of the fragments, their formation energy threshold was measured and their complementary fragments were recognized. In cellular DNA, the genetic sugar links the nucleobase and the phosphate groups in the 1', 3', and 5'carbon positions respectively. Damage to these two sugars (2-deoxy-D-ribose and D-ribose) is known to be one of the most severe forms of DNA damage induced by ionizing radiation which leads to cell death (Von Sonntag, 1987). Studies with ion impact on the RNA sugar have identified C5 site to be the most vulnerable position on the pyranose ring of D-ribose (Bald *et al*, 2006). From these results fragmentation patterns and ionization energies have been reported and appearance energies (AE) can be estimated. AE values may enable the values for heat of formation of parent and other important fragment ions to be determined.

II.1 2-deoxy-D-Ribose results

Figure 17 (bottom) shows the fragmentation pattern of 2-deoxy-D-Ribose (DNA sugar) by 23 eV photon impact. The major cations include: CH_3^+, OH^+, H_3O^+, CH_xO^+ (x=0,1,2,3), $C_2H_xO^+$ (x=1,2), $C_3H_xO^+$(x=3-5), $C_2H_4O_2^+$, $C_3H_xO_2^+$ (x=1,2,4-6), $C_4H_6O_2^+$, $C_4H_xO_3^+$ (x=6,7), $C_5H_7O_3^+$, and $C_5H_8O_3^+$. The fragmentation pattern generally appears to be diverse and scattered over a wide range of masses starting from 15 amu (CH_3^+) up to the parent molecule ($C_5H_{10}O_5^+$) at 134 amu with the two most intense peaks ($C_2H_4O_2^+$ and $C_3H_5O_2^+$) appearing at the 60-80 amu mass range.

II.2 D-Ribose results

Figure 17 (top) shows the fragmentation pattern of D-Ribose (RNA sugar) by 23 eV photon impact. The major cations include: CH_3^+, OH^+, H_3O^+, $C_2H_3^+$, $C_2H_4^+$, CH_xO^+ (x=1,2,3), $C_2H_xO^+$ (x=1-5), $C_3H_xO^+$(x=3-5), $C_2H_4O_2^+$, $C_3H_xO_2^+$ (x=1,2,4-6), $C_4H_6O_2^+$, $C_4H_xO_3^+$ (x=6,7), $C_5H_7O_3^+$, and $C_5H_8O_3^+$. The fragment peaks observed in the spectrum spans a range of masses starting from 15 amu (CH_3^+) to 116 amu ($C_5H_8O_3^+$), with the two major fragments observed at the far left of the spectrum, 44 amu ($C_2H_4O^+$) and 57 amu ($C_3H_5O^+$).

Looking at the fragmentation pattern of sugar molecules in the gas phase (Figure 17), fragments CH_3^+ (15 amu) and H_3O^+ (19 amu) and CH_3O^+ (31 amu) appear to be intense in both spectra. These three fragments have also been observed in studies involving low energy heavy ion irradiation of films of D-Ribose and 2-deoxy-D-Ribose in the condensed phase (Bald *et al*, 2006). These fragments may result from abstraction/transfer of H/H^+ via concerted bond rearrangements /dissociations upon irradiation. These results hence suggest formation of same fragments upon ion and photon induced damage in DNA and RNA sugars.

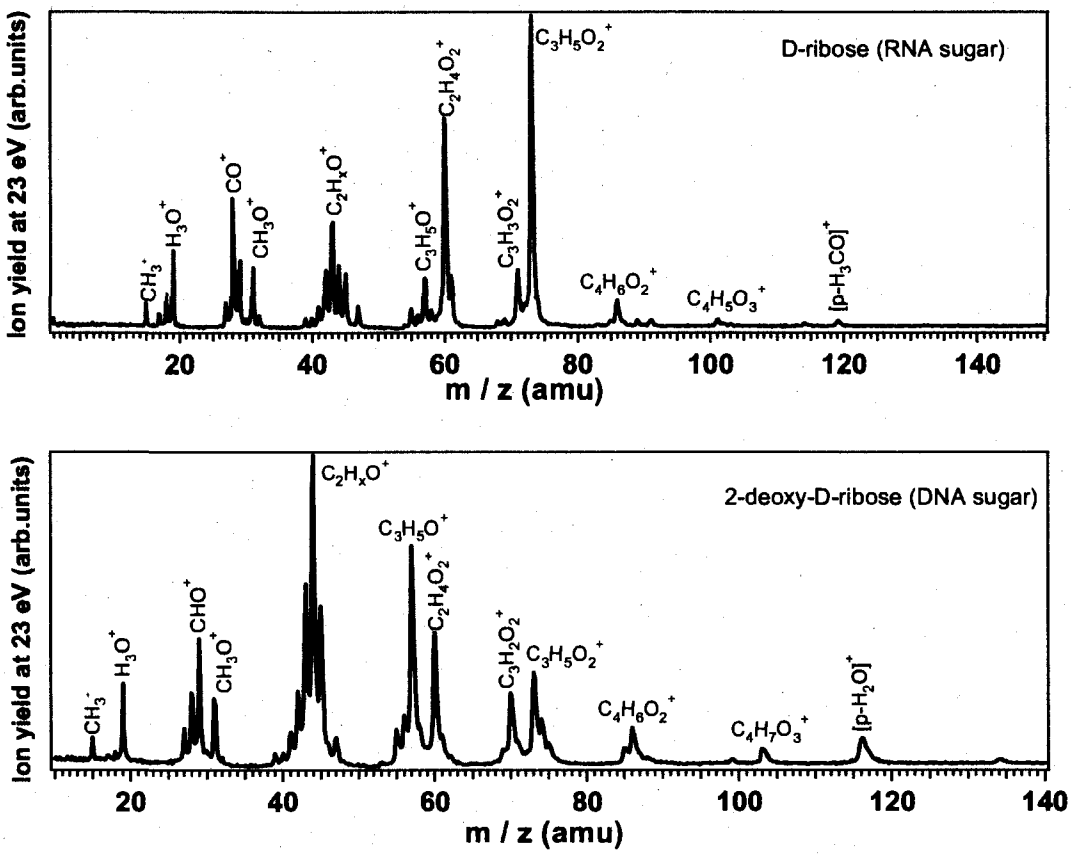

Figure 17. Fragmentation pattern of (a) D-Ribose (RNA sugar) and (b) 2-deoxy-D-Ribose (DNA sugar) at **540Å (23eV)** (Vall-llosera *et al*, paper in preparation 2008).

Looking at the results obtained for specific fragmentation sites, or cleavage planes, using isotopically labelled D-Ribose molecules, Figure 18 shows the 82-94 amu close up of the mass spectrum corresponding to the unlabeled, 1-^{13}C and 5-^{13}C labelled D-Ribose molecule upon 23 eV photon impact in the gas phase. As the results illustrate, one of the major fragmentation products, $C_4H_6O_2^+$ involves the C5 position in the D-Ribose molecule and originates from the left section of this molecule indicating a clear cleavage plane as shown in the structure of the sugar (Figure 18, right). As discussed before, this carbon atom plays a vital role in the structure and stability of D-Ribose molecule as an

RNA sugar in human genetic structure. Hence these results indicate severe damage induced in RNA upon VUV photon impact.

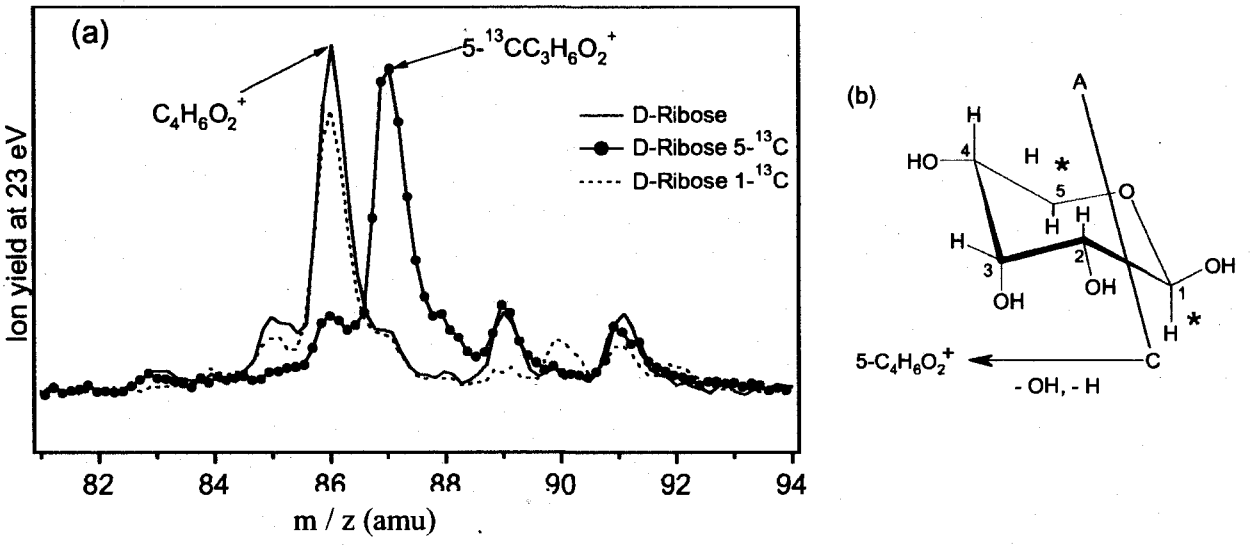

Figure 18. (a) Close up for 82-94 amu mass spectrum of D-Ribose (RNA sugar), 5-^{13}C and 1-^{13}C D-Ribose at E = 23 eV impact photon energy, (b) The cleavage pathway in D-Ribose corresponding to the graph (Vall-llosera *et al*, paper in preparation 2008).

Figure 19 illustrates the positive ion yields obtained upon fragmentation of D-Ribose (RNA sugar) by 8-11 eV VUV photons. The positive ion yields of 2-deoxy-D-Ribose after 8-11 eV photoabsorption (using a LiF filter in both cases) are demonstrated in Figure 19, where p^+ stands for the parent cation of this molecule. One of the significant excitation energy thresholds belongs to the parent cation (m/q = 134 amu) which is estimated to be (9.2 ± 0.1) eV. Looking at the two graphs (Figure 19 and 20), it is evident that the two sugars fragment in a different pattern at threshold energy. The results show that the parent cation ($C_5H_{10}O_4^+$) consistently appears in the DNA sugar fragmentation spectra. However even at threshold energy, the parent cation ($C_5H_{10}O_5^+$) does not appear in any of the RNA sugar mass spectra. Hence the results of these experiments demonstrate a higher level of vulnerability of the RNA sugar (D-Ribose) to VUV photons

compared to the DNA sugar (2-deoxy-D-Ribose) making D-Ribose a more fragile target for low energy UV radiation.

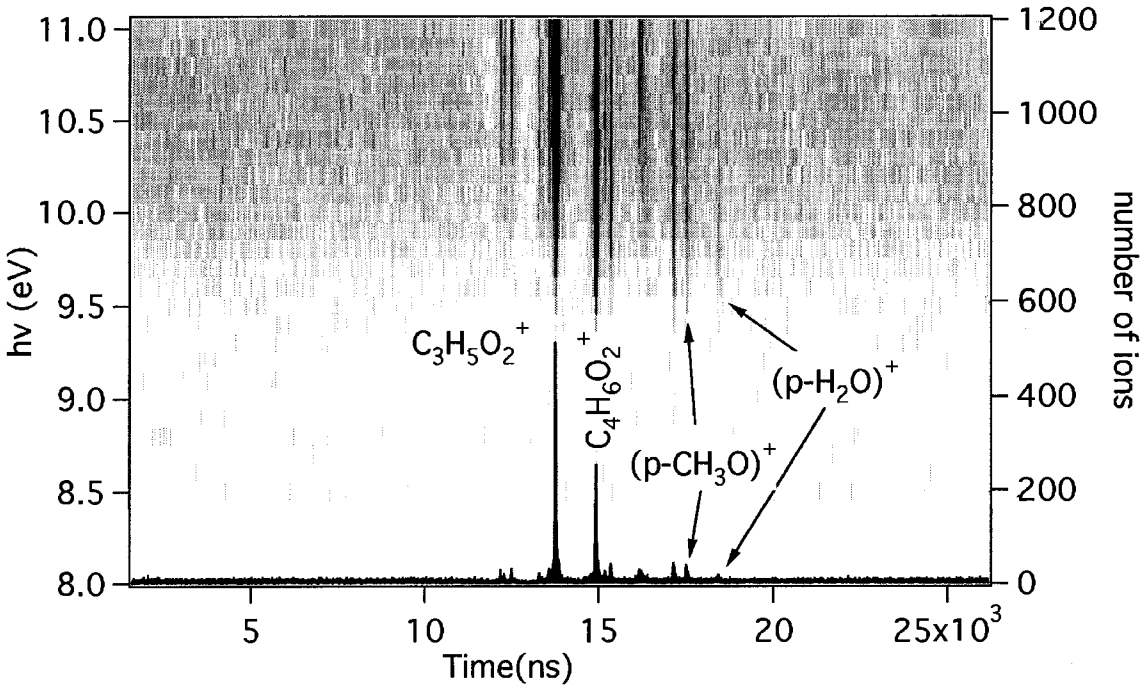

Figure 19. TOF mass spectra and topographic views of the energy dependent ion yield mass spectra after photo-absorption of VUV synchrotron photons. VUV photo-absorption using a LiF filter.(Vall-llosera *et al*, paper in preparation 2008).

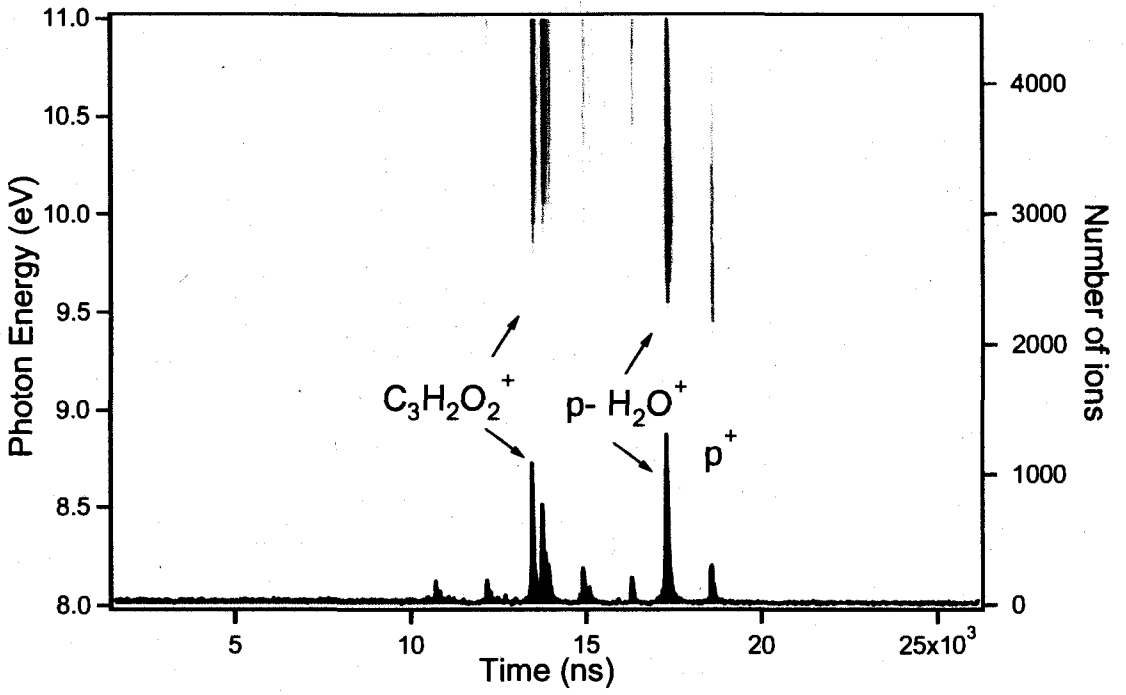

Figure 20. TOF mass spectra and topographic views of the energy dependent ion yield mass spectra after photo-absorption of VUV synchrotron photons. p^+ stands for the parent cation of this molecule (Vall-llosera *et al*, paper in preparation 2008).

Our results demonstrate that photon absorption in general leads to clusters of fragments as illustrated in Figure 17 a and b. In particular the most intense fragments appear at 50-80 amu mass range in D-Ribose, and 30-60 amu range in 2-deoxy-D-Ribose. Moreover when an electron is removed from the valence orbital of D-Ribose molecule in the gas phase, the molecule rapidly dissociates before reaching the TOF detector, since the parent cation is not observed in the ion yield mass spectra of this molecule even at threshold energy (Figure 19). In the case of 2-deoxy-D-Ribose however, the parent cation ($C_5H_{10}O_4^+$) is clearly observed even at energies higher than threshold energy. These

observations demonstrate significant implications for the stability of DNA based life compared to RNA based life in the universe.

Chapter 4. Conclusions

The success of life on earth is established on the high chemical and photochemical stability of the building blocks of life. Radiation induced alternations at the molecular level in DNA and RNA components poses significant threat to the cell and tissue environment and results in irreversible damage resulting in mutations and cancer in biological systems. These radiations span a wide range of the Electromagnetic spectrum from Ultraviolet photons to Gamma rays. Moreover low energy (1-500 eV) electrons and heavy ions (primary with track end energies or secondary) which have very high LETs and are capable of inducing complex and lethal damage including single and double strand breaks, base loss and cluster damage in DNA and RNA (Boudaïffa *et al*, 2000; Sellami *et al*, 2007).

Much has been studied on the impact of primary energy deposition in matter by electrons and photons (Inokuti, 1971; Mott *et al*, 1995). However vast amount of research is to be done to link the chain of events occurring in the time between the primary events induced by energetic particles such as X-ray photons, electrons or heavy ions and the distribution of the secondary species produced along the ionization track, low energy chemical events which cover the final stages of the primary high LET radiation.

Experiments focusing on radiation damage to biomolecules still face major challenges ahead. The production of isolated gas-phase large biomolecules (e.g. a DNA segment) presents radiobiology with an exceptionally challenging task. Nucleosides are even more fragile than nucleobases in the case of gas phase evaporation and a low vapour pressure makes it complicated to prepare sufficient target density during gas phase experiments.

Currently the efforts are made to study ion induced excitations of biomolecular species fabricate by means of electrospray ionization (using solvated biomolecules) or by utilizing laser desorption techniques such as matrix-assisted laser desorption ionization (MALDI). However it is difficult to produce neutral targets with MALDI method.

As the first part of this research, I have performed experiments with an ion beam system located at the Ion Reaction Laboratory, Sherbrooke, Canada in order to investigate the damage induced by the impact of low energy (1-200 eV) mass and energy selected heavy ions on condensed films of selected DNA and RNA bases. This work has demonstrated that, low energy Ar^+ and Xe^+ ions induce severe damage on nucleobases by ionization and fragmentation of these molecules along distinct cleavage planes, some of which have only been observed in chemical processes which induce DNA damage (e.g. deamination of Adenine, Guanine and Cytosine). Our present work demonstrates physically induced deamination of three of DNA bases in the condensed phase by impact of low energy heavy ions, a mechanism only induced in the three DNA bases containing an amino ($-NH_2$) group (As confirmed by experiments on 5-Aminouracil) which serves as an important bond breaking pathway in the radiobiological damage induced in the cell. Major types of DNA base damage in the literature include: deamination, oxidation, alkylation, ultraviolet radiation, and depurination/depyrimidation (Mol *et al*, 1999). Base damage can occur by environmental, chemical or enzymatic mechanisms. Xanthine in DNA arises as a result of guanine deamination, can mispair with thymine. Cytosine deamination is common and genotoxic since it creates uracil-guanine mispairs in DNA which results in GC→ AT transition mutations if left unrepaired before the next round of replication. These are cytotoxic effects induced in the cell (Reyes *et al*, 1998).

Nucleobase deamination products have the potential to act as biomarkers of several facets of cellular pathophsiology, with their involvement in carcinogenesis and other disease processes could involve both direct mutagenesis and, disruption of cell signalling, cycling or other facets of cell physiology (Fishbein, 2006).

Deamination of adenine, guanine and cytosine, is known to occur frequently in mammalian cells (Reddy and Vasquez, 2005). Deamination of DNA bases can occur spontaneously, leading to generation of highly mutagenic lesions such as hypoxanthine, uracil and xanthine. For instance spontaneous deamination of adenine may lead to an error in DNA transcription/replication because of resemblance of hypoxanthine to guanine (Kow, 2002). Here we have shown that the physical interaction of a slow ion leads not only to fragmentation but also to more subtle damage, such as deamination of DNA adenine, guanine and cytosine bases.

As the second part of this thesis, I have collaborated in experiments performed on DNA and RNA components using Synchrotron Radiation at BL I511 and BL 52 in Max-Lab, Lund, Sweden. In the first set of these investigations, Adenine films were irradiated with monochromatic soft X-ray (280-500 eV) to induce core specific ionization in carbon and nitrogen atoms in the biomolecule and analyzed by NEXAFS and XPS methods available onsite. The results demonstrated that Adenine films appear much more sensitive to core-specific excitations and degrade very rapidly upon irradiation. Moreover, experiments performed on pure Adenine films of 10-20 nm thickness at different angles with respect to the polarization angle of the photon beam, showed order in these films which indicates formation of ordered physisorbed films of adenine on nanocrystalline Si(100) substrate. Furthermore NEXAFS analysis of the azimuthal orientation of adenine

molecules indicated that adenine molecules lie flat or with a slight angle on the surface of Si(100) substrate, a phenomenon observed even for thick films of adenine (100 Layers of adenine e.g. 20 nm). XPS results clearly showed degradation of the adenine films and the C (1s) XPS spectra in particular demonstrated a clearly resolved C5 atomic site degrading as a function of time.

In a second set of synchrotron experiments, VUV (5-30 eV) photons were utilized to study photofragmentation of D-Ribose (RNA sugar) and 2-deoxy-D-Ribose (DNA sugar) in the gas phase at BL 52 in Max-Lab, Lund, Sweden. These experiments demonstrated fragmentation and bond cleavage at energies near 9.2 eV. Moreover the results showed significant formation of parent cation in the fragmentation pattern of one of the sugar molecules, 2-deoxy-D-Ribose (DNA sugar), a phenomenon not observed for the other genetic sugar (D-ribose, RNA sugar). The fragmentation spectra for the two molecules as well as the D-Ribose 1-^{13}C and 5-^{13}C labelled molecules, illustrated clear differences in bond cleavage pathways for the two sugars. Fragment appearance thresholds were measured and a parent excitation energy threshold (m/q=134 amu) of (9.2 ± 0.1 eV) was estimated for 2-deoxy-D-Ribose molecules. These results demonstrate a distinct vulnerability of D-Ribose to Low energy VUV radiation compared to 2-deoxy-D-Ribose, an observation which may answer extremely exciting astrobiological questions regarding the origin and formation of first primordial genetic biomolecules by passage of radiation through gaseous media in the space.

Acknowledgements

I would like to specially thank my research advisor Professor Michael Huels and Dr. Zongwu Deng and Mr.Marc Michaud at Radiobiology department, Université de Sherbrooke, Québec, Canada for their help and insight during my M.Sc. research. I would also like to thank our collaborators Professor Elizabeth Rachlew, Dr.Gemma Vall-llosera at KTH, Dr.Franz Hennies at the Swedish Light Source, Sweden, Professor Edwin Kukk and Dr.Rami Sankari from Physics department at the University of Turku, Finland, Dr.Sandrine Lacombe from Université Paris Sud, Orsay, France and Dr.Thomas Schlathölter from KVI Atomic Laboratory, Groningen, The Netherlands for constructive discussions. Also many thanks to Ms.Laetitia Michelle, Ms.Pierrette Carrier, and Ms.Francine Lussier.

Bibliography

Anderson SL (**1997**) Acc.Chem.Res. **30** 28-36.

Alvarado F, Bari S, Hoekstra R, Schlathölter T (**2006**) Phys.Chem.Chem.Phys. **8** 1922.

Akbulut M, Sack NJ and Madey TE (**1997**) Surface Science Reports. **28** 177-245.

Brahme A (**2004**) Int.J.Radiat.Oncol.Biol.Phys. **58** 603.

Burkart W, Finch GL, and Jung T (**1997**) Sci.Total Environ. **205** 51.

Bald I, Deng Z-W, Illenberger E, and Huels MA (**2006**) Phys.Chem.Chem.Phys. **8** 1215-1222.

Bowers MT (**1997**) Gas Phase Ion Chemisry, Vol.**2** (Academic Press Inc).

Brenner DJ, Amols HI (**1989**) J.Radiol. **62** 910-914.

Brenner DJ, Leu C-S., Beatty JF, and Shefer RE (**1999**) Phys.Med.Biol **44** 323.

Bell RP (**1980**) "*The Tunnel Effect in Chemistry*", (Chapman and Hall Ltd).

Boudaïffa B, Cloutier P, Hunting D, Huels MA, Sanche L (**2000**) Science. **287** 1658.

Cucinotta FA, Townsend LW, Wilson JW, Golightly MJ, and Weyland M (**1994**) *Adv.Space.Res.* **14** 661.

Deng Z-W., Bald I, Illenberger E, and Huels MA (**2005**) Phys.Rev.Lett. **95** 153201.

Deng Z-W, Imhoff M, and Huels MA (**2005**) J.Chem.Phys. **123** 144509.

Deng Z-W, Bald I, Illenberger E, and Huels MA (**2006**) Phys.Rev.Lett. **96** 243203.

Elkind MM (**1985**) DNA damage and cell killing, Cancer, **56** 2351-2363.

Fishbein JC (**2006**) "*Advances in Molecular Toxicology*", Vol **1**, Chapter 2, Elsevier.

Guler LP, Yu Y-Q, and Kenttämaa HI (2002) J.Phys.Chem.*A.* **106** 6754.

Hunniford CA, Timson DJ, Davies RJH, and McCullough RW (**2007**) Phys.Med.Biol. **52** 3729.

Huels MA, Boudaiffa B, Cloutier P, Hunting D, and Sanche L (**2003**) J.Am.Chem.Soc.**125** 4467-4477.

Hill MA (**2004**) Rad.Protect.Dosim. **112** 471.

IAEA 2008 "*Relative Biological Effectiveness in ion beam therapy*" Technical Reports Series No.461 (Vienna, Austria: International Atomic Energy Agency and the International Commission on Radiation Units and Measurements).

ICRU 1983 "*Microdosimetry*" ICRU Report 36 (Bethesda, MA: International Commission on Radiation Units and Measurements)

- **1979** *"Quantitative Concepts and Dosimetry in Radiobiology"* ICRU Report 30 (Bethesda, MA: International Commission on Radiation Units and Measurements).

- **1986** *"The quality factor in radiation protection"* ICRU Report 40 (Bethesda, MA: International Commission on Radiation Units and Measurements).

- **1992** *"Photon, electron, proton and neutron interactions in tissue"* ICRU Report 46 (Bethesda, MA: International Commission on Radiation Units and Measurements).

Inokuti M **(1971)** *"Inelastic collisions of fast charged particles with atoms and molecules-The Bethe theory revisited"*, Rev.Mod.Phys, **43** 297-347.

Jolly WL, Bomben KD, Eyermann CJ **(1984)** At.Data.Nucl.Data.Tables. **31** 433.

Kraft G, Scholz M, and Bechthold U **(1999)** Radiat.Environ.Biophys. **38** 229.

Kraft G **(2002)** *"The Physics of Highly and Multiply Charged Ions"*, Ed.F.J Kluwer Academic Publisher.

Kukk E, Sankari R, Huttula M, Sankari A, Aksela H, and Aksela S **(2007)** Journal of Electron Spectroscopy and Related Phenomena. **155** 141-147.

Kow YW, Oct 1 **(2002)** Free.Radic.Biol.Med. **33**(7) pp.886-93.

Lacombe S, Le Sech C, and Esaulov VA **(2004)** Phys.Med.Biol. **49** N65.

Löwdin P-O, July **(1963)** Reviews of Modern Physics. **Vol.35** No.3 pp.724.

Löwdin P-O **(1965)** *"Quantum Genetics and the Aperiodic Solid"*, Adv.Quantum.Chem., **2** 213.

Mott NF and Massey HSW **(1995)** *"Theory of Atomic Collisions"*, Clarendon, Oxford.

McMillan TJ, Steel GG **(1997)** *"DNA damage and cell killing"*, Basic clinical radiobiology, Arnold, London.

Morgenstern R, Schlatholter T, and Hoekstra R, Nov **(2000)** RIKEN Review. No.31.

Mårtensson N, Baltzer P, Brühwiler PA, Forsell J-O, Nilsson A, Stenborg A, Wannberg B **(1994)** Journal of Electron Spectroscopy and Related Phenomena. **70** 117-128.

Mol CD, Parikh SS, Putnam CD, Lo TP, and Tainer JA **(1999)** Annu.Rev.Biophys.Streuc.

28 101-28.

Madeja F, and Havenith M, 15 Oct **(2002)** J.Chem.Phys. **Vol 117** No.15.

Nikoghosyan A, Schulz-Ertner D, Didinger B, Jäkel O, Zuna I, Hoss A, Wannenmacher M and Debus J **(2004)** Int.J.Radiat.Oncol.Biol.Phys. **58** 89.

Östblom M, Liedberg B, Demers LM and Mirkin CA **(2005)** J.Phys.Chem.B. **109** 15150-15160.

Oshima H. and Bartsch H **(1994)** Mutat.Res. **305** 253-264.

Plekan O, Feyer V, Richter R, Coreno M, de Simone M, Prince KC, Trofimov AB, Gromov EV, Zaytseva IL, and Schirmer J **(2007)** J.Chem.Phys. .p.doi:10.1016/j.chemphys.2007.09.021.

Plekan O, Feyer V, Richter R, Coreno M, Šutara F, Skála T, Švec M, Chab V, Mantolin V, and Prince KC **(2007)** Surf.Sci. **601** 1973.

Resat SS and Morgan WF **(2004)** Cancer and Metastasis Reviews. **23** 323.

Reyes A, Gissi C, Pesole G, and Saccone C **(1998)** Mol.Biol.Evol. **15**(8) 957-966.

Reddy MC and Vasquez KM (**2005**) Radiation Research, **164** 345-356.

Routledge MN, Wink DA., Keefer LK, and Dipple A (**1994**) Chem.Res.Toxicol. **7** 628-632.

Sarabipour S, Michaud M, Huels MA (**2008**) "*Fragmentation of DNA components by Hyperthermal Heavy Ion (Ar^+ and Xe^+) impact in the Condensed phase and electron impact in the gas phase*", paper in preparation.

Sasaki MS, Kobayashi K, Hieda K, Yamada Y, Ejima Y, Maezava H, Furusawa Y, Ito T, Okada S (**1989**) Int.J.Radiat.Biol. **56** 975-988.

Schulz-Ertner D, Karger CP, Feuerhake A, Nikoghosyan A, Combos SE, Jäkel O, Edler L, Scholz M, and Debus J (**2007**) Int.J.Radiat.Oncol. **68** 449.

Sellami L, Lacombe S, Hunting D, Wagner RJ, and Huels MA (**2007**) Rev. Sci. Instrum. **78** 085111; DOI:10.1063/1.2758459.

Stelzer H (**1998**) Nuclear Physics B (Proc. Suppl.). **61B** 650-657.

Sutherland BM, Bennett PV, Sidorkina O, and Laval J (**2000**) Biochemistry. **39** 8026.

Shapiro MM (**1983**) (Ed.), NATO ASI Series C: Mathematical and Physical Sciences, **Vol. 107**, Reidel, Dordrecht.

Sigmund P, 1-5 May (**2006**) "*Ion Beam Science: Solved and Unsolved Problems , Part I*", Invited lectures presented at a symposium arranged by the Royal Danish Academy of Sciences and Letters, Copenhagen.

Schlatholter T, Hoekstra R, Morgenstern R (**2004**) Int.J.Mass.Spectro. **233** 173-179.

Schlatholter T, Alvarado F, Bari S and Hoekstra R (**2006**) Physica Scripta. **73** C113-C117.

Stöhr J (**1992**) NEXAFS Spectroscopy, Springer Ser.Surf.Sci. Vol.**25** Springer, Berlin.

Seifert S, Favrila GN, Zahn DRT and Braun W (**2007**) Surf.Sci. **601** 2291.

Sriraman S, Agarwal S, Aydil ES and Maroudas D (4 July **2002**) Nature. **418** 62-65.

Townsend LW, Cucinotta FA, Wilson JW, and Bagga R (**1994**) Adv.Space.Res. **14** 671.

Vall-llosera G, Lacombe S, Rachlew E, Hennies F, Sarabipour S, Huels MA (**2008**) "*Morphology and degradation of thin films of adenine monitored with Synchrotron photons*", paper in preparation.

Vall-llosera G ,Sankari R, Sarabipour S, Kukk E, Rachlew E, , Huels MA (**2008**) "*Photofragmentation of DNA and RNA sugars by Synchrotron photons*", paper in preparation.

Virsik RP, Harder D and Hansmann I (**1977**) Radiat.Environ.Biophys. **14** 109-121.

Von Sonntag C (**1987**) "*The Chemical Basis for Radiation Biology*", Taylor and Francis, London, UK.

Ward JF (**1981**) "*Some biochemical consequences of the spatial distribution of ionizing radiation produced free radicals*", Radiat.Res. **86** 185-195.

Ward JF **(1988)** "*DNA damage produced by ionizing radiation in mammalian cells: Identities, mechanisms of formation, and repairability*", Pros.Nucleic.Acids.Res.Molec.Biol. **35** 96-128.

Ward JF **(1994)** "*The complexity of DNA damage: relevance to biological consequences*", International Journal of Radiation Biology. **66** 427-432.

Watson JD, and Crick FHC, 25 April **(1953)** Nature, **171** 737-738.

Wiley WC and McLaren IH **(1955)** The Review of Scientific Instruments. **26** 12, 1150.

Yamada.Y **(2003)** J.Health.Sci. **49** 417.

Zeitz L, Kim SH, Kim JH and Detko JF **(1977)** Radiat.Res. **70** 552-563.